



**UNIVERSITÁ DEGLI STUDI DI PADOVA**

**Dipartimento di Tecnica e Gestione dei Sistemi Industriali**

Corso di Laurea Magistrale in

Ingegneria dell'Innovazione del Prodotto

TESI DI LAUREA

**In situ tensile tests of additively manufactured  
and wrought Ti-6Al-4V alloys**

*Studentessa*

**Ambra Celotto**

*Relatore*

**Prof. Ing. Paolo Ferro**

*Correlatori*

**Prof. Ing. Filippo Berto**

**Prof. Seyed Mohammed**

**Javad Razavi**

Anno Accademico 2019/2020





**UNIVERSITÀ  
DEGLI STUDI  
DI PADOVA**



**NTNU**

Norwegian University of  
Science and Technology

**Dipartimento di Tecnica e Gestione dei Sistemi Industriali**

Corso di Laurea Magistrale in

Ingegneria dell'Innovazione del Prodotto

TESI DI LAUREA

**In situ tensile tests of additively manufactured  
and wrought Ti-6Al-4V alloys**

*Studentessa*

**Ambra Celotto**

*Relatore*

**Prof. Ing. Paolo Ferro**

*Correlatori*

**Prof. Ing. Filippo Berto**

**Prof. Seyed Mohammed**

**Javad Razavi**

Anno Accademico 2019/2020



*Non quia difficilia sunt non audemus,  
sed quia non audemus difficilia sunt*

*(Lucio Anneo Seneca)*



# Ringraziamenti

Un ringraziamento speciale va al Prof. Paolo Ferro per la grande disponibilità e collaborazione prestata nella stesura di questo lavoro. Un grazie sentito al Prof. Filippo Berto per l'accoglienza mostrata e l'opportunità concessa di trascorrere un'esperienza così stimolante presso il suo gruppo di ricerca alla Norwegian University of Science and Technology di Trondheim. Grazie al prof. Seyed Mohammed Javad Razavi per aver guidato in maniera efficace l'attività sperimentale e aver stimolato l'interesse per la ricerca.

Arrivata al termine di questo percorso di vita, il mio grazie più sincero va ai miei genitori per avermi cresciuta consapevole delle mie potenzialità e per avermi sostenuta nella mia scelta fin dal primo momento, senza mai chiedermi nulla in cambio. Sono molto grata per aver avuto la possibilità di vivere il mondo universitario così liberamente, il quale mi ha regalato anni di grande crescita personale e accademica.

Grazie a mia sorella, che riponendo sempre grandi aspettative in me è stata lo stimolo per poterle soddisfare e, possibilmente, superare.

Grazie a tutti i miei nonni, per avermi spesso dato l'impressione di faticare con me e per essere prezioso esempio e ispirazione nelle scelte di vita e nelle relazioni con gli altri.

Grazie a tutti i miei cugini e familiari, che rendono sempre più bella condivisione dei traguardi.

Grazie a tutti gli amici che ho incontrato lungo il mio percorso. Ai compagni di scuola per aver condiviso le scelte per il futuro, agli amici e compagni di corso di Padova e Vicenza per aver alleggerito le lezioni e le sessioni di studio con qualche spritz e serata spensierata, alle coinquiline e i coinquilini tutti per aver sopportato il mio studio matto dell'ultimo minuto, alle compagne di ginnastica per aver compreso le mie scelte, agli amici di Trondheim senza i quali non avrei lucidato così bene i campioni, a quei matti di Vicenza per essere stati come una seconda famiglia, a Silvia e Valentina per essere sincere confidenti e ad Elena per preoccuparsi sempre del mio stato psico-fisico e assicurarsi che tutto venga sempre festeggiato a dovere.

Grazie ad Emanuele. Grazie per aver creduto in me più di quanto io abbia fatto, per avermi sempre dato un motivo per non sentire la stanchezza e per avermi fatto scoprire, nell'ultimo anno, una determinazione che non pensavo di avere. Grazie anche perché senza di lui questa tesi non l'avrei mai finita. Per lui un grazie non è sufficiente, questa laurea è anche un po' sua.

Ho sognato tanto questo giorno per potervi abbracciare tutti e poter condividere con voi la mia gratitudine e soddisfazione. Le circostanze mi obbligano ad aspettare ancora un po' prima di poterlo fare, ma so che succederà e sarà ancora più bello.

*La felicità è vera, soltanto se condivisa.*

Sacile, 10 Aprile 2020



# Contents

<b>Abstract .....</b>	<b>1</b>
<b>Introduction .....</b>	<b>3</b>
<b>Chapter 1 Titanium and its alloys.....</b>	<b>5</b>
1.1 Overview and properties .....	5
1.1.1 Primary production .....	7
1.2 Conventional manufacturing processes .....	10
1.2.1 Machining .....	10
1.2.2 Casting.....	10
1.2.3 Forging.....	12
1.2.4 Extrusion and rolling.....	13
1.2.5 Welding.....	13
1.2.6 Superplastic forming and diffusion bonding .....	14
1.2.7 Powder metallurgy.....	15
1.3 Classification of Titanium Alloys.....	16
1.3.1 Crystal structure.....	16
1.3.2 Alloys classification.....	18
1.4 Applications of titanium alloys .....	22
1.4.1 Aerospace .....	22
1.4.2 Biomedical .....	25
1.4.3 Chemical, petrochemical and energetic .....	27
1.4.4 Emerging markets.....	28
<b>Chapter 2 Additive Manufacturing of Titanium alloys.....</b>	<b>29</b>
2.1 Titanium alloys manufacturing introduction .....	29
2.2 Additive Manufacturing (AM) processes: a general overview.....	30

2.3 AM advantages and comparison with CNC processes .....	32
2.4 AM processes classification .....	33
2.4.1 Vat photopolymerization.....	35
2.4.2 Material extrusion .....	37
2.4.3 Material jetting.....	38
2.4.4 Binder jetting .....	39
2.4.5 Sheet lamination.....	41
2.4.6 Powder bed fusion .....	42
2.4.7 Direct Energy Deposition (DED) .....	48
2.5 AM processes for titanium and titanium alloys.....	52
2.5.1 Powder preparation for Ti-6Al-4V .....	53
2.5.2 Microstructure of Ti-6Al-4V processed with EBM and LENS.....	55
2.5.3 Mechanical properties of EBM and LENS processed parts .....	56
2.5.4 EBM and LENS processes comparison.....	57
<b>Chapter 3 Heat treatments .....</b>	<b>61</b>
3.1 Metallurgy of titanium.....	61
3.1.1 Diffusive transformations .....	63
3.1.2 Displasive transformations .....	63
3.2 Heat treatments on titanium alloys .....	64
3.2.1 Stress relieving.....	66
3.2.2 Annealing.....	67
3.2.3 Solution treating and aging .....	69
3.2.4 Quenching.....	71
<b>Chapter 4 Materials and Methods .....</b>	<b>73</b>
4.1 Specimens preparation .....	73

4.1.1 Production parameters .....	73
4.1.2 Polishing procedures .....	77
4.1.3 Heat treatments settings.....	82
4.2 Experimental works.....	86
4.2.1 Micrography.....	86
4.2.2 Microhardness tests .....	87
4.2.3 In situ investigations.....	91
<b>Chapter 5 Results and Discussion .....</b>	<b>99</b>
5.1 Microstructural properties.....	99
5.2 Fracture mechanism .....	104
5.3 Mechanical properties and size effect .....	110
<b>Conclusions .....</b>	<b>119</b>
<b>Appendix A: AM Micrographies .....</b>	<b>121</b>
<b>Appendix B: Microhardness .....</b>	<b>125</b>
<b>Appendix C: Test sequences.....</b>	<b>126</b>
<b>Appendix D: Fractographies.....</b>	<b>131</b>
<b>Appendix E: Tensile test values .....</b>	<b>141</b>
<b>References .....</b>	<b>142</b>



# Abstract

In this work microstructural and mechanical properties of additively manufactured and wrought Ti-6Al-4V alloy are investigated by means of *in situ* material characterization. Electron Beam Melting (EBM), Laser Engineered Net Shaping (LENS) and traditional wrought process combined with subsequent annealing and solution treatments have been involved in manufacturing of miniature tensile specimens which have been compared investigating microstructure and microhardness. Scanning Electron Microscopy (SEM) has been used to carry out *in situ* tensile tests and observe real-time failure mechanisms. The comparison between the obtained mechanical properties has raised the awareness of difficulties in the characterization of strain during tensile tests and on the interpretation of results due to not clearly predictable “size effect”. A graphical method has been also proposed to evaluate elongation to failure values. Microstructural properties revealed to be strongly dependent on thermal history undergone. While wrought specimens in general showed a majority of equiaxed grains, additive manufactured specimens resulted in fine basket-weaved platelets and acicular martensite grown within wide prior grains. Ductile fracture mechanism has been observed among all the cases, except for EBM where lack-of-fusion defects appeared to anticipate failure. Calculated strain hardening exponent resulted not be influenced by scale or microstructure. Elongation to failure trend showed higher values compared to that of reference standard-size specimens which is imputable to a possible “size effect”.



# Introduction

The excellent combinations of specific mechanical properties and outstanding corrosion behaviour make titanium alloys the material of choice in high performance industries [1] where reliability and functionality of the components are of major interest. About 70% of the world's titanium production is applied in commercial and military aerospace components such as engine casings, compressor blades and rotors, but it finds its wide spread also in chemical and energy plants, naval and competitive automotive applications, offshore oil and gas platforms and biomedical devices. Even though the latter cover only a small portion of the markets in which titanium is involved, the role of titanium in the production of prosthesis and others biomedical implants is unreplaceable. Its intrinsic biocompatibility assured by a superficial porous oxide layer guarantees superior osteointegration and low toxicity in human environment. Although the many benefits brought by titanium alloys and the wide availability of titanium in the Earth's crust, the costs related to titanium extraction and processing still represent a limit to its wider spread. A better understanding of the processes and procedures by which these components are fabricated is required [2]: in conventional removal processes the large amount of scrap represents the main contribute on the overall final product cost. In these terms, additive manufacturing technologies offer a valid answer compared to the conventional net-shape processes, thanks to a theoretically lower *buy-to-fly* ratio attainable [3]. Additive technologies also allow to markedly improve strength-to-weight ratio by producing very complex geometry components, already optimized, in a single-process step, reducing the need for further finishing procedures. This high production efficiency has made these techniques to rapidly develop and leave definitely the initial role of rapid prototyping tool. Moreover, while for conventional processes the product customization appears to be a constraint, for computer-aided manufacturing technologies represents an interesting opportunity. For instance, the

combination of this elevated versatility offered by additive manufacturing technologies with titanium biomedical applications is able to effectively improve the total production process. Indeed, the aerospace and medical industries have so far been the largest driver for the usage of titanium AM materials [2] in which highly topological optimized structures can be applied. In this regard, it has been aroused the importance of the control in the mechanical response of each optimized part, even the thinnest critical locations [4]. In parallel, in the last decade, there has been an increase in demand of devices whose size scale is well below that of conventional mechanical test specimens due to the miniaturization, integration, and compaction trend in the field such as electronics, consumer products, energy generation and storage, medical implants or the new generation of microelectromechanical devices (MEMS) and micro-machines [5], [6]. While macroscopic mechanical properties have been long investigated and improved with the growth of industries sectors, the awareness of possible “size effects” by changing the observation scale, induced engineers to develop reliable models and test procedures to account for the change in mechanical properties and grain size effect [5] compared to large-scale components. At this moment, the majority of small-scale characterizations are represented by tailored experimental devices and specimens that deviate from standardized procedures. This fact actually limits the comparisons possible both among same scale and large-small scale results and interpretation. This work is aimed to compare products of different manufacturing technologies on Ti-6Al-4V alloy which represent the “work horse” titanium alloy. Concerning small-scale characterization, the potentialities and the advantages of *in situ* testing have not been fully explored yet, but appears huge if combined with the rapid development of the relatively-newborn additive technologies and their continue improvement. This witness the role that this work plays in an extremely innovative and constantly evolving actual context.



# Chapter 1

## Titanium and its alloys

### 1.1 Overview and properties

Titanium is the fourth most abundant structural metal in the Earth's crust, after aluminium, iron and magnesium, representing 0.6% of its composition. This abundance is to some extent illusory, however, in that titanium is not so frequently found in economically extractable concentrations [7]. The concentrated sources of the metal that are commonly used to extract it and obtain titanium sponge are the minerals ilmenite and rutile (Figure 1.1). Several are the advantages of titanium and its alloys due to their high specific strength and excellent corrosion resistance that make them stand out primarily towards competing material such as aluminium, steels and superalloys. This justifies their early success in the aerospace, the chemical installations and many other highly performing markets [8].



*Figure 1.1: Ilmenite mineral ( $\text{FeTiO}_3$ ) and Rutile needles ( $\text{TiO}_2$ ) on Hematite mineral*

Table 1.1 summarizes the main physical and chemical characteristics of titanium. Thanks to its unique low density, titanium, together with its alloys, is the metal with the higher values of relative properties reported to mass. In absolute terms, considering its tensile strength performances, alloyed titanium results to be

comparable to any other lower-strength martensitic stainless steel and better than austenitic or ferritic steel; In terms of ultimate strengths, alloys can be comparable to iron-base or cobalt-base superalloys [9]. Instead its great advantage appears when these properties are reported to its weight: the same object, of equal weight, will be much more resistant if made of titanium instead of steel, or even better in case of a certain mechanical strength required for a specific component, the weight saving will be considerable if realized in titanium alloy. Hence the density of titanium is only about 60% of that of steel or nickel-base superalloys and this is only one of the some significant benefits offered by titanium alloys which illustrate the basis for its widespread use.

<b>Atomic Number</b>	22
<b>Atomic Weight</b>	47.88
<b>Density</b>	451 g/cm <sup>3</sup>
<b>Melting Temperature</b>	1670°C
<b>Boiling Temperature</b>	3260°C
<b>Thermal Conductivity</b>	19 W/mK
<b>Specific Heat</b>	523 J/kg°C at 25°C
<b>Coefficient of Thermal Expansion</b>	841 x10 <sup>-6</sup> cm/°C (1-100°C)
<b>Young's Modulus</b>	110 GPa

*Table 1.1: Main physical and chemical characteristics of titanium*

Furthermore, titanium has exceptional corrosion resistance that often makes it more effective than stainless steel in most aggressive environments, above all in the human body. This is made possible by the formation of a protective oxide passivating film on its surface, which exactly in same way steel do, avoid the material to be attacked by aggressive reagents. Service temperatures are relevant too: dependently on composition, commercial titanium alloys can be applied between 538°C and 595°C or even more in the case of titanium aluminides.

Biocompatibility and chemical stability have made this material the best candidate for structural medical implants inside human body.

On the other hand, all these numerous valuable qualities are balanced by a cost that is of the same magnitude of superalloys, namely four times that of a stainless steel [9]. A short cost comparison will be reported in Chapter 2.

### 1.1.1 Primary production

The aforementioned Ilmenite mineral is haematite ( $\text{Fe}_2\text{O}_3$ ) in which half of the iron has been replaced by titanium ( $\text{FeTiO}_3$ ). Rutile is  $\text{TiO}_2$  and it's the mineral from which titanium was discovered in about 1790. Anyway, titanium has never been purified until early 1900s and it did not become widely used until the second half of the twentieth century [9], when it started to be more easily available in a wide variety of types and forms. Nowadays the 50 years accumulated experience in modern industrial production and the many virtues of this material have made it find its niche in many application fields.

Since the overall demand for raw material is not subject to the same fluctuations as the demand for the metal, it is very important to have a wide raw-material base to draw from in case the material demand would be subjected to relevant increases at any time. The titanium industry, in this regard, can rely on a plentiful and stable supply of the basic ore, allowing to manage unexpected increased requirements for this metal. The production of titanium dioxide, in the form of sponge (Figure 1.2), is broadly diffused in high volumes and for many industries, so strongly that in 1977, for example, only a few percent of the global titanium mineral produced was destined to metallic sponge refinement while most of the mined ore was employed in paint pigments [7].

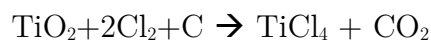
Despite its wide availability on the earth's crust, the process of titanium refinement is highly energy intensive making its obtainment as final product hardly sustainable from an environmental overall point of view. This fact has to be taken into account

as a negative note above all if considering the industries' growing awareness about energy conservation and interest on improving *Life Cycle Assessment*. It has been estimated that for the production of a ton of sponge-titanium can reach 16 times the amount needed for a ton of steel[7]. This high energy consumption explains also the notable cost percentage equal to 47% that refinement process occupies on the total cost for the production of a 1" plate [10].

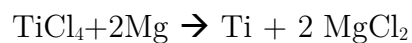


*Figure 1.2: Titanium sponge, result of titanium extraction from minerals*

The most well-known method to convert rutile mineral  $\text{TiO}_2$  in titanium sponge is the Kroll process that provides the reduction of  $\text{TiCl}_4$  by magnesium. Firstly, a colorless titanium tetrachloride is gained passing  $\text{Cl}_2$  gas through charge the ore:



Then  $\text{TiCl}_4$  is purified by fractional distillation. At the end, the liquid form of  $\text{TiCl}_4$  is reacted with magnesium under an inert atmosphere to obtain titanium sponge while  $\text{MgCl}_2$  is electrolytically recycled:



The Kroll Process is schematized in Figure 1.3. Once titanium sponge is obtained and purified, it has to be melted to form ingots. During the melting step, alloying elements can be added. Ingots are produced by means of Vacuum Arc Remelting (VAR) technique. A cylindrical electrode of appropriate chemistry is melted by an arc in a vacuum and solidified in a water-cooled crucible. Electrodes for making titanium ingots are compacted aggregates (“compact” or “briquettes” as showed in

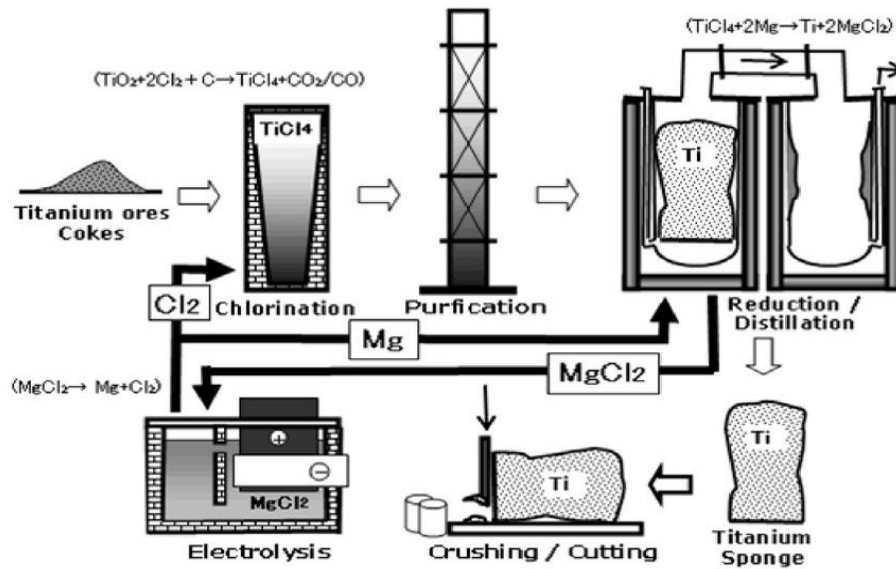


Figura 1.3: Kroll extraction process of Titanium sponge

Figure 1.4) of sponge and alloy elements, including both master melt and elemental materials [9]. Primary fabrication is what it is defined as conversion of ingot into general mill products. Generally, the first breakdown of production ingot is a press cogging operation. Following operations of extrusion, rolling and forging are performed in order to obtain bras, plates, sheets, wires and tubing to be further shaped by secondary fabrication processes. Heat control is very important in this phase for the obtainment of desired microstructure.

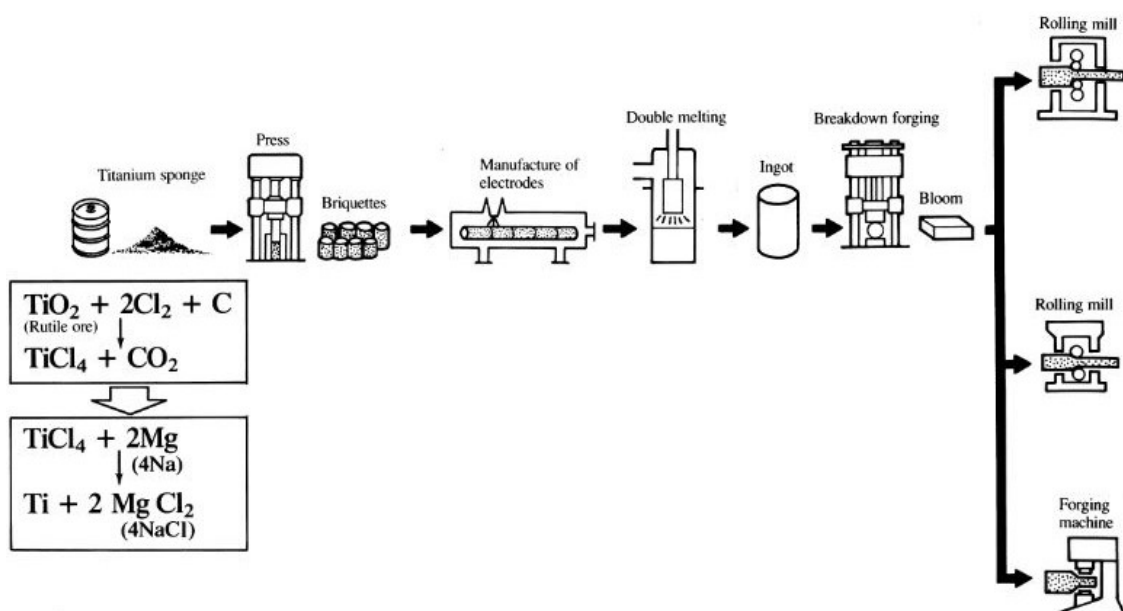


Figure 1.4: Overview of the production cycle for ingot and mill products [9]

## **1.2 Conventional manufacturing processes**

Above all due to its unique physical and chemical properties, some restrictions have to be recognized for titanium to be shaped. An outline on the most popular production techniques is described in this paragraph.

### **1.2.1 Machining**

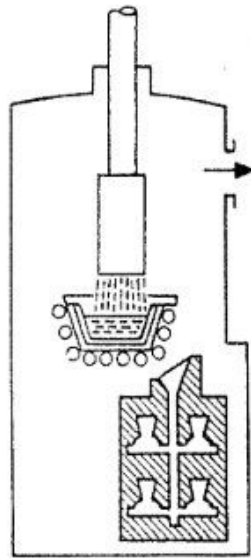
Titanium alloys machining presents some constraints. Firstly, the low thermal conductivity of titanium impedes quick dissipation of heat generated by machining, leading to the necessity of higher wear resistant tools. Valuable spring back after deformation under load are also possible because of titanium low Young's modulus. Moreover, galling tendency is highly probable due to titanium low hardness and high chemical reactivity.

Hence, some general guidelines have to be followed for conducting an effective machining process. Cutting tools should be sharp and replaced at the first sign of wear, which is a sign of occurring failure. The workpiece should be subjected to few vibrations possible being mounted into the grips of the working machine, which have to be stiff. Copious coolant is required to perform positively the operation, but to also to prevent fire which can occur from titanium chip that are fire hazardous. Low cutting speeds should be used while feed rates should be high. Tools mostly used are high-speed cobalt-based steel tools, effective for their flexibility and low cost. However, in case of higher feed rates and speeds or rough surfaces, cemented carbides cutting tools may be needed. Grinding operations highlight titanium low thermal conductivity, in which almost a half or one third of conventional operating wheel speeds have to be adopted [8].

### **1.2.2 Casting**

Casting is a (near-)net-shape process. Indeed, if compared to machining, it has a high cost saving potential because of the large amount of material scrap produced

by subtractive processes on ingot and often post-processing steps are not as extensive. Complex geometries, otherwise not reachable, are producible with casting economically. On the other hand, cast components are penalized on strength and ductility if compared to forged parts but these defects can be partially compensated by proper procedures. In these terms, the most common process to achieve low thickness, close tolerance a good surface quality is investment casting. Investment casting, also called lost- wax process, need to be carried out in vacuum and with water-cooled crucibles. The process consist in separate steps. At first, a wax model have to be realized from an aluminium die, which have to be bigger than the required final titanium part in order to compensate the shrinkage both of wax and the titanium alloy. A cluster is made assembling several wax models which is then coated with ceramic slurry and dried. Wax is then melted in an autoclave while the refractory is stabilized for the actual casting process. Subsequently casting is performed in a vacuum arc furnace with a self-consuming electrode (Figure 1.5).



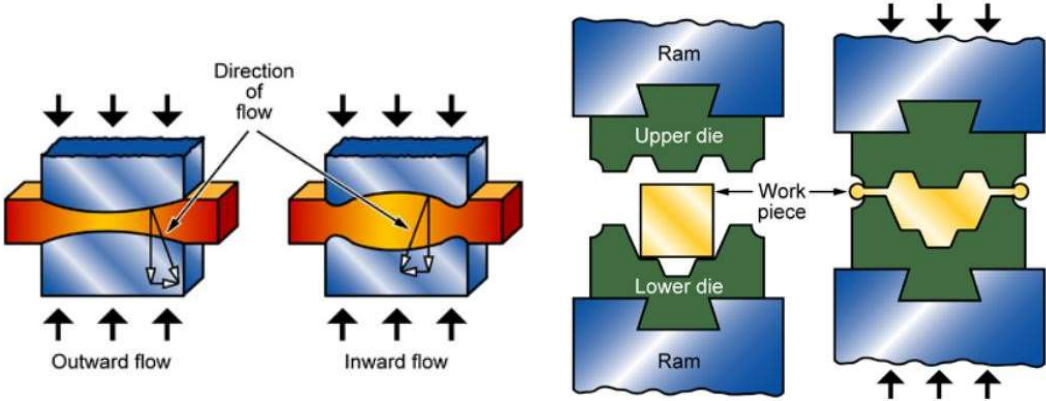
*Figure 1.5: Principle of Titanium investment casting (Courtesy: Tital, Bestwig) [8]*

The melt metal is dropped on a water-cooled copper crucible in order to forms a thin titanium layer on it, which then acts as the crucible and feed the final ceramic mold, where centrifugal casting is applied. After cooling, the ceramic mold is broken

(lost wax) and titanium part is extracted and stays, risers, and channels are removed in order to obtain the final cast piece. An Hot Isostatic Pressure (HIP) procedure below beta transus and at pressure of around 100 MPa is commonly carried out to reduce porosity. Titanium casting is mostly employed for high performance parts for the aerospace and non-aerospace industries [8].

**1.2.3 Forging**

The selection of forging process depends on the desired shape. Forging process include open-die, closed-die, rotary forging and others. The main advantage of forging, apart from shape control, the possibility to obtain a combination of tensile strength, creep resistance and fracture toughness not otherwise obtainable in bars or billets. Open die forging is necessary in case of large volume or dimensions components that are not processable in close die. However, close die forging gives the greater contribute in the production of forged titanium[9]. Figure 1.6 shows the schematic of the two processes. The employment of hot-die or isothermal forging techniques can also achieve more precise geometries. Indeed, an hotter die makes the filling process easier and prevents component to crack during the process [9]. The process temperature is able to affect considerably the final microstructure and its predisposition to be modified with further heat treatments.



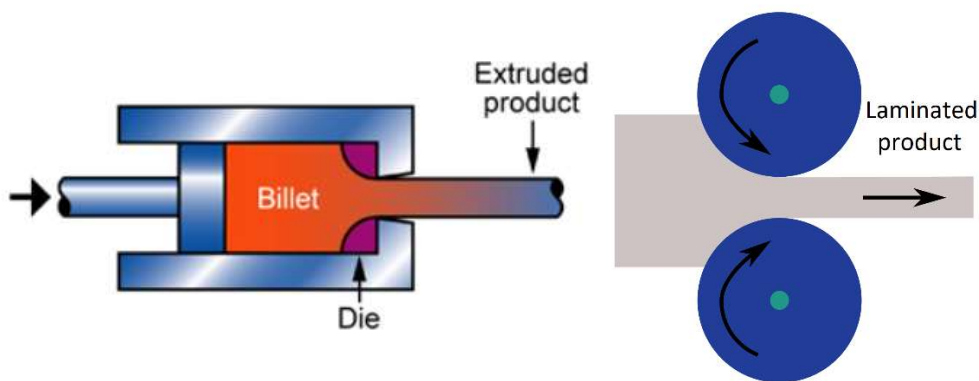
*Figure 1.6: Open die forging and close die forging in comparison*



### 1.2.4 Extrusion and rolling

Extrusion and rolling processes exploit plastic deformation of the material to obtain respectively fixed cross section objects and sheets of controlled thickness (Figure 1.7).

During extrusion process, a billet is pushed through a die of the designed shape. A rolled product instead is realized by a material stock that is passed between one or more couples of rollers and reduced in thickness. Both technologies provide highly deformed products in which material encounters only compressive and shear stresses, which may lead to grains deformation and anisotropic behaviour due to the stretched grains along the working direction. These process are classified according to the stock temperature: if the material is heated above its recrystallization temperature, the processes are cold hot extrusion and hot rolling, otherwise they are called cold extrusion and cold rolling. Higher temperatures reduce anisotropy of the product, allowing the nucleation of equiaxed grains; Major deformations are also achievable without the occurrence of residual stresses.



*Figure 1.7: Extrusion and rolling processes*

### 1.2.5 Welding

Titanium joints are realized by means of a wide range of welding techniques available. Besides, welding process has to be monitored in order to avoid that melt titanium comes into contact with oxygen and nitrogen from the air, causing undesired reactions. The main approach used in the common practice is Gas

tungsten-arc welding (GTA) and Gas metal-arc welding (GMA) where an inert gas shield protect all the metal parts exposed to temperature greater than 250-400°C [8]. In case of more high quality applications, electron beam, plasma, laser or friction welding are employed, where a vacuum chamber is needed [8]. Figure 1. shows the comparison between Gas Tungsten Arc (GTA) welding and more accurate Electron Beam welding (EB). In the GTA weld the heat affected zone (HAZ) Embrittlement problems may occur in case of welding titanium with other materials because of the formation of intermetallic phases[8].

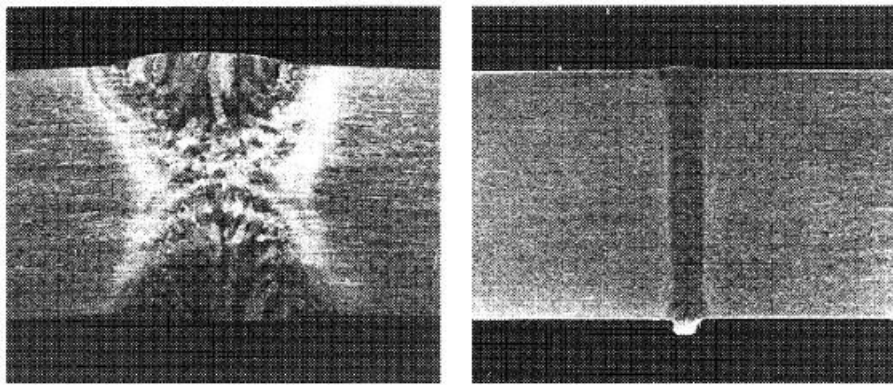


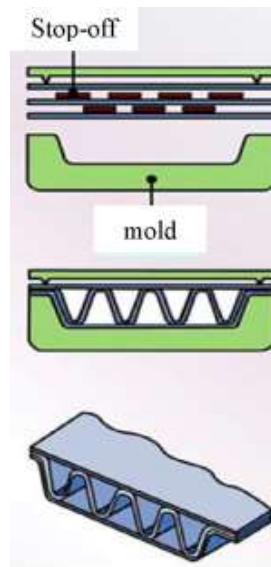
Figure 1.8: Comparison of Ti6Al4V GTA and EB welds [8]

### 1.2.6 Superplastic forming and diffusion bonding

Superplastic forming (SPF) is based on a fascinating property of titanium and its alloys. In a range of high temperatures and very slow strain rates, titanium shows a so-called *superplastic behaviour* which allows plastic deformation of 1500% without macroscopic necking. Very complex thin walled components can be manufactured by means of this process. Often superplastic forming is combined with solid-state diffusion bonding (DB) to produce hollow or honeycomb structures [8].

Superplastic forming consists in heating a die up to about 90% of its beta transus temperature, which is about half of the melting point. A titanium sheet is then placed between the two halves of the die and then with a proper pressure the sheet is forced versus the lower die by hot argon gas that is pumped into the die and it

deforms superplastically. As all other fabrication processes, also SPF should be carried out in vacuum or inert gas atmosphere due to titanium high reactivity with air. Thanks to the combination with diffusion bonding mechanism, which is schematized in Figure 1.9, high quality three dimensional sheet structures are also achievable. Since high strains at high temperature are caused by creep phenomenon, deformation performance is improved by a fine and stable microstructure at this temperatures [8].



*Figure 1.9: Principle of Superplastic forming combined with Diffusion Bonding to process a thin sandwich and three dimensional structure*

### **1.2.7 Powder metallurgy**

Powder metallurgy results particularly convenient when expensive materials are processed and an extensive scrap would not be reasonable. For this reason powder metallurgy of titanium is a widespread technique that allows to produce complex parts with only little machining post-processing, thus keeping costs down. Powder metallurgy of titanium includes powder production, compaction and sintering of the green part by hot isostatic pressing (HIP). The metal powder is manufacturable by means of arc or electron-beam melting methods.

Inert atmosphere is needed to conduct arc melting and pulverization is make possible by the rotation of a titanium self-consuming electrode or crucible which let

melt titanium drop. While material droplets are falling, they cool rapidly due to the inert atmosphere and retain their spherical shape. This is an economical method, but unfortunately it has found that leads to undesired tungsten impurities from the tungsten cathode, reason why it is no longer applied today. The solution was found in substituting the arc with a plasma for the melting process of titanium electrode. Electron-beam process requires to be conducted under vacuum so lower impurity levels are guaranteed. Then resulting powders have to be encapsulated, degassed, and evacuated in order to ensure that no gases remain on the particle surfaces. Eventual gases can lead to pore formation during HIP and compromise compaction. Typical HIP parameters for Ti-6Al-4V are temperatures included between 920°C and 970°C, at a pressure of 200 MPa for 1-3 hours.

Products of powder metallurgy have normally mechanical properties comparable to that of forged components, higher than cast ones.

At the beginning of the development of this technology, powder metallurgy should have been an economic production of near-net shape products. However, this method can be considered cheap as long as the powder production is cheap, which is not for titanium. Currently, the only reason why high process cost could be justified is the case in which new alloys are not otherwise manufacturable for example to produce particle reinforced titanium alloys. Moreover, recently the production of titanium powder has become fundamental to accomplish all additive manufacturing processes, based on powder bed fusion principle. The latter will be deepen in Chapter 2.

## **1.3 Classification of Titanium Alloys**

### **1.3.1 Crystal structure**

As many other metals, titanium can crystallize in different crystal structures which are stable only in certain ranges of temperature. This metallic phenomenon is called allotropic behaviour and the temperature that defines the allotropic transformation

is called transus temperature. Pure titanium and mostly of titanium alloys at room temperature have hexagonal close packed structure (hcp), called  $\alpha$  titanium. However, at  $882\pm 2^\circ\text{C}$  pure titanium transforms into a body-centered cubic structure (bcc), defined  $\beta$  titanium[8]. The atomic unit cells of  $\alpha$  and  $\beta$  titanium are represented in Figure 1.10.

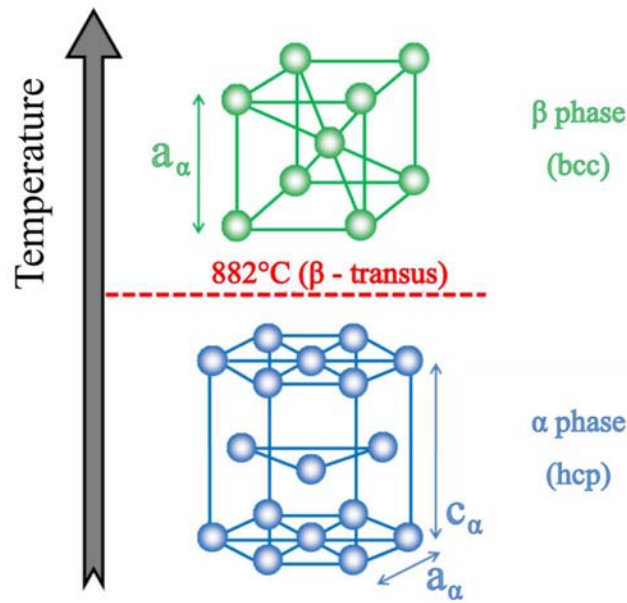


Figure 1.10: hcp  $\alpha$  and bcc  $\beta$  atomic crystal lattices in their stable temperatures field

The body-centered cubic (bcc) lattice allows an higher plastic deformation if compared to the hexagonal close packed (hcp) structure because of the major number of slip systems, that correspond to the number of dislocation glide opportunities, in bcc than in hcp lattice which are 12 in the first case and only 3 in second case. Indeed, the planes and directions with highly dense packed atoms energetically promote plastic deformation and the number of slip systems is obtained by multiplying the number of these slip planes and slip directions. Normally a higher density of atoms packing in a slip plane would lead to easier dislocation gliding. This would mean that hcp structure with a packing density of 91% would be favoured in plastic deformation compared to the bcc structure which is only 83% dense. Though, the length of the minimal slip path also affects the energy amount required for plastic deformation. Defining  $a$  as the lattice parameter,

this length is equal to  $b_{\text{MIN-hcp}} = 1 \cdot a$  for hcp whereas for bcc is valid  $b_{\text{MIN-bcc}} = 0.87 \cdot a$  that means the latter, in turn, is favoured. Furthermore, a valuable elastic anisotropy of hexagonal lattice is appreciable in  $\alpha$  titanium: elastic modulus of a single hexagonal crystal varies between 145 Gpa for a vertical applied load and 100 GPa if loaded perpendicularly to the previous [8].

### 1.3.2 Alloys classification

Alloying elements influence on  $\beta$  transus temperature is variable and creates a range of temperature in which, depending on the alloying element fraction, both crystal structures can coexist. Thus, phase transformation, in case of alloyed titanium, does not occur at a precise temperature but rather in a range of temperatures. Alloying elements classification is based on their effect on the  $\beta$  transus temperature and divides them into neutral elements,  $\alpha$ -stabilizers and  $\beta$ -stabilizers. There can also be primarily non-metallic elements that are classified as impurities when present on the order of 100 ppm [8]. As schematized in Figure 1.11, neutral elements have only a negligible effect on phase diagram,  $\alpha$ -stabilizer elements rise the allotropic transus temperature,  $\beta$ -stabilizers instead make  $\beta$  phase stable also at low temperatures.

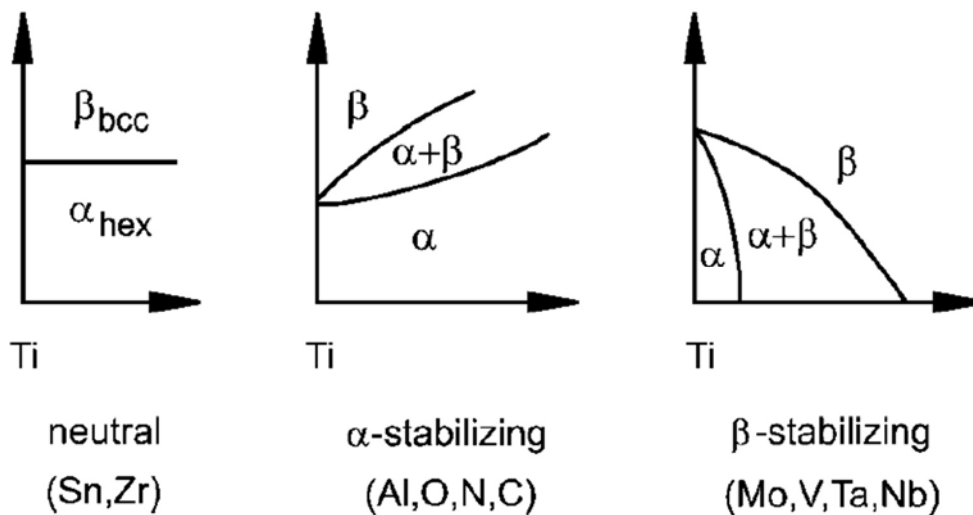


Figure 1.11: Effect of alloying elements on phase diagrams of Ti alloys[8]

Tin and zirconium are considered neutral concerning the  $\alpha/\beta$  boundary, but they have a valuable strengthening influence on  $\alpha$  phase. Interstitial elements as oxygen, nitrogen and carbon are considered  $\alpha$ -stabilizers and they also have a solid-state hardening effect. However, among  $\alpha$ -stabilizers aluminium is so far the most important alloying element of titanium. Molybdenum, vanadium and tantalum are  $\beta$ -stabilizers with high solubility in titanium [8].

Conventionally titanium alloys are subdivided as  $\alpha$ ,  $\alpha+\beta$  and  $\beta$  alloys depending on the stable phases guaranteed by alloying elements at room temperature. Further classification are made into near- $\alpha$  and metastable near- $\beta$  alloys. A three-dimensional diagram can outline the classification combining an  $\alpha$ -stabilizer phase diagram with a  $\beta$ -stabilizer one (Figure 1.12). By sectioning this diagram, a ternary-like diagram can be obtained. The following paragraphs will briefly describe the most common titanium alloys, which correspond to first level of classification. A schematic overview of some properties trend among alloys depending on their content is shown in Figure 1.13.

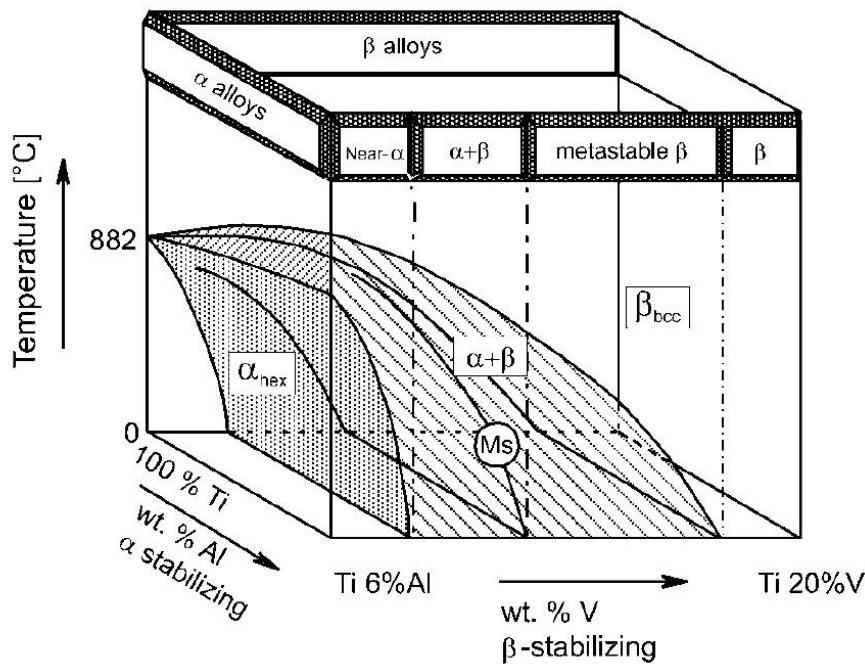


Figure 1.12: Three-dimensional phase diagram to classify Ti alloys[8]

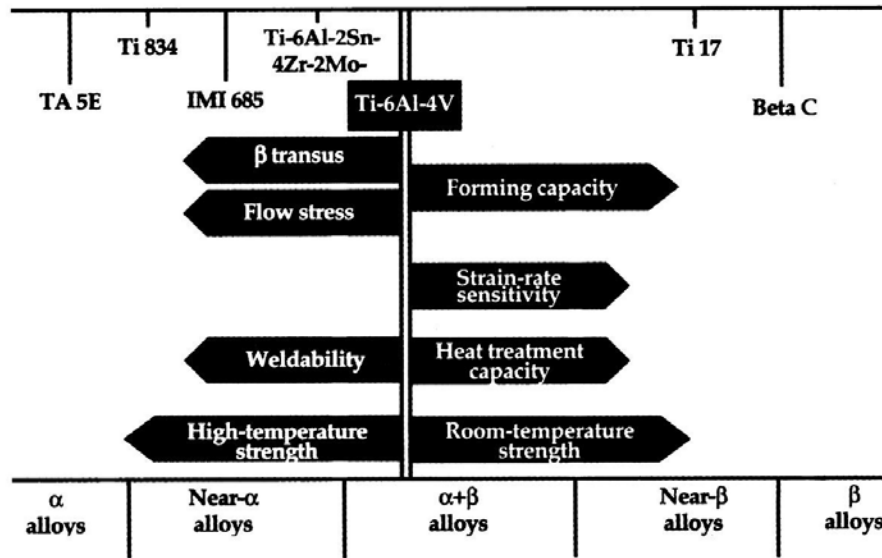


Figure 1.13: Overview on some properties trend among titanium alloys with regard to the most popular *Ti-6Al-4V* [9]

### 1.3.2.1 $\alpha$ alloys

These alloys are constituted only by  $\alpha$  structure at room temperature. High corrosion and oxidation resistance are the these alloys' the stronger point. Due to these performances,  $\alpha$  alloys are primarily employed in chemical and process engineering industry. Another distinctive property is the excellent ductility that is favoured with increasing interstitial elements content. A negative point of these alloys is the moderate mechanical strength which is neither improvable by heat treatment because of  $\beta$ -transus temperature is hardly reachable. Only stress relief treatment can be done on these alloys. Fatigue behaviour is the best if compared to the others categories, but cold working hardening is not practicable. High temperature Near- $\alpha$  alloys contain a maximum of 2% content of  $\beta$ -stabilizers with the aim of improve  $\alpha$ -alloys weak tensile performances.

### 1.3.2.2 $\beta$ alloys

These kind of alloys find use for structural applications thanks to their high toughness. They usually have molybdenum and vanadium in high contents and often are stabilized with aging treatments between 350°C and 550°C for long times,



in order to achieve optimal mechanical performances. Cold working possibility is evaluable. A near- $\beta$  alloy of primary concern is Ti-8Mn, employed in the aerospace industry because of its high-level performances.

### ***1.3.2.3 $\alpha+\beta$ alloys***

The highest performance in mechanical strength is achieved by  $\alpha+\beta$  alloys. These alloys present double phase structure at room temperature and a combination of properties are achievable through the interaction of the two crystal structure. Even greater mechanical properties are achievable by quenching from the  $\alpha+\beta$  field, followed by an aging treatment at high temperature in order to let  $\alpha$  coherent particles precipitate from the metastable  $\beta$ . Many heat treatments are available for this class of alloys and they will be further explained in detail in Chapter 3. Maximum  $\beta$  phase content at room temperature may not exceed 20% to be weldable [7]. The most popular alloy among  $\alpha+\beta$  ones is undoubtedly Ti-6Al-4V.

#### ***1.3.2.3.1 Ti-6Al-4V***

Ti-6Al-4V titanium alloy has been defined by many the workhorse of titanium alloys and it's the material considered for this work. Being one of the first developed titanium alloys, more than 50% of all alloys in use today are of this composition [8]. This double phase alloy is also known as Grade 5, according to the ASTM International standard on commercially pure titanium. Its success has to be attributed to the fact that it's a perfect comprise solution of all virtues of titanium alloys, but also it is so far the most intensively developed and tested titanium alloy [8]. Except for a lower thermal conductivity, this alloy has a significantly higher strength than commercially pure titanium (Grades 1-4) while having the same stiffness and thermal properties [11]. Moreover this grade is easily heat treatable, workable and weldable. Elevated are also its corrosion resistance and biocompatibility. In the prosthetic field, indeed, this alloy is undoubtedly the

material mostly used. Nevertheless, biomedical applications are only a small part of the all industries in which this alloy finds application (Figure 1.14).

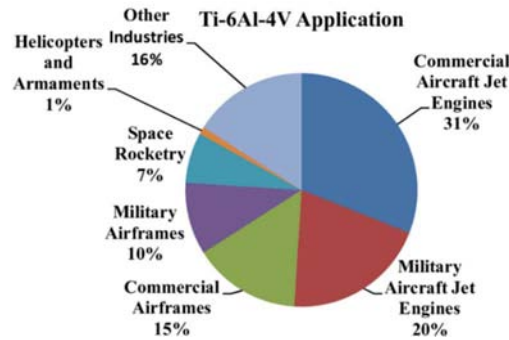


Figure 1.14: Ti-6Al-4V alloy applications [12]

## 1.4 Applications of titanium alloys

Thousands of titanium alloys have been developed and their properties are related to chemical composition, lattice structures, processes and heat treatment that they have undergone before service. Anyway, a general overview on the most common applications is possible because of the excellent properties offered by alloyed titanium alloyed that fit perfectly with some typical requirements of many field of application.

The type of titanium demand is different between countries: while aerospace covers half of the demand in the USA, in Europe and Russia, industrial applications are the dominant purpose of titanium exploitation in the Asian continent [13]. It is important to notice that almost 95% of titanium consumption is destined to the production of titanium dioxide, employed in pigments for paints, paper or plastics; 2% is involved in welding, 1 % in other employments, but only the 3% of the extracted titanium is exploit as a metal.

### 1.4.1 Aerospace

The aerospace market is the sector where metal titanium products are mostly employed, covering over 50% of the totality. Both in commercial and in military aerospace market, titanium has a fundamental role. Everything concerning

producing aircrafts or spacecrafts has to deal with the everlasting compromise between strength and lightness. For many of these components, wide ranges of temperature service are also required. These are the constraints that most of all titanium alloys can effectively fulfil, thanks their excellent strength to weight ratio and high temperature tolerance and stability.

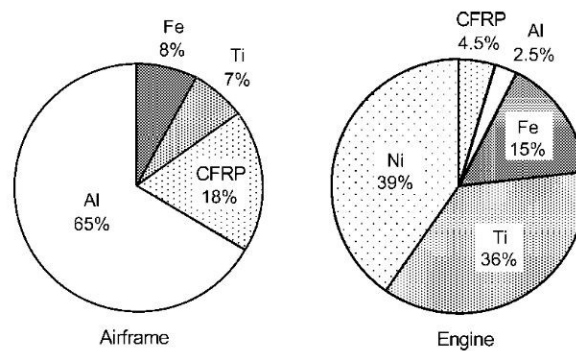


Figure 1.15: Percentage of aluminum, titanium, steel alloys and FRP of the structural weight in modern large commercial aircraft and gas turbine engines [12]

Figure 1.15 shows the percentage of structural weight for various material classes in modern large commercial aircraft, distinguished between airframe and engine materials. Nearly two thirds of aluminium is involved in the manufacture of the fuselage of the Airbus A330/340, for example. At about 7%, titanium alloys have a similar share of the structural weight as steels. However, at over a third the structural weight, titanium is the second most common material in the jet engine following Ni-based superalloys. By volume, titanium alloys are the most abundant material in the engine [12]. The main area of application for aerospace titanium alloys is in the gas turbine engine. The first jet engines was presented in the early 1950s: the content of titanium in that occasion was quite low but since then it has steadily increased. Besides, over the years alloy design has evolved from the employment of  $\alpha+\beta$  alloys to the more thermally efficient near- $\alpha$  alloys. At the beginning only compressor blades were made from titanium, subsequently compressor disks and then the large front fan blades in modern jet engines are now often made from titanium alloys too (Figure 1.16) [12].

Another reason of the notable expansion in use of titanium within the aerospace industry can also be attributed to the increasing demand of Carbon Fiber Reinforced Polymer (CFRP) for newer aircraft designs. By sharing the same thermal expansion rates as many popular composite materials and thanks to its compatibility with polymer matrix composites, titanium is highly favored as a composite interface material.

It is also worth mentioning military aircraft application which for nearly sixty years now largely exploit the high performance of titanium alloys. Figure 1.17 shows the first example of beta alloys using on military SR71 aircraft. Highly involved during Cold War by Americans, this extremely performing aircraft was able to reach the highest speed ever achieved by an aircraft with pilot, 3530 km/h [13].



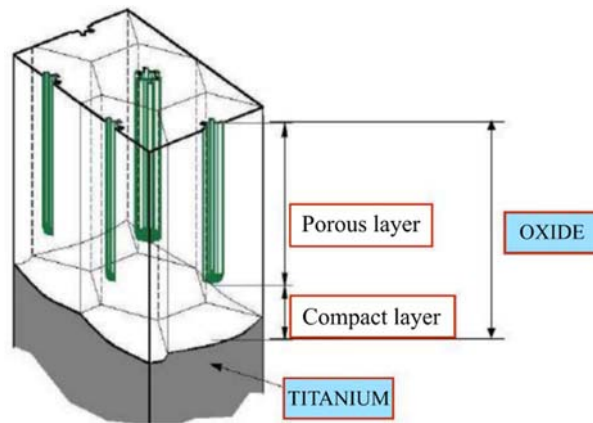
*Figure 1.16: The large front fan blades in modern jet engines are now often made from titanium alloys[13]*



*Figure 1.17: SR71 aircraft: first use of beta alloys in aerospace structures. (Courtesy of Lockheed California Co) [9]*

### 1.4.2 Biomedical

Although the percentage of the employment of this material in the medical industry is only a small amount in the totality of its applications, the role that titanium gains in this field is irreplaceable. Together with its high corrosion resistance and biocompatibility that make it survive and resist within human environment without contaminating it, titanium has another priceless property that has made it become a staple of the medical field: the outer porous oxide layer. Equally to stainless steel, the corrosion resistance is guaranteed by an oxide film, few tens Ångstrom thick, that forms instantly upon exposure to air and it is immediately replaced if damaged. This protective oxide layer confers passivity to the material, preventing it to be subjected to corrosion. This very thin film, as described in Figure 1.18, presents an inner compact layer and a deeper porous layer that grows outward. The porous morphology is very similar to human bone tissue and allows the material to be well joint to human bone. This osteointegration capability prevents the titanium implant to be recognized as a foreign body and let human tissues grow around.

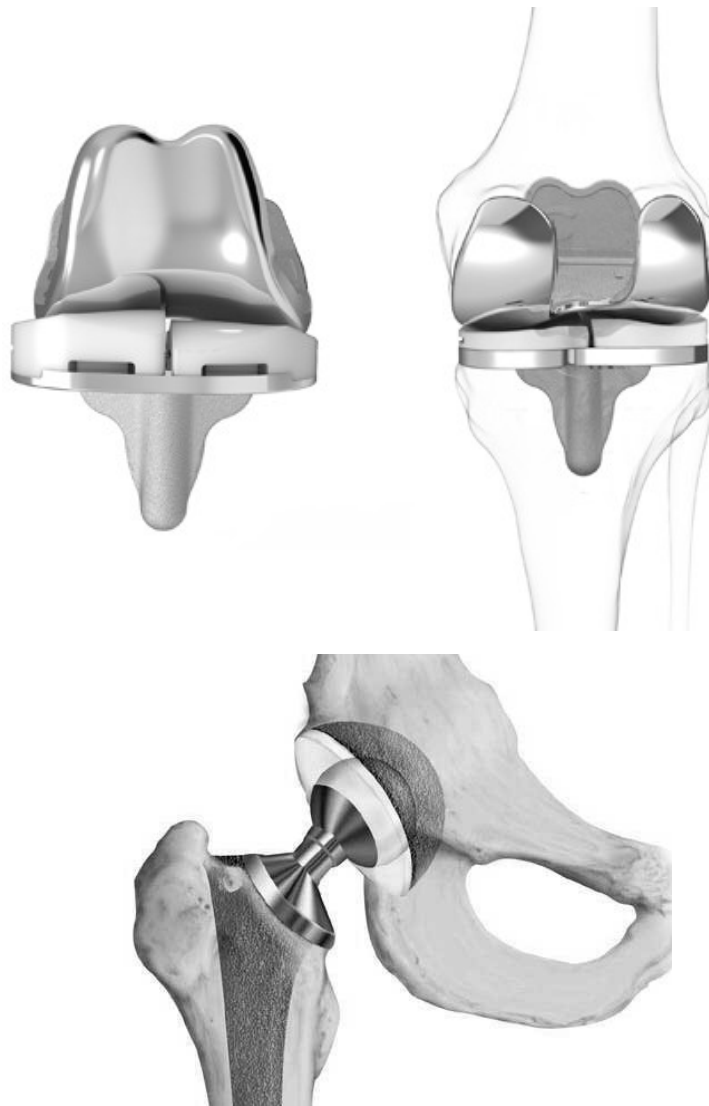


*Figure 1.18: Porous oxide layer is responsible for titanium osteointegration*

Titanium chemical stability is another important requirement for this application: no metallic ion can be ceded to external environment due to its hazardousness. For these reasons, titanium has truly become the fundamental material used in medicine. The most common titanium applications in the medical industry are hip and knee

joints prosthesis (Figure 1.19), bone screws and plates, dental implants, surgical devices, pacemaker cases, heart valves, pharmaceutical equipment, wheelchairs.

It is expected that uses for titanium within the biomedical industry will continue to grow in the coming years above all due to the development of additive manufacturing process which will fully exploit the synergic benefits given by the combination of this material and production processes. These technologies, that will be deeply described in Chapter 2, turned out to be undeniable in the production of titanium medical implants due to their flexibility to create efficiently high quality components characterized by an high customization and complex geometries.



*Figure 1.19: Titanium medical implants: knee and hip joints prosthesis*

### 1.4.3 Chemical, petrochemical and energetic

The use of titanium for chemical and energetic implants is justified not only by better performances compared to stainless steel, but also to cost efficiency. The higher corrosion resistance of titanium allows almost 3% annual saving on the initial investment because no painting is needed and lower maintenance frequency is required. Having longer service life compared to that of other materials means reducing in cost of material replacement, of production and maintenance labor and of downtime. Employing titanium in these types of implants results also in a considerable weight reduction. With consideration to heat exchangers on offshore oil platforms (Figure 1.20), where sea air has strong corrosive ability, the cost efficiency is translated into a service life equal to that of the platform which is over 30 years; This means that, compared to 5 years life of heat exchangers made of steel, even a 6 times higher investment cost for the titanium ones would be still cheaper, added to the fact that an offshore substitution intervention is 27 times more expensive than one on mainland. Reduction in weight is estimated to result in 1 ton for the emerged part which can pay off the higher cost per kilo. These advantages can be reported with the same virtuous effects on many other types of implants subjected to corrosive attack or located in aggressive environments.



*Figure 1.20: Offshore oil platform implants in the North Sea*

#### 1.4.4 Emerging markets

Several are the niche applications where titanium has been employed. Generally, due to its manufacturing and raw material costs, titanium is mostly used in highly performing scopes, namely where cost can be justified by ambitious objectives and where the combination of its properties are not otherwise findable. For the energy recovery, geothermal tubulars, drilling risers, downhole tooling and tapered stress joints are being produced using titanium alloys. Titanium distributors are quickly finding also more widespread uses for titanium tubing in recreational products, including sports equipment such as bicycles, golf clubs (Figure 1.21) and tennis racquets [13]. Moreover, due to its extraordinary lightness and less tendency to be less allergenic to skin, spectacle frames are being developed by some eyeglasses designers. After anodic treatment, titanium can be coloured which makes it also more attractive for these markets. In the early 1980s, titanium was firstly applied within engine parts of racing cars. Since then, the range of applications for titanium has expanded but only for limited models of high-performance cars and others niche markets because the automotive industry is very price sensitive and titanium in these terms is not competitive compared to steels and aluminium [13].



*Figure 1.21: Titanium finds application also in sports equipment*



# Chapter 2

## Additive Manufacturing of Titanium alloys

### 2.1 Titanium alloys manufacturing introduction

Despite the large variety of titanium and titanium alloys applications reported in the previous Chapter, the largest demand of the global titanium production comes from the aircraft manufacturing field: just think about a Boeing 787 whose empty weight is about 220 tons and 15% of that is made up of titanium alloys [14]. Furthermore, from 2012 to 2031, the estimated growth in number of aircrafts all over the world should be in the order of 20.000 [15]. Such a large volume of production leads, and had led in the last fifty years, to the well-known issue of minimization of the cost and forced the research to a huge effort in this direction. The cost of extraction of titanium is pretty much higher than that of comparable metals such as steel and aluminum (Table 2.1).

	Steel (€/kg)	Aluminum (€/kg)	Titanium (€/kg)
<b>Ore</b>	0.04	0.02	0.43
<b>Metal</b>	0.2	2.17	10.74
<b>Ingot</b>	0.3	2.27	17.9
<b>Sheet</b>	0.59 – 1.18	1.97 – 9.87	29.61 – 98.7

*Table 2.1: Comparison in extraction costs of raw materials [2]*

Not only the extraction but also the production process is strongly energy-intensive: the relatively low processing temperatures and surface cracks that need prior to further fabrication bring to a high energy consumption. For example, the energy required to produce 1 ton of sponge-titanium from its ore is 16 times than that needed to produce 1 ton of steel, 1.7 times than that of aluminum and just a bit

more than that of magnesium. Finally, it must be taken into account that a part of the raw material is wasted in standard machining processes resulting in final products which own a weight several times lower than the initial raw part. The ratio among the weight of the latter to that of the final product is usually referred to as “buy-to-fly” ratio and the titanium industry average of such a value is equal to 11 [3]. It means that to obtain a 10 kg component, more than 100 kg raw material is needed. Such a background therefore, makes one to understand the strong necessity of effective manufacturing processes for titanium and titanium alloys that can keep up the increasing demanding industry requests and fit the compromise of saving energy. Among these processes, additive manufacturing seems to cover to a large extent these requests and to leave definitely the only role of rapid prototyping tool. The buy-to-fly ratio attainable in such processes can be theoretically lower than 1.5 [3] and, with Computer Aided Design techniques, the optimization in terms of strength-to-weight ratio can be markedly improved even in very complex geometry components (topological optimization).

In this chapter, the additive manufacturing process will be generally introduced and, after a general overview about AM processes, the focus will be given to those processes that are nowadays mostly involved in 3D printing of metals such as Direct Energy Deposition (DED) and Powder Bed Fusion (PBF) methods.

## **2.2 Additive Manufacturing (AM) processes: a general overview**

The development of additive manufacturing processes begun on the late 80’s and the principal aim was to build models and prototypes in a very fast way. Rapid prototyping was, and still is, widely used in a variety of industries to describe a process for rapidly creating system or part representation before the final release or commercialization. However, after 40 years of improvements such an equivalence among AM and rapid prototyping seems not to fit properly anymore since

additively manufactured components are nowadays functional or structural parts of working machines, tools, equipment or sometimes even applied when prompt spare parts need to be quickly replaced. The generic AM process always starts from a virtual CAD description of the physical part to be printed. Usually 3D modeling software are used at this stage and the result is a solid or surface model which is converted in STL format. This describes the model's surfaces by mean of a simple code, ready for slicing operations where the part is divided by several layers and the path that the tool shall follow is determined.

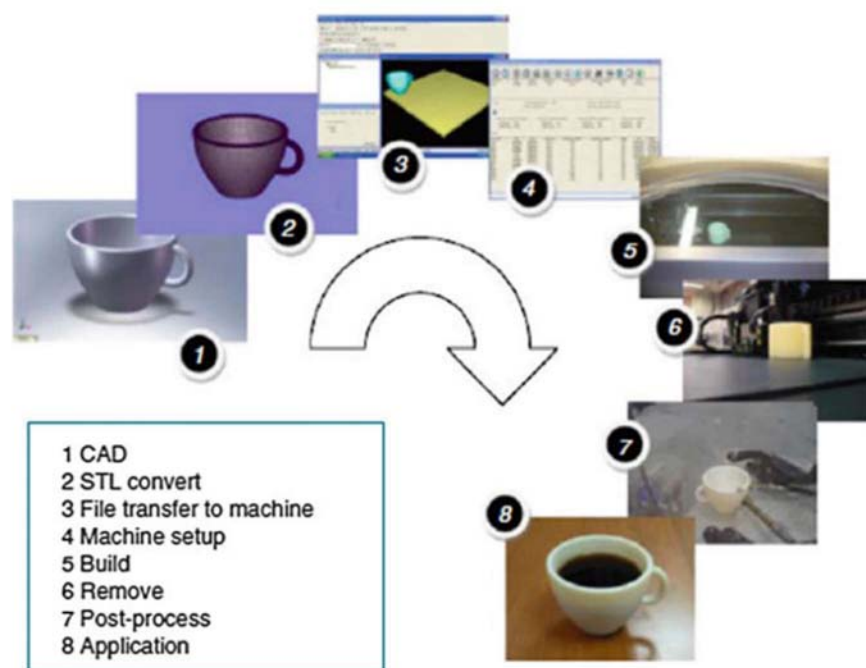


Figure 2.1: Steps of a general AM process [16]

The machine must be previously set up in order to tune the energy source, layer thickness, timings and material constraints whereas the model must be oriented and positioned in the most convenient way depending on the printing technique. Building the part is an automated process and hence the machine can carry on without any supervision except that part focused on checking errors both from the machine (like material run-out or glitches) and software (bugs). Finally, the component is completed and must be removed together with eventual supporting features. In some cases, when an acceptable surface texture or finish is required, a

further machining process is needed. In Figure 2.1 the aforementioned AM process is summarized. In conclusion, the core of such process relies on the possibility of build up a component by addition of layers which are the stacking cross-sections of the latter: from here the attribute “additive”, which represents the opposite to the typical material removal methods belonging to CNC machine processes.

### **2.3 AM advantages and comparison with CNC processes**

The main advantages of AM technology can be summarized within two aspects: the speed at which the final product is obtained and the opportunity to realize complex geometry in one single comprehensive stage. The speed of the process not only consider the building part, but also the direct link among the CAD design and final working machine; such interface is seamless and does not imply criticalities on data conversion or interpretation. Criticalities that instead can often occur in CNC where the set-up part of the machine requires experience and an in-depth knowledge of the machine in order to adjust the correct parameters. Moreover, regardless of the geometry complexity of parts to be built, all the procedure is nearly every time fulfilled in one single step or requires at most a limited additional number of post-processes. Other manufacturing procedures typical of CNC applications instead require several and iterative steps and even when only a small feature must be changed, the result may be a dramatic increase in the number of operations.

Despite the development of AM was originally about polymeric materials, waxes and paper laminates, nowadays it is possible to additively produce composite, metals and ceramics. CNC machines on the other hand can shape softer materials but usually this occurs in a pre-processing stage in order to get them ready for further process like casting. CNC machines are more accurate on working with hard and relatively brittle materials having as a result mostly homogeneous isotropic material. AM parts instead may present voids or defects and different degree of

anisotropy depending on the orientation of the component and process parameters. As a consequence, AM products own a less predictable quality. The higher is the complexity of the geometry, the higher would be the advantage that AM has over CNC. For example, the spindle of CNC machine cannot have free access to all the points of a solid surfaces if it contains undercuts or constraints and the solution is always to previously split the part and re-assemble the components together after the machining. AM nozzle instead can sweep all the volume with the only constraints of contemporary build all the supports requested, making the likelihood to encounter a part that is not printable much lower. The resolution of both CNC and AM machines is not straightforward to be compared since can depend on the geometry and the properties of the build material. CNC tools are governed by motors and gearboxes that decide the position but since removal nature of the process, the product can have very thin and fine walls and surfaces. The same can occur for AM, that can have different resolution in different axis, sometimes governed by motors but sometimes by different techniques (like galvanometric mirror drives in laser-based technologies). And the thickness of the layer as well can both depend on the material and on the diameter of the nozzle or the laser. Finally, the programming task at the interface 3D model - machine is much more complex in CNC. The setting of parameters requires a greater effort both to obtain a good quality of the piece and to avoid several damage of the machine, which difficultly can occur on AM machine.

## **2.4 AM processes classification**

It is important to note that AM processes sometimes fall outside of process standards due to their large variety and pretty new exponential increase in large scale applications and huge effort is being invested on it. To classify AM processes there are several proposals, but two of them are most common. The first one is

from [17] and it is reported in [16] with some modifications as in Figure 2.2. The raw dimension refers to as the method of layers build-up: in the earliest applications the use of a single point source was common and probably it is the currently most known due to the diffusion of commercial cheap 3D printer machines available out of the industrial field. Two nozzles technology can mix the properties of two materials or offer different colors whereas array of source points, both 1D and 2D, decrease dramatically the time of model building and the number of moving parts.

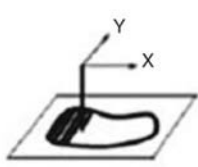
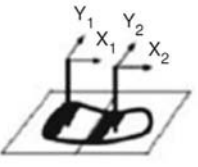

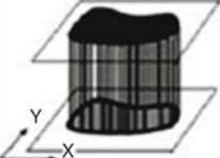
	1D Channel	2x1D Channels	Array of 1D Channels	2D Channel
Liquid Polymer	 SLA (3D Sys)	 Dual beam SLA (3D Sys)	 Objet	 Envisiontech MicroTEC
Discrete Particles	SLS (3D Sys), LST (EOS), LENS Phenix, SDM	LST (EOS)	3D Printing	DPS
Molten Mat.	FDM, Solidscape		ThermoJet	
Solid Sheets	Solido PLT (KIRA)			

Figure 2.2: AM process classification by [17]. Acronyms as follow: SLA = Stereolithography, SLS = Selective Laser Sintering, EOS = Electro Optical System, LENS = Laser-Engineered Net Shaping, SDM = Shape Deposition Manufacturing, FDM = Fused Deposition Modeling, PLT = Paper Lamination Technology. Other acronyms refer to company or technology brands [16]

In the column dimension instead, four groupings of materials are reported i.e. liquid polymers, discrete particles, molten materials and solid sheets. Liquid polymers are specifically photopolymers and the single or double point source used is typically made by a laser. It has indeed a curing effect on the polymer chains, like in SLA processes, whereas droplets of liquid polymers are more common in array sources. Discrete particles i.e. powders are usually uniformly sized and distributed. As a

general rule, finer powder corresponds to a better quality of the final product but more difficult results the control over their sizes and distribution. In this case a laser would be a better option for single and double point source: the effect is to focus enough energy into a small area in order to melt the material and make it glued with the adjacent layers. SLS and EOS fall within the most common technology for these materials. For array sources, an example of application uses droplets of a binder in order to stick the particles together and build the layers. Even if the single point source is the slowest, a wide variety of such machines is available due to the low cost both of the material and the machine. Two sources improve the quality of built-up part including a second supporting material that contemporary sustain the structure without flawing the surface. Finally, the solid sheets include very limited applications: a blade driven by a 2D plotter cut out the part profile from stacked sheets and uses an adhesive activated by laser printing technology to bond them together. The empty tiles of the table represent further future developments as well as a hypothetical extension of the raw up to a third dimension array (3D holography) where the material is fabricated in one pass.

The second classification has been proposed by [18] in accordance with the baseline technology in use, like lasers, printer technology, extrusion, etc. Despite this standard was withdrawn on 2015, the terminology is still in use and it helps to have a more practical view on the various technology groupings. A subsection is dedicated to each grouping, with a greater emphasis on processes that involve metals, in particular Powder Bed Fusion and Direct Energy Deposition technologies because of the direct interest of such thesis.

#### **2.4.1 Vat photopolymerization**

Photopolymerization processes use liquid resins which have the capability of being cured when undergoing the effect of different radiations. Such resins are called photopolymers. Most of them react to UV radiation but also gamma rays, X-rays,

electron beams, UV and visible light can be adopted. Vat polymerization is a more general term that includes stereolithography technologies, which is instead used when pointing at macroscale laser scan photopolymerizations. SL was the first developed technology and only later extended to the more general VP.

Benefits	Drawbacks
<ul style="list-style-type: none"> <li>• Accuracy and surface finish: surface finish ranging from submicron Ra for upfacing surfaces to over 100<math>\mu</math>m in slanted angles.</li> <li>• Flexibility of machines among different light sources and pattern generators.</li> <li>• Isotropic mechanics and less shrinkage than thermoplastics</li> </ul>	<ul style="list-style-type: none"> <li>• Only photopolymers can be used as printing materials (acrylates and epoxies in commercial applications).</li> <li>• Material bad quality in terms of loss of mechanical properties over time.</li> <li>• Parts emerge wet and must be post-cured</li> <li>• Expensive materials</li> </ul>

Table 2.2: Benefits and drawbacks of VP processes

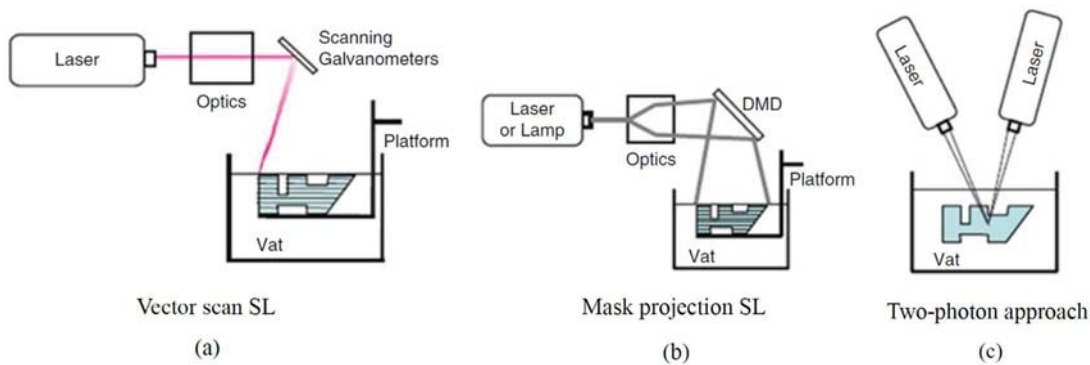


Figure 2.3: The configurations of typical VP techniques

Three configurations of VP are the most used (Figure 2.3):

- Vector scan: typical of SL machines, where a laser scanning operation cures the photopolymer;
- Mask projection: a large radiation beam is patterned by another device in order to obtain an entire layer section;



- Two-photon: the photopolymerization occurs at the intersection of two scanning laser beams. The part is fabricated below the resin surface.

In Table 2.2 the main benefits and drawbacks of VP are summarized.

### 2.4.2 Material extrusion

Extrusion-based technologies are the currently most popular on the market where cheap FDM machines are available for a large range of customers, from companies to private persons. Heat is furnished in a portable chamber where the material is melted and after pushed through by a tractor-feed system that creates the pressure drop to extrude it. The most common printable materials are thermoplastics since they can melt once and the melt again to get stuck with new layers: ABS, PLA, PET, PA, TPE and HIPS are the most popular among the private and industrial applications. In Table 2.3 the main benefits and drawbacks of FDM processes are summarized. Applications of FDM products can be prototypes and concept models, manufacturing tools and finished goods as aircraft interior parts and ducts.

Benefits	Drawbacks
• Low cost	• Limited materials (only thermoplastics)
• Simplicity	• High accuracy is not always possible due to
• Good bondage among layers	the fixed shape of circular nozzle
• Good mechanical properties and durable over time	• Layer-by-layer finish
• Fully functional parts can be built in standard plastics	• Require supports
• Allow rapid prototyping	• The final product can be porous and anisotropic due to layer orientation

*Table 2.3: Benefits and drawbacks of FDM processes*

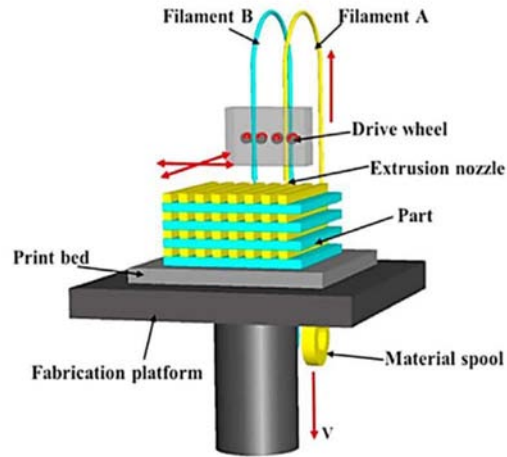


Figure 2.4: Schematic FDM machine [19]

### 2.4.3 Material jetting

Industries and researchers have introduced so far printing machines that use waxy polymers and acrylic photopolymers exclusively, corresponding to two methods: the first includes the heating of wax and its deposition whereas the second is based on the deposition of a liquid-state acrylate photopolymer, wherein droplets of liquid monomer are formed and undergo ultraviolet light to polymerize. Promising future applications involve polymers, ceramics and metals.

Benefits	Drawbacks
<ul style="list-style-type: none"> <li>• Low cost of printing machines when compared to other AM machines</li> <li>• High speed of build-up and scalability</li> <li>• Different colors at one step</li> <li>• Accuracy and surface finish</li> <li>• Fully-cured final parts</li> <li>• Homogeneous mechanical properties</li> </ul>	<ul style="list-style-type: none"> <li>• Limited materials (only photopolymers and waxes)</li> <li>• Fragile final products</li> <li>• Supports required</li> </ul>

Table 4: Benefits and drawbacks of material jetting technology

The material jetting has a good potential in terms of becoming a successful AM technology but some shortcoming prevented it from further growth: it relies on the phase change of the printed material and the conversion from droplets to a solid geometry represents a hard challenge that involves the deposition of a liquid-state

particle impacting on a pre-existent substrate either of the same or different material. Support structures are built in different materials, which is easy to remove by hand and water jetting.

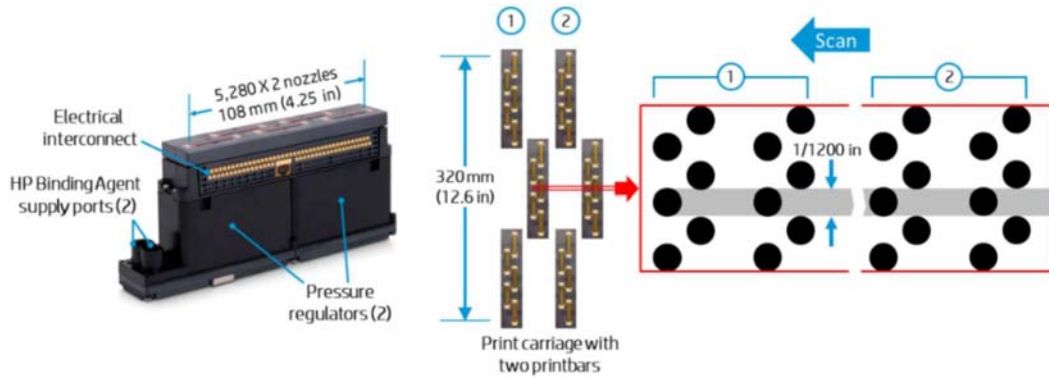


Figure 2.5: Nozzles' arrangement on HP Metal Jet printer [20]

Recent applications from HP [20] can print metals drops and more precisely place up to 630 million nanogram-sized drops per second of a liquid binding agent onto a powder bed to define the part's cross-section layer by layer. In Figure 2.5 the schematic organization of nozzles on a printhead of HP Metal Jet printer. Typical applications are rapid prototyping, also multi-material and multi-colors, jewelry products and anatomical models.

#### 2.4.4 Binder jetting

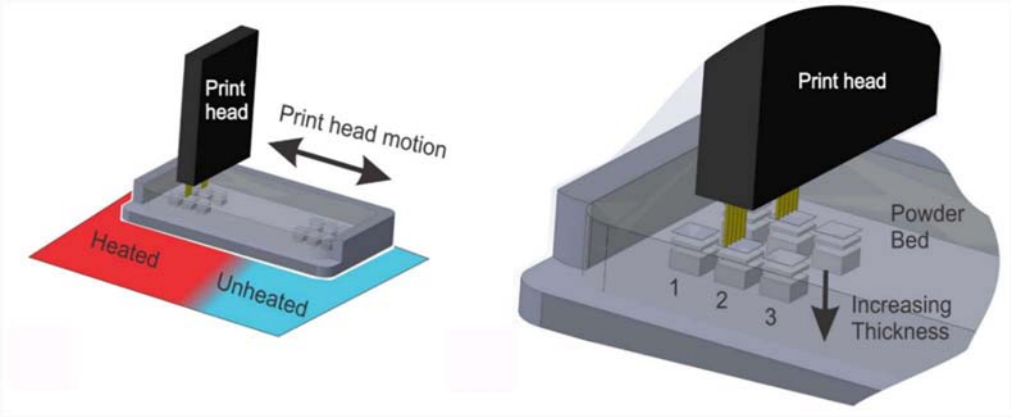
Conversely to the material jetting, in this system a binder is injected against a powder bed to form spherical agglomerates of both binder and powder and to provide bonding among the previous layers. Once the layer is built, the bed is lowered and a new layer of powder is spread onto it by a recoating mechanism. A schematic representation is given in Figure 2.6. The printer head contains multiple nozzles as well as in material jetting technology, but the material is left into the powder bed once printed in order to let the binder fully act. The unbounded powder is then removed by pressurized air. Several parts can be also built at the same time and even joints and assemblies are attainable by simply removing the loose part of powder. There is a strong similarity among this process and the powder bed fusion

processes explained in section 2.4.6. At the beginning of the development of such a technology in the 90's, the material used was starch-based and the binder a water-based glues. Current systems use plaster-based powder and still water-based binders but also polymer powders are available. Like the material jetting machine, having several nozzles allow the fabrication of multi-color parts like sculpture, attractive prototypes and investment casting component.

Benefits	Drawbacks
<ul style="list-style-type: none"> <li>• Only a small fraction of the total part goes through the printhead</li> <li>• Solid content is higher compared to final product from material jetting</li> <li>• Multi-color parts are feasible and the machine can be scalable</li> </ul>	<ul style="list-style-type: none"> <li>• Need of an additive step for recoating</li> <li>• Poor accuracy and surface finishes compared to final product from material jetting</li> <li>• An infiltrant is needed to improve the mechanical properties of the part</li> </ul>

*Table 2.5: Benefits and drawbacks of binder jetting technology*

Since the final products own low mechanical properties, it is common to add the so-called infiltrant with a strengthening effect. Some machine can even use metal or sand powders for metal parts or sand-casting molds. In the case of stainless steel for example, the infiltrant used is bronze, which provides a fully dense final product, and polymers as binders, so that they can be removed by mean of furnace cycles at the end of the printing.



*Figure 2.6: Binder jetting machine, schematic running operation [21]*

The future challenge in this field may be the achievement of a fully dense material comparable to the wrought one. Ceramics can be used as well. The main benefits and drawbacks of binder jetting technology are summarized in Table 2.5.

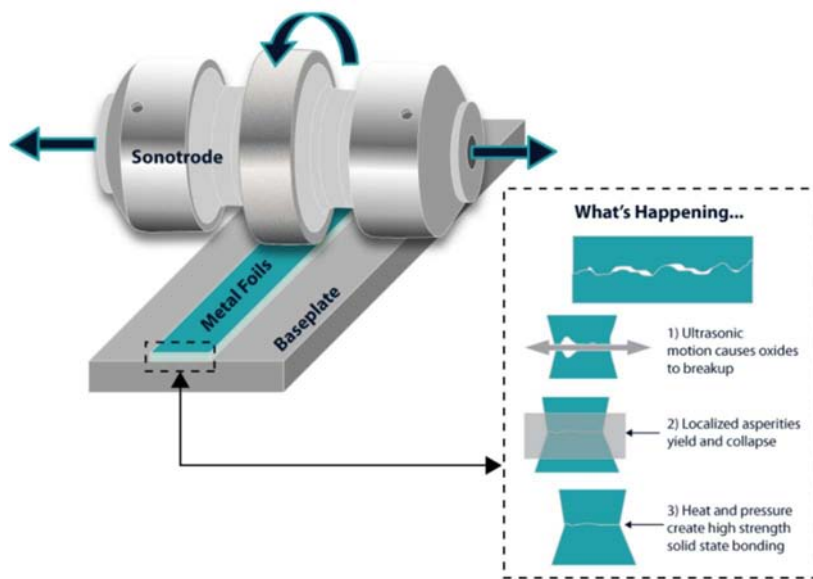
#### **2.4.5 Sheet lamination**

Sheet lamination was born for paper sheets applications but based on the same concept was further extended to different sheet materials and cutting strategies. The principle of cutting involve only the outer contours to be removed and the sheets can be either cut and then stacked (form-then-bond) or vice-versa (bond-then-form). Looking at the bonding mechanism among the layers, sheet lamination systems can be categorized in four groupings: adhesive bonding, thermal bonding, clamping and ultrasonic AM. The latter technology is a hybrid technique combining ultrasonic metal seam welding and CNC milling and it is also applied to titanium alloys. In ultrasonic AM, the object is built up on a heated plate up to 200°C from bottom to top and each layer is composed of multiple metal foils close side by side and trimmed by CNC milling. A visual description is given in Figure 2.7. A rotating sonotrode (a tool that applies vibration on the material) holds the sheets in contact with the base plate and oscillates at high frequency with a pre-set amplitude. Foil after foil, a layer is built up and typically four layers form a level in the UAM terminology. Every time a level is attained, the CNC milling machine provide to material removal shaping the contour of the current level. In such a way the accuracy of depends only on the resolution of the milling instead of the sheet thickness. UAM gives the opportunity to manufacture complex geometries even from multiple material stacking. Different internal patterns and features can be obtained such as honeycomb structures and enclosed cavities. Theoretically each material that can be ultrasonic welded can be used, from titanium and aluminum to copper, from nickel to brass, and moreover fiber embedment is allowed, including

optical fiber and every type of sensing device for smart structure applications. In Table 2.6 benefits and drawback of sheet lamination processes are reported.

Benefits	Drawbacks
<ul style="list-style-type: none"> <li>• Low shrinkage and residual stresses</li> <li>• Low cost in term of material, machine and process (paper-based processes)</li> <li>• Flexibility on the materials usable</li> <li>• No material state change</li> <li>• Smart structure and closed internal channels are feasible</li> </ul>	<ul style="list-style-type: none"> <li>• Paper-based products are sensitive to moisture absorption</li> <li>• Anisotropy among the directions parallel and perpendicular to the stacking direction</li> <li>• Large waste of material</li> <li>• Need of a post-process</li> </ul>

*Table 2.6: Benefits and drawbacks of sheet lamination processes*



*Figure 2.7: Ultrasonic Additive Manufacturing*

#### 2.4.6 Powder bed fusion

Powder bed fusion (PBF) processes are widely used worldwide and represent the fastest growing area in AM field. PBF is suitable for a large range of materials such as polymers, metals, ceramics and composites and the mechanical properties of the final products are comparable to those of many engineering materials at the stage of end-use. The first commercialized PBF process was the Selective Laser Sintering

(SLS), but successive branches of the same technology kept the same basis elements: one or more heat sources for powder fusion, a method for focusing the thermal energy to a well-controlled region and finally a mechanism of re-coating, that is, adding or smoothing powder the new layer. A schematic representation can be observed in Figure 2.8. The name Laser Sintering refers to as the most common heat power source, a laser light, that makes the powder to attain a temperature high enough to allow the formation of a cohesive solid mass. It is underlined that “sintering” points to a particular high temperature phenomenon which happens at lower temperature than the melting point of the material, but still allow the solid mass formation.

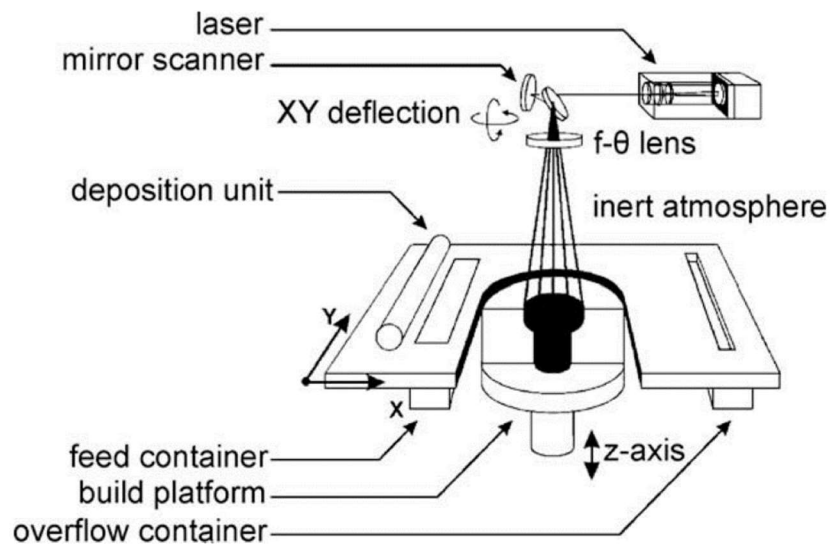


Figure 8: Selective Laser Sintering machine [22]

The polymer and metals LS are pretty much different but shares the same fundamentals concepts. A thin layer of powder is first spread over the area of interest by a leveling roller and it is then fused in 0.075-0.1 mm thickness. The operation occurs in inert atmosphere to minimize oxidation or degradation of the material. Some IR heaters are used to maintain an elevated temperature both around the region that is going to be sintered below the melting point of the powder and the feeding containers to pre-heat the powder for the next layer. Such pre-heating helps to minimize the amount of energy spent from the laser and avoid

warping of the building up region due to differential thermal expansion coefficient. Different types of laser can be used including CO<sub>2</sub>, Nd:YAG, fibre lasers, disc lasers, etc. [23] and the choice of each can be fundamental for two reasons: the absorptivity of the materials depends on the wavelength of the laser and the metallurgical mechanism for powder densification is governed by its energy density. The beam size is important too: it determines the time of the laser laying in one point and consequentially the scan speed (typically between 0.5 to 25 ms). Unheated powder remains as a support for further layers and the bed platform is lowered of a layer height in order to start again the cycle. Among the polymers used, PA is the most common thermoplastic involved and the quality of the final product depends on its degree of crystallinity. As a general rule indeed, crystalline materials have a well-defined melting point and are better processed. The microstructure obtained is usually porous but unique among other process. A wide range of metals is suitable too: steels and stainless steels, titanium and its alloys, aluminum and cobalt-chrome alloys have been processed in commercial applications. Finally, ceramics such as aluminum oxides and titanium oxides are available together with different composites forms. Under the short time of laser scan, the entire thermal cycle must occur and the sintering or melting mechanisms take action in four different appearances:

- Solid-State sintering: it means that the particles are fused together as soon as they reach a half of the melting point and not the melting point itself. Smaller particles own a smaller surface area and consequently a smaller surface energy that allows the diffusion mechanism to act and make the particles stuck together, like two ice cubes in a glass of water. The rate of sintering increases with the temperature and sometimes isostatic pressure is applied within the sealed chamber to enhance it. It is anyway the slowest mechanism among PBF processes.



- Chemically induced sintering: primarily utilized for ceramic materials. The sintering occurs by mean of thermally activated reactions among two or more types of powder or between the powder and atmospheric gases. The reaction products bind together the particles. High porous final parts often need costly and long-time post-processes.
- Liquid-Phase sintering (LPS): the most versatile mechanism in PBF technologies. A binder is added in different way among the powder and is melted in order to glue the particles. There is no need to directly sinter or melt the material particles. The binder can be made of separate particles, can be mixed within each particle (composite particle) or as a coating of a particle. In some cases, larger polymer particles can be melted only at the surface and glued by other smaller totally-melted particles (partial melting). The same results when using metal powders from alloying with low-melting-point components.

<b>Benefits</b>	<b>Drawbacks</b>
<ul style="list-style-type: none"> <li>• Flexible in terms of number of suitable materials</li> <li>• Powder surrounding the part is a sufficient support in polymer applications</li> <li>• Complex geometries are available including internal channels</li> </ul>	<ul style="list-style-type: none"> <li>• Supports are required for metals, also in order to avoid residual stresses</li> <li>• Post-processing could be long and expensive</li> <li>• Finish and accuracy depend on powder size; solid particles give lower finish than liquid-based ones</li> <li>• Pre-heating and cooling time can represent an increasing in the process speed</li> </ul>

*Table 2.7: Advantages and drawbacks of PBF processes*

Full melting: the most commonly used process with metal alloys and semi-crystalline polymers. In this case, the entire region under the heat source effect is

melted also including a portion of the previously solidified structure and creating a well-bonded and high-density structure. PA is the most used polymers whereas various metals are suitable such as Titanium alloys, Stainless Steel, CoCr, etc. The microstructure presents unique feature and the mechanical properties can result more desirable than casted or wrought part.

The required laser power increases with the melting point of the powder and also depends on the absorptivity characteristics of the powder bed, which is in turn influenced by the material type, the powder shape, size and packing density. Even though within the term PBF falls a wide range of different technologies, the general advantages and benefits of PBF processes are reported in Table 2.7. The heat sources may be also different from laser-based lights and for example very effective machines based on high-energy electron beam are considered successful technology in the metals field. Electron Beam Melting (EBM) is one of them and its greatest difference between the other LS processes, is the energy transfer mechanism: while in LS the powder absorbs photons to gain energy, in EBM it absorbs the kinetic energy coming from electrons and gains a negative charge (see Figure 2.9). If the particles around the negative-charged region have got a negative charge too, and the strength of the repulsive magnetic field is high enough, there might be the risk of particles push-out with the formation of powder clouds.

For the same reason moreover, such particles have an effect of diffusion on the beam coming from the electron source. This therefore requires both the material to be conductive enough and the beam to be a bit more diffuse to avoid a very high-density region of negative charges. The technical consequences are a larger resolution of EBM than it should theoretically be and that suitable materials for EBM must be conductive. Nevertheless, the greatest benefit of EBM is the effectiveness of the energy conversion inside the heat source unit. When a laser is generated, only 10 - 20% of the initial electrical energy is utilized whereas the other

part is lost in heat dissipation. Electrons generation instead occurs with almost no wasting part and furthermore the power converter units are cheaper than laser ones. Another fundamental difference is that not only the temperature of EBM heat source is higher than LS, but also the powder bed is maintained at higher temperature. The building part would become hotter and hotter during the printing, thus giving a bad gradient along the height. In order to avoid such gradient, the substrate of powder is scanned before the recoating by a defocused electron beam. This allows a steady-state and uniform temperature throughout the build without the need for alternative heaters (IR heaters in LS) and, more fundamental, gives different microstructures from LS. In LS printed parts for example, it is common to find distinguishable scan lines whereas in EBM these are difficultly visible. The powder bed in LS is held at lower temperature and the gradient among the building region and the surrounding part is higher. Thus, a rapid cooling occurs generating small-sized grains that do not overcome the layering effects.

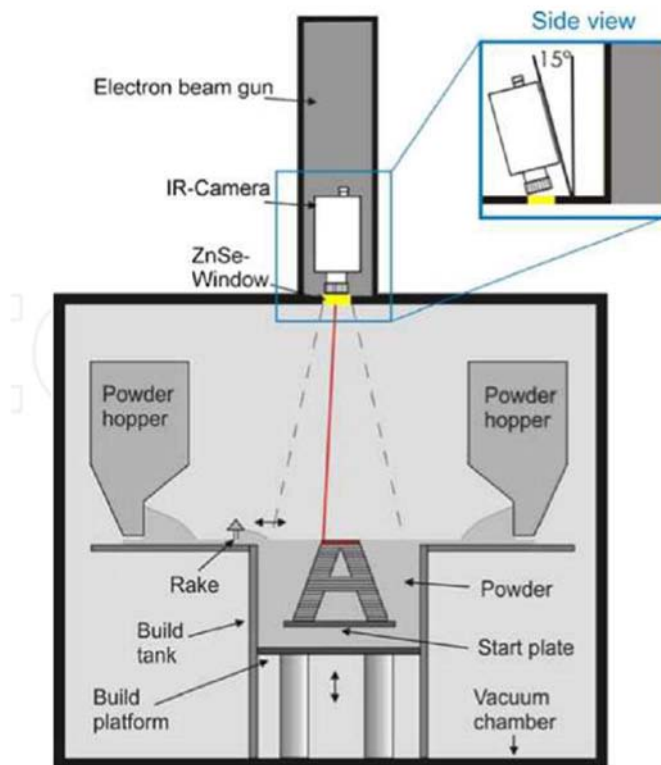


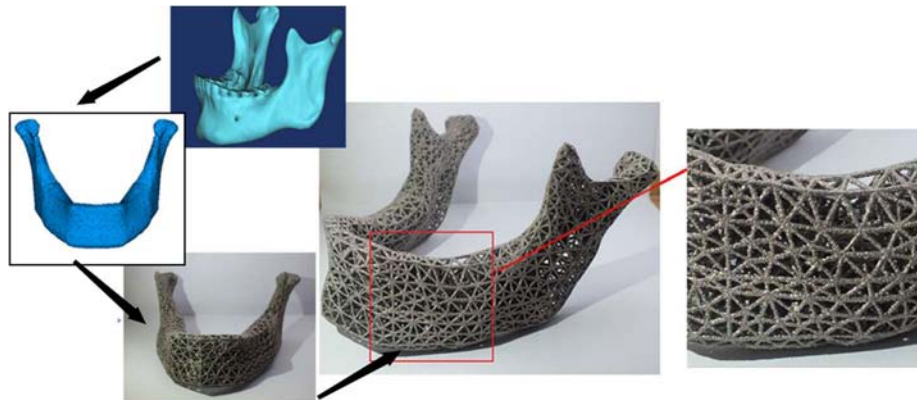
Figure 2.9: Schematic graph to show the working principle of an EBM [24] equipment

EBM microstructure emerges as less porous and comparable to that of cast parts. Such differences of course depend on the material and it is not uncommon to observe grains that grow across the layers both for EBM and LS, especially for titanium alloys and high-melting-temperature metals. High temperature powder bed, in addition, leads to much lower residual stresses. The last fundamental advantage of EBM is the possibility to melt multiple regions at the same time, thus dramatically improving the speed of building with the respect to LS process. The applications of EBM, as explained above, are suitable only for metals but the quality of the final product and the freedom on the design, make this process desirable in an increasing number of cases. Typical applications go from rapid prototyping to functional parts, from high-precision medical products and fitting implants both in orthopedics and dentistry (Figure 2.10) to structural parts in aerospace and automotive, functional engine components, bodyworks and basis component that even require long life cycles and high safety and undergo high level of mechanical and thermal loading.

#### **2.4.7 Direct Energy Deposition (DED)**

Even if DED processes can be applied to polymers and ceramics, they most involve metal powders and sometimes they are even referred to as “metal deposition” technologies. As in PBF, a heating source is focused on a region of a powder substrate which is melted, but the crucial difference is that the melting occurs as soon as the material is being deposited. The heat source can be either a laser or an electron beam, but the building-up of the part is apparently more similar to extrusion-based processes, where the moving head leaves a track of material and position the new layers close to the old ones. The resulting part however attains a high density and microstructure more similar to PBF processes. Several different names are given to different DED machines depending on parameters such as laser type, powder delivery method, inert gases and so on: the most famous are Laser

Engineered Net Shaping (LENS), Direct Metal Deposition (DMD) and Laser-Based Metal Deposition (LBMD).



*Figure 2.10: The process chain of a rapid prototype model for  $Ti6Al4V$  mandibular prosthesis [24]*

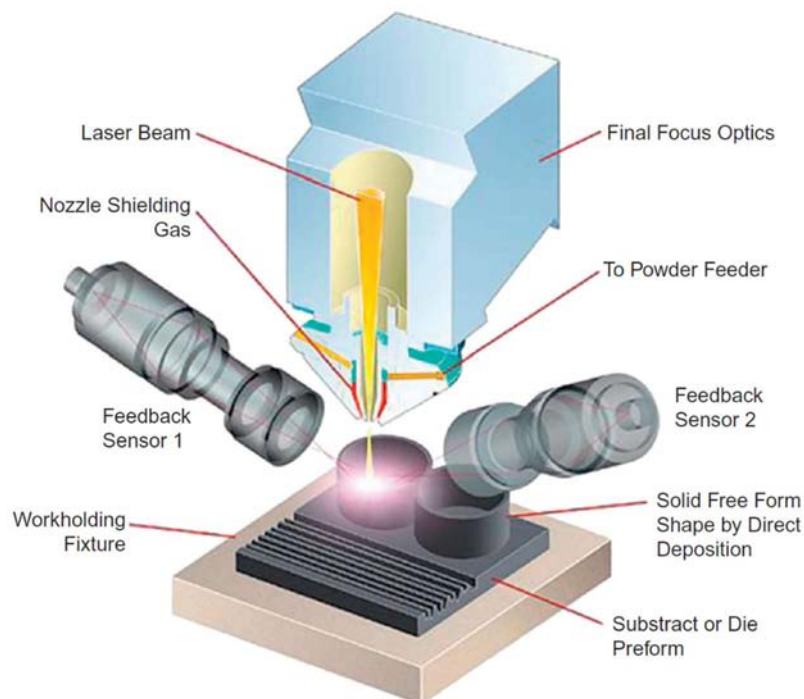
DED machines can also be used with the same approach for laser welding and cladding applications. In Figure 2.11 a scheme of a LENS machine and its fundamental parts are shown.

In laser-based deposition processes the head is responsible on placing both the heat source and the powder onto the substrate. The deposition is controlled by the relative motion among the head and the substrate motions, meaning that both of them can give a contribute on one or more axis movement. The axis number can be up to 4 or 5 and even robotic arms are available with interchangeable heads owning standard CNC tools. Since the feeding nozzle distribute the powder at high kinetic energy, multiaxial distribution also on pre-existent material is one of the greatest advantages of such technology.

The laser generates a small pool of molten materials in contact with the pre-existent part and usually the powder melts as soon as enter in the pool. Some uncommon systems are also available in which the molten state is attained before the powder touch the pool. Finally, after the head moves away, the powder solidifies thanks to the growth of a large thermal gradient. This makes the material to undergo a rapid cooling and, depending on the head speed, can result on unique grain shapes in the

microstructure. The track overlaps a part of the previous pass originating a second partial melting on it and typical layer thicknesses are within 0.25 – 0.5 mm range. DED machines usually work in sealed chamber under inert conditions (typically using Argon with a very low ppm content of oxygen) to avoid oxidation. About the methods of distributing the material, there are two main ways:

- Powder feeding: the powder is typically first fluidized in a container by bubbling up a gas through it or applying ultrasonic vibrations and after is transferred out with a pressure drop. The powder size ranges are 20-150  $\mu\text{m}$ . Single or multi-nozzles systems are available, with different arrangements but being the coaxial or toroidal the most effective. Usually, excess of powder is utilized since a small fraction is always lost at this stage.
- Wire feeding: more effective for simple geometries like blocks without thin transitions or coating of surfaces. The volume of material lost is even smaller, but a certain amount of porosity must be always taken into account as in extrusion-based AM processes.



*Figure 2.11: Schematic DED machine. All the DED machines can be reconducted at the same scheme of working*

Like PBF machines, DED can use a large variety of lasers (CO<sub>2</sub>, Nd:YAG, fiber lasers and disc lasers) but also a electron beams were developed with the advantages of saving electrical energy and work within a vacuum but non-inert atmosphere. These are typically fed by wire feeding but mostly adopted in aerospace applications. About the materials processed, theoretically all the weldable metals are employable but those with high reflectivity and thermal conductivity such as gold, aluminum and copper result of difficult application. Powders from pure elements can be delivered by separate feeders in precise fractions against a localized region with the opportunity of in-situ alloying and building customized compounds. Ceramics are often used in a composite form with a metal matrix.

About the microstructure, DED parts show a macroscopic layered structure with an extremely fine solidification substructure. The region at the layer interface does not exhibit porosity and the heat-affected zone results very thin. Some materials display pronounced columnar grain structure aligned in the laser scan direction, while others show equiaxed structures. The overall deposit materials do not usually show porosity except from excess on powder moisture absorption or entrapped-gases during the building up. Layer-to-layer bonding is excellent and at most, lack-of-fusion defects can form at layer interfaces where the energy density in the melt pool is not enough. Residual stresses are generated as a result of rapid cooling and the formation of brittle intermetallic phases formed at the interface of dissimilar materials can also lead to cracking. Rapid cooling rate can have some advantages on the microstructure with the formation of very fine secondary phase particles (see section 2.5.2). The overall microstructure is very close to that of welded structures in the layer-like component but can be assimilated to that of high-cooling rate cast metals. In Table 2.8 benefits and drawbacks of DED processes are reported.

Benefits	Drawbacks
<ul style="list-style-type: none"> <li>• Fully dense parts</li> <li>• High control on the microstructure: production materials with gradual variation on the composition, composites in-situ</li> <li>• High control on the cooling rate</li> <li>• It can be used for repairing in-service damaged high-precision components</li> <li>• Perfect for features addition and coating since there is no need for a substrate</li> <li>• Hollow components are feasible</li> </ul>	<ul style="list-style-type: none"> <li>• Poor resolution and finish</li> <li>• Slower build speed; higher accuracies needs longer time</li> <li>• Finish and accuracy depend on powder size; solid particles give lower finish than liquid-based ones</li> <li>• Pre-heating and cooling time can represent an increasing in the process speed</li> <li>• Lower complex geometries than PBF processes</li> <li>• Post-machining and stress relief heat treatment required</li> <li>• Requires supports</li> </ul>

*Table 2.8: Advantages and drawbacks of DED processes*

## 2.5 AM processes for titanium and titanium alloys

Titanium and its alloys have been produced by various AM methods: the most common include PBF processes (SLS, SLM and EBM) and DED processes (specifically, LENS and DMD). Other AM systems applied to titanium alloys are Direct Manufacturing (DM), Shaped Metal Deposition (SMD), Wire Arc Additive Manufacturing (WAAM) and ultrasonic AM that use titanium foils as feed stock. The research studies have focused on various aspects such as the microstructures, mechanical and corrosion properties and more important, on the biomedical aspects and compatibility. Titanium bones and dental crowns have been fabricated by SLM by 3D modelling geometries [25], titanium implants have been produced by LENS and tested on the in-vivo bone ingrowth response in rabbits [26], showing mechanical strength and elastic moduli suitable to biomedical applications. In



particular, AM studies of Ti-6Al-4V have received greater attention than wrought titanium and other alloys due to its broader range of applications. For example, cellular structure manufactured by EBM showed mechanical properties similar to those of human bone [27] and dental frameworks made by SLM were found to fit the proper strength and corrosion resistance [28]. Finally, the aircraft applications field is currently in strong expansion and high-precision components made by SLM in already end-use forms are very desirable for the high strength-to-weight ratio [15]. Since the majority of AM system are powder-based and the interest of the current work involves EBM and LENS more emphasis will be given to PBF and DED technologies applied to Ti-6Al-4V.

### **2.5.1 Powder preparation for Ti-6Al-4V**

The powders can be either made from elemental metals (Ti, Al and V) that undergoes alloying during the building or provided in a pre-alloyed form. A classification can be given according to the shape of the particles [2]. As a general rule, spherical particles are more desirable than angular-shaped particles due to their more favorable attitude to flow. Angular-shaped particles are less expensive and are obtained as electrolysis products of titanium reaction. They can be both elemental or pre-alloyed and sometimes used as a pre-stage in the process for spherical particle fabrication. The effectiveness of PBF process strongly depends on the control of the powder manufacturing and handling. In particular the following parameters have a fundamental influence:

- Size and size distribution: just recall the notions about energy transfer mechanism among particles in PBF in processes. Particle size affects the surface energy exchanged and therefore the density of the built part; it also affects the part finish and the minimum buildable feature. In PBF, sizes range in 20 – 40  $\mu\text{m}$  whereas in DED in 45 – 150  $\mu\text{m}$ .

- Powder morphology: as explained below, spherical particles are desired since they optimize the compaction of the final part, especially in PBF technology. Various morphologies are acicular, flake, granular, irregular, needle, nodular, platelet, plates, and spherical.
- Chemical composition: it determines the fraction of alloying of the final part. EBM, since it works under vacuum, can lead to the loss of aluminium and therefore an extra amount of it is usually desirable.
- Flow: it is more critical in DED since it leads to the final consistency of the layers. In PBF, it coincides with the recoating quality.
- Powder density: hollow particles lead to a porous final part.
- Contamination, handling and moisture: contamination is obviously to be minimized and the handling method is fundamental in that. Moisture absorption can generate voids in the building stage.
- Recycling: a part of the powder is always lost and, even though it can undergo a severe thermal effect and degrade, the attempts of recycling are economically fundamental for the sustainability of PBF and DED.

Another big issue about the Ti-6Al-4V powder is the price (Figure 2.12), that can approach values even one order of magnitude higher than that of raw materials ( $\text{TiO}_2$ ), intermediate materials ( $\text{TiCl}_4$ ) and different types of powders produced by different methods (Kroll, Hunter, HDH).

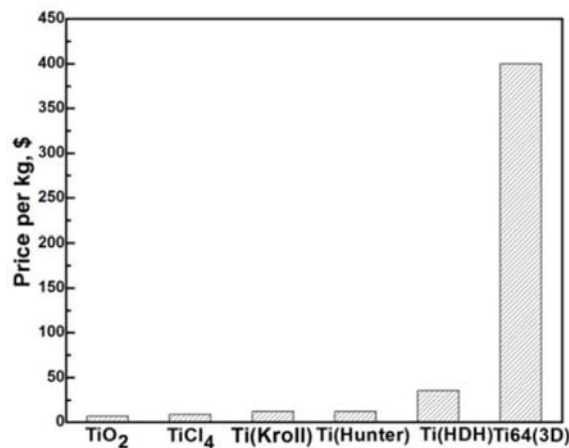
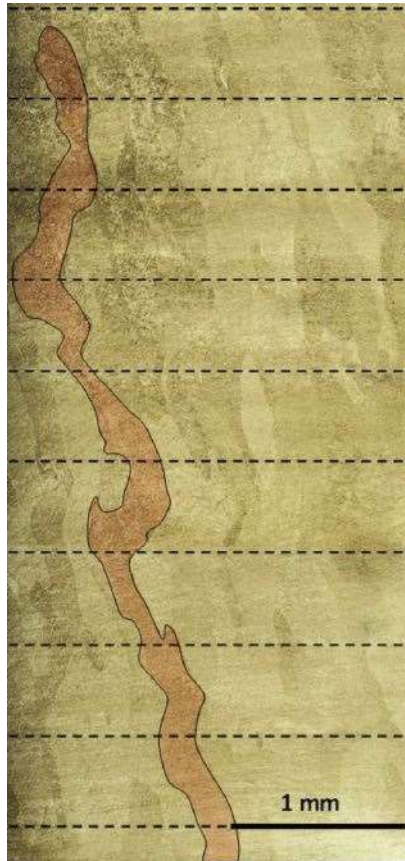


Figure 2.12: Cost comparison for Ti-6Al-4V AM powder

### 2.5.2 Microstructure of Ti-6Al-4V processed with EBM and LENS

In EBM and LENS approaches the densification process during the build-up occurs by solidification from a liquid phase, thus deviating from a regular sintering that would occur mostly through solid-state sintering. As explained in section 2.4, this means that the melting point is not achieved and sintering temperature are normally selected within the  $\beta$  phase region around 1300°C; the liquidus temperature for Ti-6Al-4V instead stands approximately around 1660°C. In DED and EBM processes instead, the microstructure is mainly a game played by phases role and hence led by the temperature of the process, the gradient of temperature along the part and the cooling rate (typically  $10^4 - 10^6$  K/s).



*Figure 2.13: Columnar prior- $\beta$  grains in Ti-6Al-4V AM processes [29]*

In both of the processes, the epitaxial growth of grains perpendicular to the substrate direction i.e. along the z-axis is observed, giving prior- $\beta$  grains with a columnar nature and slightly tilted in the direction of the beam motion. It is common to find some of them even growing across multiple layers. This effect is

visible in Figure 2.13 and it becomes stronger when the gradient of temperature around the beam is sharper, meaning therefore that it is more noticeable in laser-based processes where indeed  $\beta$  phase is predominant. This strong gradient allows a rapid cooling of the phases and hence the possibility of a martensitic  $\alpha'$ -phase formation. The cooling rates required must be at least  $525^\circ\text{C}/\text{s}$  as reported in [2]. Microstructure from electron beam instead, shows  $\alpha + \beta$  phases grains for the opposite reason, that is the constant high temperature held at the substrate ( $600^\circ\text{C}$ ) and the slower cooling rate underwent.

### 2.5.3 Mechanical properties of EBM and LENS processed parts

It is clear that mostly laser-based technology leads to the formation of a higher strength final product with a low ductility due to the presence of a martensitic phase. EBM instead, with a slower cooling rate in vacuum atmosphere, gives materials that exhibit lower tensile strength but higher ductility. In Figure 2.14 this effect is visually summarized also over other AM processes. The microstructure is coarser in cast material whereas wrought material shows equiaxed  $\alpha + \beta$  grains. Moreover, the mechanical properties of the material as-built (before eventual post-processing) are strongly different from that of heat-treated or hot-pressed material. The residual stresses indeed can present values higher than the ultimate strength of the titanium alloys itself and could lead to a premature fracture especially in dynamic and fatigue loading. For such reason, in many applications a collection of different heat treatment is available, such as annealing for laser-based DED and hot isostatic pressing (HIP) for EBM, whose effects are basically two: a change in the material phase balance from a co-existence of  $\beta$ -phase and martensitic  $\alpha'$ , to a co-existence of  $\beta$  grain boundaries and intergranular precipitated coarse  $\alpha$ -phase and the relaxation of residual stresses. The columnar grains are broken down and move toward the equiaxed state. The mechanical properties are therefore markedly

affected and in general a decrease on the ultimate tensile strength and an increase in ductility are observed.

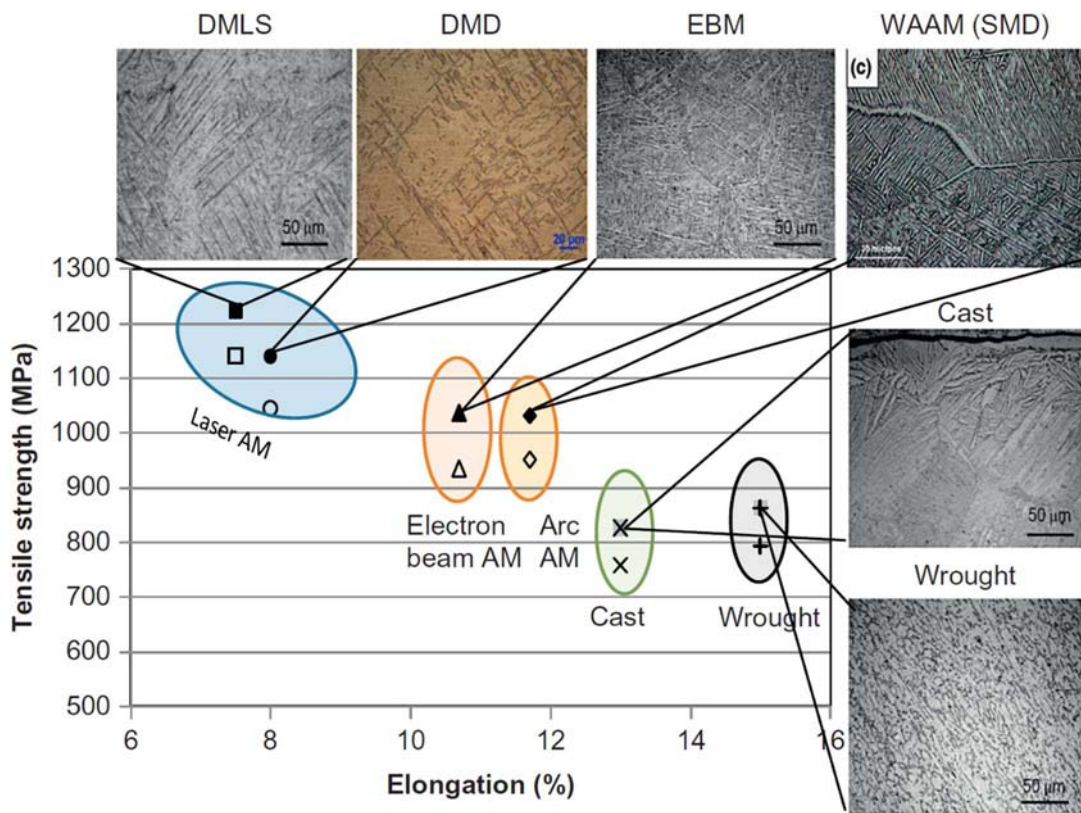


Figure 2.14: Tensile behavior of AM Ti-6Al-4V alloys produced using various AM technologies and their comparison with cast and wrought material properties. Closed and open symbols represent UTS and yield strength respectively [2]; LENS and DMD both fall within the DED process grouping and own slight differences

#### 2.5.4 EBM and LENS processes comparison

The EBM inherits the advantages and drawbacks of the Powder Bed Fusion processes whereas LENS is one of the DED processes mentioned in the previous sections 2.4.6 and 2.4.7. PBF are suitable for more complex geometries with hollows and internal unsupported channels and gives a finer surface finish respect to DED. DED is mostly adopted in simple geometry especially in terms of repairing, coating or substituting features in already existing parts. Both of them need some form of

machining to reach the end-use stage. Typical technical parameters for EBM and LENS machines set-up for Ti-6Al-4V building are reported in Table 2.9.

	<b>EBM</b>	<b>LENS</b>
<b>Power Supply</b>	7 kW max	3.5 kW max.
<b>Beam size</b>	200 – 1000 $\mu\text{m}$	500 – 4100 $\mu\text{m}$
<b>Atmosphere</b>	Vacuum, $10^{-1}$ - $10^{-3}$ Pa (at most partial pressure of He)	Argon flow
<b>Scanning speed</b>	125 – 802 mm/s (up to 8000 mm/s)	2 – 40 mm/s
<b>Feed type</b>	40 – 100 $\mu\text{m}$ (standard)	10 – 200 $\mu\text{m}$
<b>Layer thickness</b>	20 – 100 $\mu\text{m}$	40 – 100 $\mu\text{m}$
<b>Build temperature</b>	640°C - 700°C	Naturally heated
<b>Build density</b>	99.4% - 100%	>99.9%
<b>Substrate</b>	Stainless steel, heated at 720°C - 800°C	Ti-6Al-4V or Ti, room temperature or heated at 200°C

*Table 2.9: EBM and LENS machines parameters for Ti-6Al-4V [24]*

LENS presents larger beam diameters and layer thicknesses but as consequence shows higher deposition rates. DED processes in general can repair and add features to cast or wrought components. The structure obtained is fully dense and the heat affected zone on the modified component is minimized. A calibrated vision system integrated with the machine allows automatic identification of part location in the machine coordinate system and resulting on precision processing. Titanium components that can be repaired include turbine blades, housings, bearings, casing flanges, seals, and landing gears. EBM gives a good surface finish in the order of

$R_a = 25 - 35 \mu\text{m}$  and reduces the residual stresses in comparison with laser-based DED. EBM does not need support and is better indicated when components with small porosity size or controlled porosity content are required (e.g. in prosthesis replacing human bones). Multi-material built-up are an option owns by DED processes that can attain even different grades of alloying within the same component.



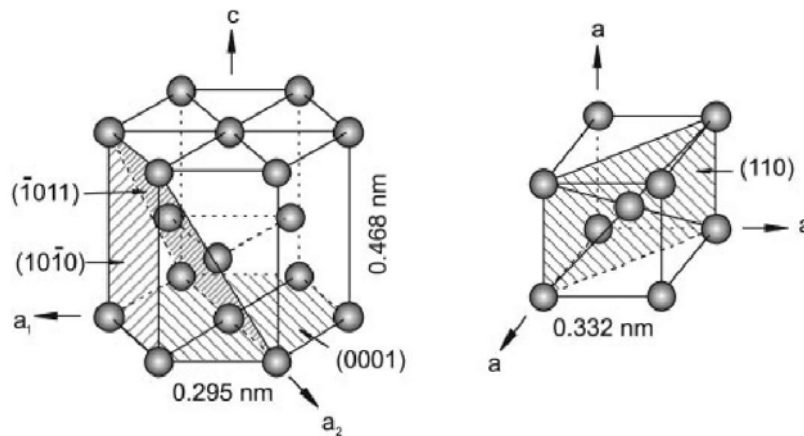


# Chapter 3

## Heat treatments

### 3.1 Metallurgy of titanium

The wide range of properties offered by titanium alloys is based on their allotropic behaviour. Phases  $\alpha$  and  $\beta$ , as introduced in Chapter 1 and shown in Figure 3.1, are respectively characterized by hexagonal close packed (hcp) and body centered cubic (bcc) structures. The existence of two stable phases plays a central role in plastic deformation and diffusion mechanisms.



*Figure 3.1: Atomic crystal structure of hexagonal close packed (hcp)  $\alpha$  phase and body-centered cubic (bcc)  $\beta$  phase with their most densely packed planes and directions highlighted [8]*

Alloying elements can be in solution within the titanium lattice until their content reaches a solubility limit related to both atomic lattice dimensions. At the equilibrium, this solubility limit implies that, if exceeded, particles precipitate and contribute to form a new phase. Hence, allotropic transition temperatures and the consequent phase stability fields are controlled by this phenomenon.

Figure 3.2 is a schematic representation of the pseudo-binary Ti6Al-V phase diagram. This diagram can be thought as if it was extracted from the three-dimensional one reported in Chapter 1, by choosing an aluminium content of 6%

and considering the diagram by varying of vanadium content. If fixed the 4% value, the resulting  $\beta$ -transus temperature for Ti-6Al-4V alloy is about 980°C and martensite start temperature is 200° below, namely at 780°C.

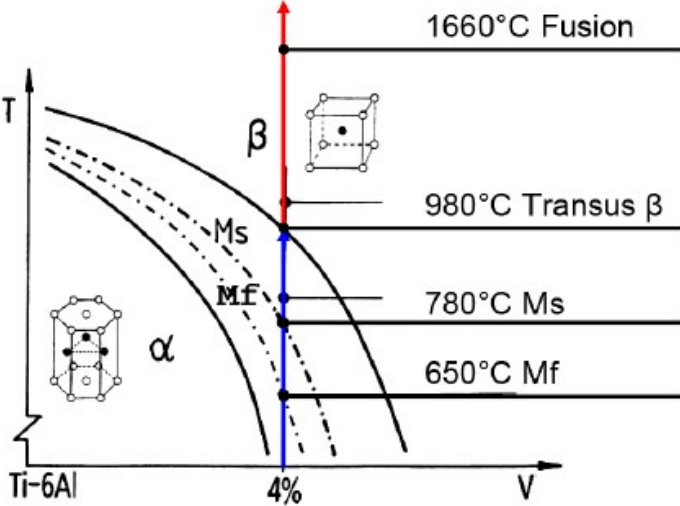


Figure 3.2: Pseudo-binary phase diagram representation of Ti-6Al-4V alloy [30]

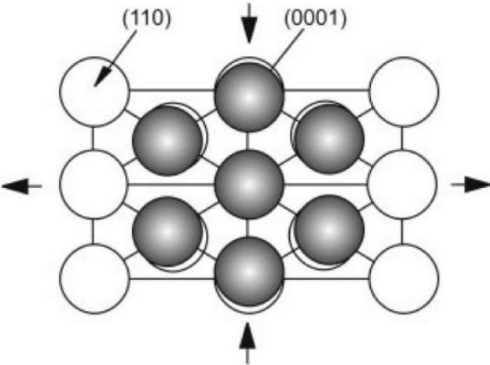


Figure 3.3:  $\beta/\alpha$  transformation according to Burgers relationship [8]

Cooling process from the  $\beta$  field to the  $\alpha$  one is followed by a slight volumetric increase (Figure 3.3) due to the transformation of the most densely packed planes of the bcc  $\beta$  phase  $\{110\}$  into the basal planes  $\{0001\}$  of the hcp  $\alpha$  phase which are more spaced out. The transformation of  $\beta$  titanium slip planes into  $\alpha$  titanium basal planes allows 12 orientation possibilities of  $\alpha$  grains growth, which derive from the combination of six slip planes and two slip directions of  $\beta$  phase. Indeed, microstructure reflects this variety in possible orientations:  $\alpha$  lamellar grains

nucleate and grow within the prior  $\beta$  grains according to the previously mentioned 12 orientation relationships. Thus, microstructure results in multiple repetitions of lamellar  $\alpha$  differently oriented which in some cases reminds to the weave pattern of a basket or to more regular Widmanstätten structures (Figure 3.4a-b).

### 3.1.1 Diffusive transformations

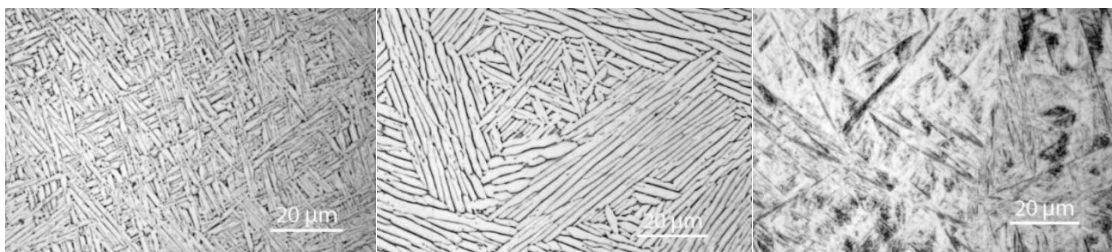
Diffusion mechanism is considerably promoted in bcc  $\beta$  structure due to its lower packing density with a diffusion coefficient that is orders of magnitude higher than  $\alpha$  phase. This relevant difference in diffusion coefficients strongly affect mechanical properties of the two phases at high temperatures as creep behaviour, hot workability and superplasticity [8].

Below the  $\beta$  transus temperature diffusion process depends on time and temperature but generally it is slower and a lamellar microstructure is obtained. Hence, the lamellae thickness depends on cooling rates: very fine lamellar structure is reached upon fast cooling, coarser lamellae if cooling is slower. The individual lamellae nucleation takes place not only at grain boundaries but also, upon enough cooling rate, on the growth front of lamellar packets, spreading radially in a parallel plane to the  $\{110\}$  planes of  $\beta$  phase [8].

### 3.1.2 Displasive transformations

Fast cooling from a temperature above the martensite start temperature causes a diffusionless nucleation mechanism, also said *displasive* mechanism, which involves the complete transformation of  $\beta$  phase into metastable  $\alpha$  martensitic structure. As all displasive transformation results, titanium martensite has acicular, or plate-like, microstructure. The martensitic structure does not automatically lead to an embrittlement effect, above all for dual phase alloys, however the material is slightly strengthened compared to  $\alpha$  titanium. Indeed,  $\alpha$  martensite can be further divided into two species: hexagonal  $\alpha'$  martensite and  $\alpha''$  orthorhombic martensite. The

latter is a soft martensite that have been observed by quenching from temperature lower than about 900°C [8], above all in case of  $\beta$  phase rich in  $\beta$ -stabilizer content [31](in that case it was 10% of vanadium). Moreover, it has been found that the precipitation of orthorhombic martensite leads to softening and loss in yield strength, which means also increase of plastic deformation. However,  $\alpha''$  martensite it is a very difficult phase to detect only by microstructure observation [31]. Hexagonal  $\alpha'$  martensite has a similar orientation relationship to  $\beta$  as that of  $\alpha$  and it is recognizable by its typical basket-weave structure composed of thin  $\alpha$  needles [8] (Figure 3.4) that cross each other growing from the prior  $\beta$  boundaries. Titanium martensite is so called because of its formation mechanism and its typical acicular shape, but it must not be understood as steel martensite for what concerns mechanical properties. Indeed, since crystal lattice distortion in titanium martensitic structure is not that accented as in that of steels, the hardening and strengthening effects are only moderate [8].



*Figure 3.4: Examples of lamellar microstructure in additively manufactured Ti-6Al-4V alloy: (a) Basket-weave (b) Widmanstätten colony and (c) acicular martensitic microstructures [32]*

### 3.2 Heat treatments on titanium alloys

Thermomechanical treatments are able to change an alloy mechanical response by means of modification of its microstructure. Grains shape, dimensions and compositions affect considerably material properties and heat treatments are often the only way to improve them. A crucial role in heat treating titanium alloys is covered by  $\beta$  transus temperature since it is the boundary between the double-phase  $\alpha+\beta$  and the single  $\beta$  phase fields. As previously explained, upon cooling

from the  $\beta$  field,  $\alpha$  starts nucleating and growing with lamellar shape from the  $\beta$  boundary within the grain. Instead, an equiaxed microstructure is achievable only as result of recrystallization. Hence, since recrystallization takes place only after a complete solubilization in the  $\beta$  field of a sufficiently cold worked structure in the  $\alpha+\beta$  field, equiaxed microstructure is a result of a thermomechanical treatment. However, in this paragraph, only thermal effect will be discussed because it has represented the theoretical basis on which subsequent heat treatment operations have been planned. The types of heat treatments commonly performed on titanium alloys are mainly two: solution annealing and aging. Their typical thermal cycles and process variable are reported in Figure 3.5. In the first instance, solution annealing differs from aging for higher temperature ranges required and the possibility to gain different microstructure by varying the cooling rate. Aging instead, by definition, consists in longer maintaining time, well below of  $\beta$  transus temperature. Depending mostly on their objective, these treatments can be further divide in subclasses of treatments which are mentioned hereafter.

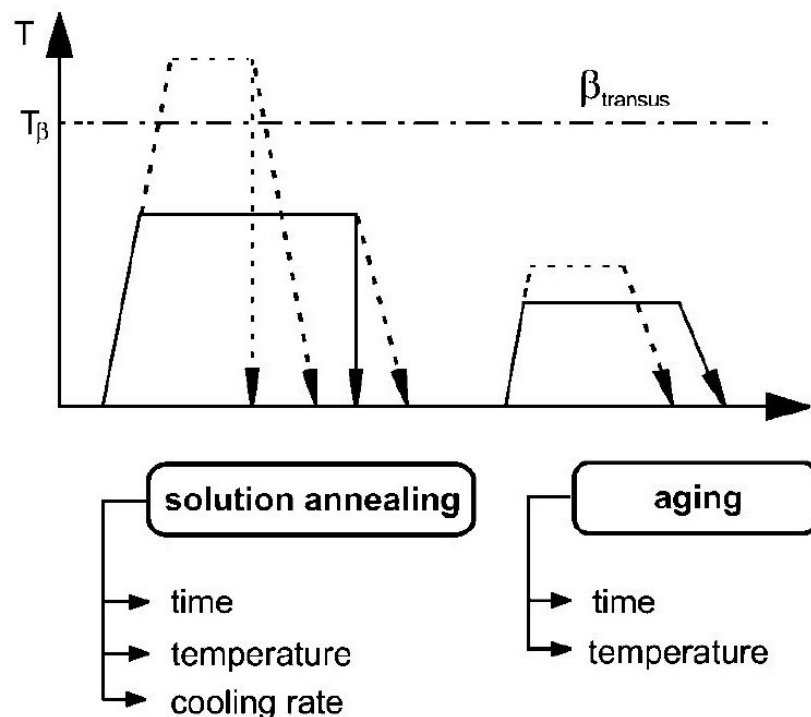


Figure 3.5: Thermomechanical treatment commonly performed on titanium alloys [8]

### 3.2.1 Stress relieving

Stress relieving is probably the most broadly applied heat treatment among all classes of titanium alloys. It is aimed to remove or reduce the undesired internal stresses caused by nonuniform forming such as hot forging deformation, cold working and straightening, by asymmetric machining, by welding and rapid cooling of castings and also by additive manufacturing processes. This heat treatment is not used to control microstructure, except when it is performed together with other thermal treatments.

The reason of its widespread on titanium alloys lies on its relative low operation temperatures which allows these alloys to be stress relieved without compromising their strength or ductility. Potentially, it doesn't have negative sides. Indeed, relieving stresses has a beneficial effect on shape stability, enhancing service life and other undesired conditions as the decrease of compressive yield strength, also known as Bauschinger effect, very common on titanium alloys. The only circumstance in which stress relief treatment is not convenient is when other treatments at higher temperature have been planned, as they are able to loosen stresses too. Process temperature must not be too high to avoid excessive amount of precipitation or strain aging, but enough to reduce internal stresses[9]. If otherwise a further stress relief treatment is required on solution treated and aged titanium alloys, care have to be taken to prevent material from overaging, which would lead to a decrease in strength. This usually implies a proper selection of times and temperatures that partially provides stress relief.

Commonly, for most effective treatment, higher temperatures are combined with shorter time and vice versa. For titanium alloys, cooling rate from the stress-relief temperature is not critical, whereas the uniformity of cooling it is, especially between 480°C and 315°C. Hence, furnace or air cooling are preferred instead of quenching which would induce new residual stresses. Efficiency of a stress relief

cycle can be measured only with x-ray diffraction by monitoring the decrease of stresses by passing of time. An example is reported in Figure 3.6.

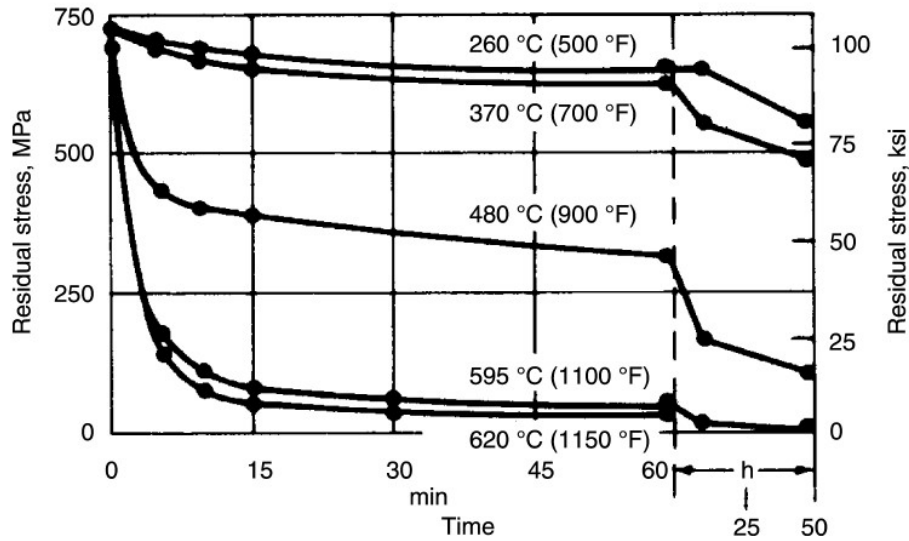


Figure 3.6: Residual stresses after stress relieving treatments at various stress-relief anneal temperatures for Ti-6Al-4V alloy [9]

### 3.2.2 Annealing

Commonly, annealing treatment is conducted in order to improve the material workability by refining the grain size. The material is heated up to the proximity of its  $\beta$  transus temperature and begins to dissolve. Annealing treatment on titanium alloys can be carried out both above and below the allotropic transus temperature, depending on purposes. Atoms migrate in the crystal lattice and the number of dislocations decreases, thus, leading to ductility and toughness improvement. Dimensional and thermal stability are also increased and, due to a loss in hardness, the material is ready to be easily shaped or machined.

Maintain time depends on the objectives of the treatments, while cooling rate is generally slow to let the constituents separate and reach their stable phases. Therefore either air or furnace cooling can be adopted from higher-temperature annealing and they can result in different levels of tensile properties, which are higher in second case. Since an improvement in one or more properties generally is

given by a comprise with some other properties, it is important to select the annealing cycle according to treatment objectives.

Annealed titanium alloys often results in a wider property variability than solution treated and aged alloys because of the lower control on these treatments. Solution treatment is frequently considered an annealing process, as is mill annealing. Even stress-relief heat treatment frequently is called stress-relief annealing. Depending on process parameters, common treatments identified as annealing are mill annealing, duplex annealing, recrystallization annealing and  $\beta$  annealing that are following described [33].

Mill annealing is a general-purpose thermomechanical treatment given to all mill products to reduce their anisotropy. It is not fully definable as annealing and may leave cold or hot work marks on hardly worked products, particularly sheets.

Duplex annealing, instead, is conducted to improve creep resistance and fracture toughness. It modifies shapes, sizes, and distributions of phases. For example, duplex anneal of Ti-6Al-4V alloy consists in a first anneal near the  $\beta$  transus to let deformed  $\alpha$  globularize and minimize its volume fraction. Secondly, a lower-temperature anneal is carried out to make  $\alpha$  precipitate as new lenticular (acicular)  $\alpha$  between the primary globular  $\alpha$  particles. Acicular  $\alpha$  is the responsible for improvements in creep strength and fracture toughness.

Recrystallization annealing is primarily used to improve fracture toughness. During this treatment the alloy is brought up to the upper limit of the  $\alpha+\beta$  field, maintained for a certain time and then cooled at very low rates.

Beta annealing, just as the previous treatment, is aimed to increase fracture toughness but it is the only treatment that provides heating above the  $\beta$  transus temperature. If excessive grain growth is not accepted, the process temperature must exceed  $\beta$  transus only slightly. Annealing times are dependent on section thickness and process has to last long enough to let all  $\alpha$  solubilize within  $\beta$  phase.



Fan or water cooling should be done on larger sections to avoid the formation of  $\alpha$  phase at the  $\beta$  grain boundaries[33]. Figure 3.7 shows the positive effect of grain growth on fatigue behavior.

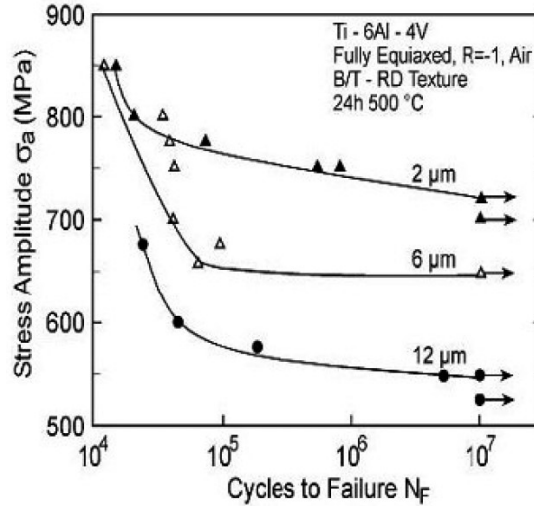


Figure 3.7: High cycle fatigue strength of the Ti-6Al-4V alloy with fully equiaxed microstructures and different grain size [34]

### 3.2.3 Solution treating and aging

Solution and aging treatment share a common objective which is the material strengthening, by increasing its yield strength.

Solution treatment is based on the heating of the alloy to a suitable temperature that allows its soluble phases dissolution and subsequent maintaining at that temperature enough time to let these constituents to enter into a solid solution. A fast cooling is then needed to keep them in solution, preventing them from precipitating.

Precipitation, instead, is the strengthening mechanism that is meant to be achieved by aging treatment. Indeed, aging consists in keeping the alloy at elevated temperature for hours to let precipitation to take place within the metal structure. This time delay is called "aging" and it is based on precipitation hardening mechanism. At high temperature, solid solubility of phases changes and fine particles of an impurity phase are generated. These impurities at the grain boundary, just as particle substances in particle-reinforced composite materials, impede the

movement of dislocations and other defects within the crystal lattice, leading to limitation of plasticity and, thus, to material hardening. However, no titanium alloy of conventional composition has been found to be truly age hardenable [35]. Therefore, depending of treatment purposes, solution treatment and aging are often carried out sequentially and materials treated by that thermal cycles are sometimes specified as "STA" in certificates. The combination of solution treatment followed by aging treatment is the treatment cycle that makes titanium alloys reach the higher strength values. This is due to a higher ratio of  $\beta$  phase that is produced when a  $\alpha+\beta$  alloy is heated to the solution treating temperature and this partitioning of phases is kept by quenching at room temperature where  $\beta$  phase is in its unstable form; During subsequent aging, these unstable phase decompose and provides high strength.

**Effect of solution treating temperature on tensile properties of Ti-6Al-4V barstock**

Solution-treating temperature		Room-temperature tensile properties(a)				Elongation in 4D(c), %
		Tensile strength		Yield strength (b)		
°C	°F	MPa	ksi	MPa	ksi	
845	1550	1025	149	980	142	18
870	1600	1060	154	985	143	17
900	1650	1095	159	995	144	16
925	1700	1110	161	1000	145	16
940	1725	1140	165	1055	153	16

*Figure 3.8: Effect of temperature in solution treating of Ti-6Al-4V on its tensile properties [9]*

Usually process parameters are determined by the thickest section and depends on the alloy type. With regard to  $\alpha+\beta$  alloys, selection of a solution-treatment temperature is crucial because affects the amount of  $\beta$  phase dissolved and so the magnitude of aging effectiveness. Hence, temperature has to be selected according to the desired mechanical properties. Figure 3.8 gives an outline of how solution

treating temperature influences the obtainment of tensile properties. If stress corrosion resistance or fracture toughness are priorities, solution treatment above the  $\beta$  transus may be desirable. However, this would cause a significant loss in ductility for an  $\alpha+\beta$  alloy, therefore experience has shown that an optimum balance of ductility, fracture toughness, and creep properties in  $\alpha+\beta$  alloys is better achievable by heating slightly below the  $\beta$  transus temperature, normally no more than 85°C less.

### **3.2.4 Quenching**

Even though quenching does not fall into the class of heat treatments, it is worth mentioning its effects. Quenching consists in the rapid cooling of a material generally in water, oil or air and it is aimed to avoid undesired equilibrium processes that occur in certain low temperatures ranges. Indeed, effectiveness of quenching techniques is based the reduction of the window of time during which these undesired reactions are both thermodynamically favoured and kinetically possible. Submerging the workpiece in a fluid after it has been treated means affecting the cooling rate of the process, in relation on its thermal conductivity and on the alloy characteristics. As previously mentioned, upon a rapid cooling martensite phase can appear on the material, which is non-equilibrium phase distinguishable by the needles-shape of the grains, produced by displasive transformation occurred during rapid cooling. The quenching media that can be used are forced air, oil and water until the more thermally efficient brine and mixtures of water and glycol polymers. However, the most commonly used are water and oil. Water gives one of the highest cooling speeds allowing to reach maximum hardness, but on the other hand may increase the risk of distortion and tiny cracking. Mineral oils are instead less drastic as quenching media and they can be employed when hardness is of secondary importance.

Anyway, after solution treatment of  $\alpha+\beta$  alloys, it is common practice to use water, 5% brine or caustic soda solution upon quenching. For quenching of sheets, low viscosity oil has to be preferred in order to prevent them from distortion.

Apart from heavily  $\beta$ -stabilized alloys for which a slower cooling can be performed still obtaining a good result in terms of uniformity in strengthening, for  $\alpha+\beta$  alloys a faster cooling is required otherwise coarse  $\alpha$  could precipitate resulting in a weaker strengthening effect. Quicker quenching also helps in reducing the formation of  $\alpha$  at grain boundaries that, once again, can cause poor ductility[36].

# Chapter 4

## Materials and Methods

A deep comprehension of mechanical properties comes through different types of investigations. In this study, five types of miniature specimens, that differ only in the production method, have been tested. The results of static tests have been evaluated together with microstructure characterization, microhardness values and failure mechanisms examined by *in situ* fracture surfaces observation. Special precautions must be taken in regard of specimens preparation and experimental procedures, since the potentialities and the advantages of *in situ* testing are huge and they have not been fully explored yet. Together with the rapid development of the relatively-newborn additive technologies, their continue improvement and increasingly widespread industrialization, the growing interest in functionally graded materials and the enhancement of materials performance, the investigation methods adopted in this work testify the extremely innovative and constantly evolving context in which this studies have been conducted. Therefore, experimental procedures and equipment will be described in detail in this Chapter, giving an explanation on the limits that have been encountered, on the existing constraints and the uncertainty of the results, emphasizing especially the numerous possibilities offered by this experimental approach.

### 4.1 Specimens preparation

#### 4.1.1 Production parameters

Ti6Al4V alloy have been employed for the fabrication of all specimens. An overview on the alloy's properties has been previously presented in Chapter 1. According to ASTM standards on commercially pure titanium, its chemical composition is given in Table 4.1.

Nominal composition wt%, impurity limits wt%	
Al	6.0
V	4.0
N (max)	0.05
C (max)	0.10
H (max)	0.0125
Fe (max)	0.30
O (max)	0.20

Table 4.1: Ti6Al4V alloy chemical composition [9]

Miniature specimens of the same geometry have been used in order to conduct *in situ* investigations. Unlike for macro ones, miniature specimens sizes are not normalized, thus their geometry has to be properly designed for that purpose. The first design criteria that was followed is maximizing the grip section: the bigger the grabbed area is, the higher would result the friction force between each clamp and the specimen surfaces, which will allow the specimen to be held still within the clamps. At the same time, the useful section has to be very narrow. These two conditions mean having an high difference in width between the central section and the side section of the specimen. As the failure should occur approximately in the center of the specimen, it is important, in the geometry designing phase, not to concentrate stresses in other single points to avoid them from early fracture. For this reasons, the chosen geometry is a dog bone shape with two gentle curvatures [37] instead of a drastic one commonly adopted in conventional tests. In this way, at the two fillets the  $K_t$  factor is lower, ensuring a more homogenous flow of stresses instead of the single curvature profile. As illustrated in Figure 4.1, the gauge geometry is 5 mm x 2 mm x 1,5 mm. According to their production method, specimens can be firstly divided into two categories: conventionally wrought and additively manufactured specimens.

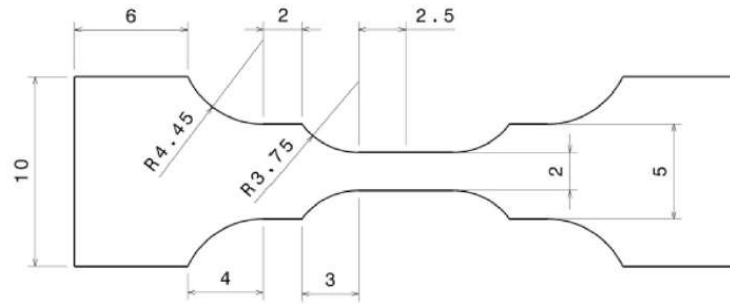


Figure 4.1: Tensile specimen geometry in mm. Medium thickness= 1,5 mm

The wrought ones were manufacture by rolling and subsequently they underwent a recrystallization annealing treatment in order to remove any possible anisotropy effect given by working. Then the rolled-annealed plate has been machined to obtained specimens geometry. Thereafter, some of them have been heat treated, as better described in 4.1.3, with two different thermal cycles. Notice that it would not have been convenient carrying out the desired heat treatments directly on the bulk plates and subsequently cutting specimens from them because machining operation may have caused residual stresses occurrence and superficial microstructure alteration on the specimens, which being very small, would have resulted in most of their section affected by the undesired effects of machining, hiding the ones given by the treatment. Moreover, heat treatment may lead to the formation of hard phases that would have made the material more difficult to be worked at a later time.

	<b>EBM*</b>	<b>LENS</b>
<b>Powder size</b>	45-100 $\mu\text{m}$	44-149 $\mu\text{m}$
<b>Laser power</b>	7000 W	325 W
<b>Layer height</b>	100 $\mu\text{m}$	508 $\mu\text{m}$
<b>Preheating</b>	700°C	-
<b>Stress relief</b>	-	600°C -1h
<b>Building direction</b>	vertical	vertical

Table 4.2: Process parameters comparison for additively manufactured specimens;

\*Example of recommended data for Arcam printers

The specimens fabricated by additive manufacturing processes were obtained by machining of vertically printed thin prisms. Powder Bed fusion (PBF) and Direct Energy Deposition (DED) technologies have been applied for their fabrication, as it was anticipated at the Chapter 2, where these methods have been deepened. The PBF prisms were manufactured by means of Electron Beam Melting technology (EBM) using metallic powder of particle size included between 45 and 100  $\mu\text{m}$ , following the recommended process parameters provided for *Arcam* EBM machines. An example of typical *Arcam* parameters is reported in Table 4.2 and, more generally for EBM applications, in the previous comparison presented in Table 2.9. The foils obtained by DED method were built adopting Laser Engineered Net Shaping technology (LENS). LENS specimens were fabricated as in [29], where process parameters can be found in detail, over a mill-annealed Ti-6Al-4V substrate. Spherical Ti-6AL-4V powder for their production was provided by Timet with a mesh size of -100/+325 (SAE AMS 4998C) obtained by gas atomization. The printer used was an *Optomec LENS 850-R* machine powered by a 1 kW Nd:YAG laser. After specimens fabrication, prisms underwent a stress relief treatment in a preheated furnace at 600°C for one hour followed by cooling at room temperature.

<b>Process</b>	<b>Process Type/Treatment</b>	<b>Name</b>
Wrought	As received	W
Wrought	Heating up to 970°C in 2h Maintenance at 970°C for 1h Water quenching	W970-WQ
Wrought	Heating up to 1015°C in 1h Maintenance at 1015°C for 2h Furnace cooling	W1015-FC
Additive Manufacturing	Electron Beam Melting	EBM
Additive Manufacturing	Laser Engineered Net Shaping	LENS

*Table 4.3: Specimens process parameters and terminology*



In Table 4.2 some comparable process parameters of both AM technologies are summarized; Notice that without EBM precise data, only an example for the recommended parameters is reported. Subsequently, both types of specimens have been cut from the printed prisms. Therefore, in this study five cases have been evaluated and Table 4.3 contains their description.

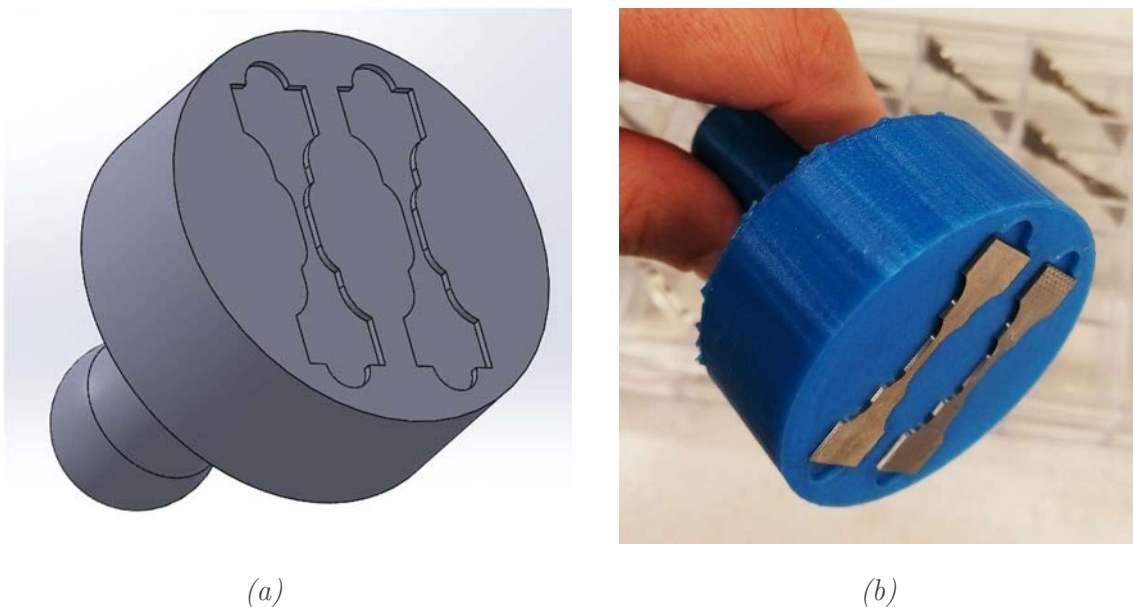
#### **4.1.2 Polishing procedures**

Since the planned experimental works consist in the use of optical devices, the specimens need their surface to be smooth and with mirror finish. Low roughness is required also in the heat treatment processes to obtain an homogenous microstructure trough the section: an high number of roughness peaks means a likewise high number of sites where new grains can nucleate. This leads to the formation of fine grain microstructure near the surface, differently from with material core where grains would be coarser. Hence, specific polishing procedures have been carried out before both tests and heat treatments to reduce surface roughness due to the production process. Basically, the specimens selected to be heat treated have been polished twice: once coarsely before being heat treated and then after the treatments as accurately as the others, in preparation for the optical analysis. Two polishing methods have been explored: mechanical polishing and electropolishing.

##### ***4.1.2.1 Mechanical Polishing***

The mechanical method is the most common procedure to polish samples. If done properly, mechanical polishing can provide very smooth and flat surfaces, on the other hand is time consuming and requires careful manual skill, above all for titanium alloys. Since the specimens under examination must be tensile tested, they cannot be mounted and thereby the use of automatic polishing machines is not possible either. To facilitate specimens handling, a holder has been designed

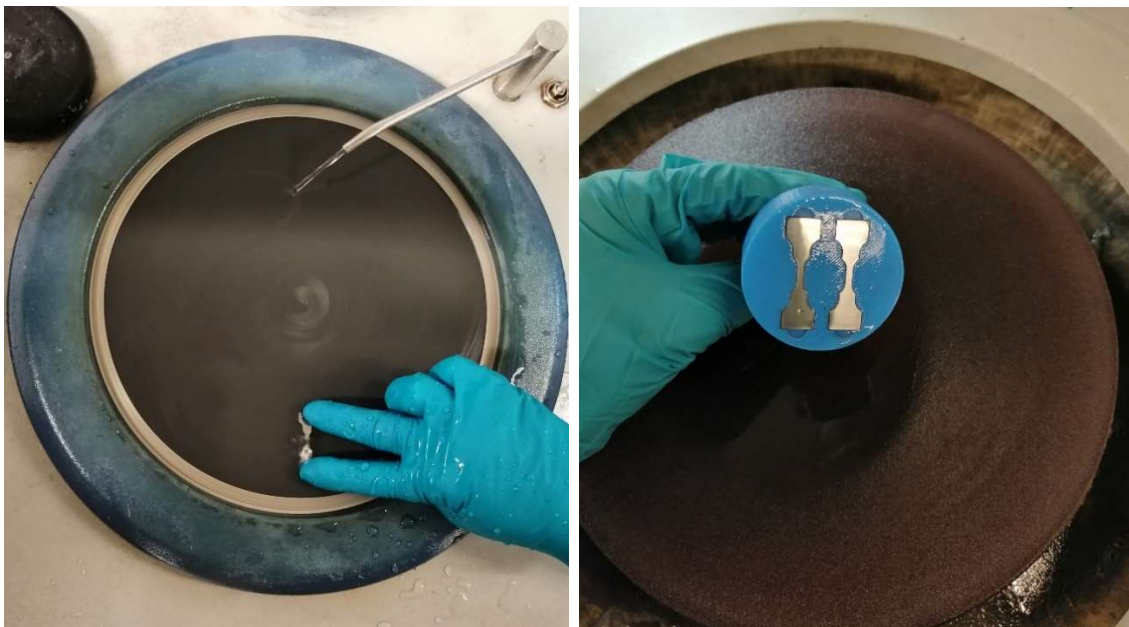
(Figure 4.2.a) and then FDM printed, made of generic PET (Figure 4.2.b). This cylindrical holder allows to hold two specimens at a time, speeding up the polishing procedure. Compared to the specimens sizes, the cavity dimensions have been increased of 2% in width and 5% in length to let specimens fit inside it. The cavity is 1 mm deep to make approximately one third of the specimen thickness stick out to be polished. Notice that both sides of the specimen need to be smoothed to get the same surface properties. However, practice has shown that the holder is effective only for the very last stages of polishing because it makes the specimens horizontality less controllable compared to holding them with hands: during the grinding phases the amount of material removed is high and even a slight slope of the specimens or a light difference in pressure along them may lead to obtain specimens significantly tilted.



*Figure 4.2: Holder for specimens handling during polishing; (a) CAD model, (b) PET holder realized by means of FDM printing, showing raw specimens wedged in and sticking out from it*

Indeed, the procedure consists in two stages: grinding and polishing. During the grinding step, grade #200, #500, #1000, #2000 silicon carbide papers have been used in this order on turntables to flatten specimens. The paper was changed once each ground surface was uniform in scratches and the specimen was 90° rotated in

a way that all the previous grooves can be removed, creating new ones. Giving a uniform pressure is fundamental and a lot of water is necessary as coolant and to take away the removed material particles (Figure 4.3.a). For polishing steps, suspensions of diamond of decreasing granules size have been sprayed on different clothes, which have likewise decreasing abrasive effect (Figure 4.3.b). Pastes of 6, 3,1  $\mu\text{m}$  granule size were used lubricated with ethanol. At this stage, specimen were moved radially from the center to the side of the disk, while this was rotating. Ultimately, 20 minutes of final polishing was carried out with colloidal silica suspension of 0,25  $\mu\text{m}$  particles dimension. At the end, mechanically polished specimens appeared very smooth to the naked eye, some grains were also recognizable (Figure 4.4). However, if quickly checked at the optical microscope some striation was still visible which could interfere with an accurate consequent microstructure analysis. In addition, not all the specimens presented visible grains, not even under the microscope, necessitating chemical etching for micrographies on those.



(a)

(b)

Figure 4.3: (a) Grinding process was carried out holding specimens manually one by one;  
(b) Polishing process allowed the use of the holder



*Figure 4.4: DED specimen after O-PS polishing step; Some prior grains are visible to the naked eye*

#### ***4.1.2.2 Electropolishing***

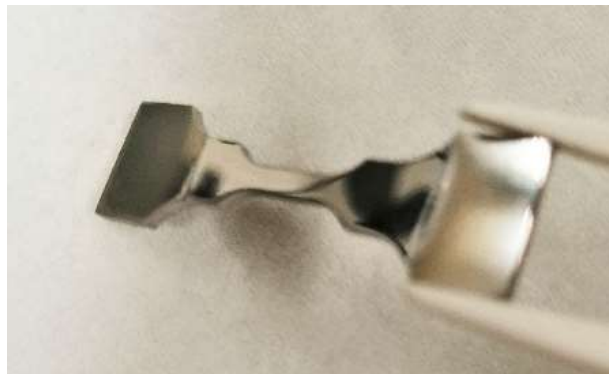
Electropolishing is an electrochemical process that can effectively remove a controlled amount of surface material and contaminants embedded, giving the surface a high luster. During electropolishing, metal is anodically dissolved, but due to the preferential passage of current at the raised portions of the roughness, these dissolve more quickly compared to the surface gorges.

In the considered case (Figure 4.5), an electrolyte containing methanol and 2-butoxyethanol was chosen. The affected area was 1 cm<sup>2</sup> large and the bath was operated at 25°C for 25 seconds. The selected voltage was 33 V and flow rate was 14  $\mu\text{m}/\text{min}$ . As literature shows ([38], [39]), electropolishing of titanium alloys provides lower surface roughness values than conventional polishing. In this study roughness has not been quantitatively measured, but a qualitative comparison has been conducted. However, even though electropolishing is considered an alternative instead of mechanical polishing, the electrolytic method requires a grinding pre-treatment [40] and, preferably, polishing down to a 3  $\mu\text{m}$  step. Therefore

electropolishing procedure has been carried out downstream of the mechanical one. As Figure 4.6 shows, it is clear within the same specimen the difference in luster between the electropolished zone (the useful area) and the endpoints conventionally polished.



*Figure 4.5: Electropolishing apparatus*



*Figure 4.6: The electropolished area is only a part of the specimen surface and the difference in luster is clear*

Moreover, when observed under the microscope, microstructure was clearly visible in all the specimens. Therefore, the use of electropolishing has made further microstructure analysis possible without chemical etching, which would have

involved the use of hydrofluoric acid. Since chemical etching implies the selective corrosion of material, the possibility to avoid it means preserving specimens surface integrity and reducing the risk of microstructure damaging. For these reasons, in this study, electrochemical polishing has been considered favourable compared to the mechanical method.

#### **4.1.3 Heat treatments settings**

Some of the aforementioned wrought specimens have been heat treated in order to examine the possibilities given by different microstructures upon mechanical properties. Wrought specimens have been subjected to rolling and subsequent recrystallization annealing, therefore an homogenous globular microstructure is expected in their case. Heat treatments planification has been guided by the willingness to obtain different grain sizes among the specimens by experiencing two opposite treatments aimed to swell and refine the as-received grains. An attempt was done also towards the efficiency of the treatment by choosing reasonable process parameters among the lower ends of the temperature and time ranges suggested in previous works [9], [34]–[36], [41], [42], relying on the fact that, unlike those, in this study miniature specimens are being considered and even a slight increase in their grain size, as a consequence of a shorter treatment, could have significantly affect mechanical response, as well. Indeed, defining with  $d$  the average grain size and with  $t$  the transversal section thickness, a small specimen, having lower  $t$ , would show bigger grains in its section than a conventional tensile specimen for the same  $d/t$  ratio. Therefore, in the case of a grain coarsening treatment, attaining an equally high grain size-thickness ratio in a bigger section would require much more time to let grains grow and thus a more time consuming heat process. On the other side, the possibility of accomplish an homogenous quench is also reasonable because of the reduced dimensions of the sample section. However, despite these observations and reported experiences, the treatment effectiveness

cannot be fully guaranteed due to the uncertainty on the actual temperature reached by specimens during the thermal cycle. As already extensively discussed, titanium alloys show a high reactivity with air especially at high temperatures and this behavior implies the need of an inert or vacuum atmosphere during the alloy treatment, preventing it from oxidation or the creation of a brittle surface layer beneath the surface called alpha-case [32]. Since the thermal conductivity of a rarefied atmosphere is significantly lower than that of normal air, the actual achievement of the set temperature by the workpiece is not to be taken for granted. In addition, the possibility of installing a thermal camera to monitor the sample temperature is complicated by the fact that it should not compromise the airtightness of the furnace. Hence, the full control of the heat treatment process would be achieved by means of a controlled atmosphere furnace which allows to install a thermal probe within. Anyway, for what this study concerns, an Across International TF1700 Tube Furnace was used to perform the projected thermal cycles. This type of oven is equipped with high quality alumina fiber insulation and molybdenum silicide heating elements and it is shown in Figure 4.7.



*Figure 4.7: Tube furnace used to heat treat the specimens*

Vacuum atmosphere was assured by enclosing specimens in glass capsules with vacuum inside (shown in Figure 4.8). Notice that the glass surface that separates

specimens from the external environment may represent another additional obstacle to effective specimens' heating. Despite the awareness of these experimental limits and variables, two thermal cycles have been performed on encapsulated specimens. As mentioned before, specimens needed to be previously polished down to at least the 3  $\mu\text{m}$  step so that eventual grain nucleation during the treatment could have been as homogenous as possible across the section.



*Figure 4.8: Specimens encapsulated in a vacuum glass case to avoid them from oxide formation during their heat treatment*

Thermal cycle adopted to heat treat the specimens has been anticipated in Table 4.2 and they are charted in Figure 4.9. The first one was aimed to activate displacive mechanisms by fast quenching after solubilization of  $\alpha$  phase within the  $\beta$  one in order to obtain microstructure refinement. Thus, an attempt of solution treatment has been performed by putting the encapsulated specimens into the center of the tube furnace, then heating the latter up to 970°C in 2 hours and then keeping it for 1 hour at that temperature. At the end, the capsule has been quickly extracted from the oven and immediately broken in the water (W970-WQ). Hence, the Ti-6Al-4V specimens have been brought to the upper limit of the  $\alpha+\beta$  field, 10°C below the  $\beta$  transus temperature as common practice for  $\alpha+\beta$  alloys (see previous section 3.2.3). If the time has been enough for  $\alpha$  phase to partially dissolve into  $\beta$ , the subsequent water quenching should kept this phase partitioning at room



temperature in acicular shape. However, due to the aforementioned difficulties in controlling the actual temperature of specimens, this effect has to be verified.

The second heat treatment type was meant to cause grains swelling, so it was necessary to exceed  $\beta$  transus temperature and treat as long as the  $\alpha$  phase can complete its solubilization into  $\beta$  phase and the latter can begin to swell itself; Then a slow cooling would allow secondary alfa to grow and become coarser. Thus, furnace was heated up to 1015°C in 1 hour, kept at that temperature for 2 hours and then cooled switching off the furnace (W1015-FC). Thermal cycles are clearly described in the Time-Temperature diagram reported in Figure 4.9.

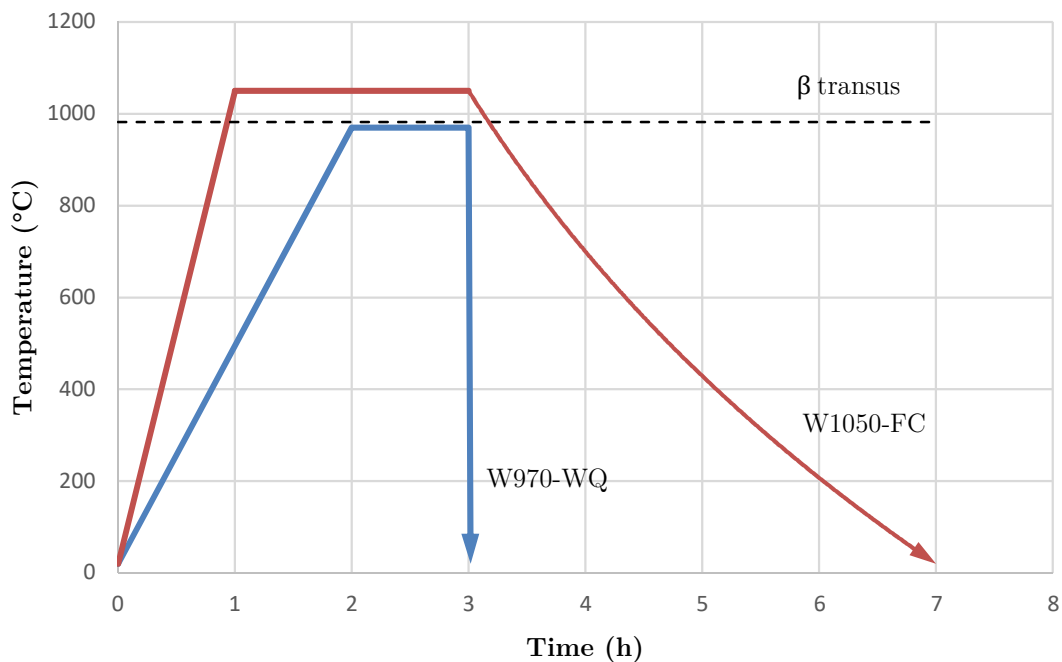
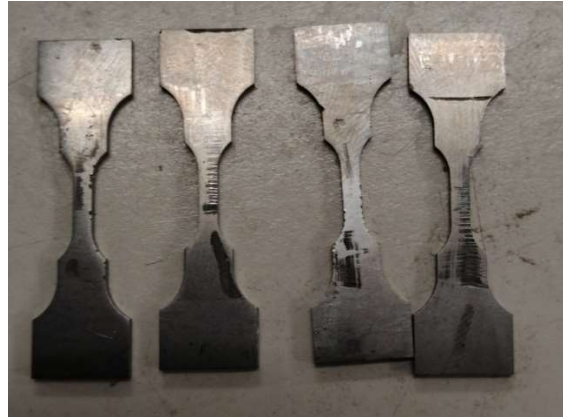


Figure 4.9: Schematic diagram of thermal cycles applied on specimens

An undesired condition occurred in the W1015-FC specimens at the end of the process. Once removed from the furnace and broken the capsule, some specimens weld together along their outlines. This phenomenon has been caused by diffusion mechanism that the high temperature promoted between the surfaces that were overlaid and touching. Figure 4.10 shows W1015FC specimens that could have been separated without visible deformations. A slight oxidation has been observed on all

treated specimens (also visible in Figure 4.10) although they have been heated under vacuum atmosphere. Hence, all of them have been re-grinding starting from the lowest paper grade, up to polishing and electropolishing steps.



*Figure 4.10: Specimens after heat treatment need polishing from the beginning; Some of W1015-FC welded together in some lines*

## **4.2 Experimental works**

### **4.2.1 Micrography**

As mentioned in Chapter 1, titanium alloys in their entirety present a wide range of mechanical properties that are not given only by different alloying elements, but also due to their influence on crystal structure, to grains shape and dimensions which in turn depend on manufacturing techniques and thermal processes that they may have undergone. In other words, the material behaviour is strongly correlated to microstructure configuration. For these reasons, microstructure analysis have been undertaken with the aim of finding the bridge between fabrication process and tensile behaviour.

As explained in 4.1.2.2, thanks to the excellent surface finishing obtained by electrochemical polishing, hydrofluoric acid etching was not necessary anymore. This allowed to analyse a wide portion of surface on each specimen, without further corrosion. The examinations were carried out with an Olympus optical microscope, showed in Figure 4.11. The use of the dedicated software enabled pictures to be taken, as will be reported in the next Chapter. Several pictures have been captured

at 4 different magnifications (5x, 10x, 20x, 50x). The use of polarized lens was excluded because, although it gave a 3-dimensional appearance of grains, it hid some features that laid on the same plane. Different phases have been distinguished by grains arrangement and shape, taking example from literature. By doing so, as most of the configurations were easily recognizable and could be lead back to their thermomechanical history, the more accurate EBSD examination was not performed.



*Figure 4.11: OLYMPUS optical microscope used for microstructure examinations*

#### **4.2.2 Microhardness tests**

Microhardness measurements have long been used as a microprobe of the mechanical response of materials [43] but it can also be a supporting parameter for the identification of material phases. Therefore in this study, Vickers microhardness tests have been performed on each type of specimen, getting a mean value each. Vickers test provides an indentation made on the specimen by a pyramidal diamond indenter with a  $136^\circ$  included angle through the application of a constant load  $P$  (Figure 4.12). After a defined application time, the load is removed and the resulting rhomboidal footprint diagonal  $d$  is measured. The Vickers hardness value

$H_V$  is defined as a function of the applied load divided by the indentation projected area, in the following form:

$$H_V = 1854.4 \times \frac{P}{d^2}$$

where load  $P$  is expressed in kgf and the diagonal  $d$  in mm.

In microhardness testing, typical adopted loads are in the range of 1-100 gf that correspond to the range of 9.81 - 9810 mN[43].

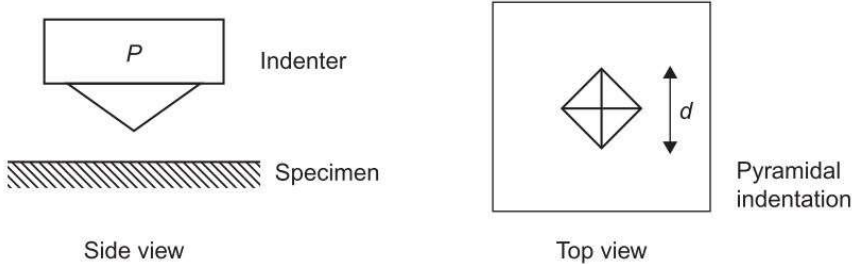
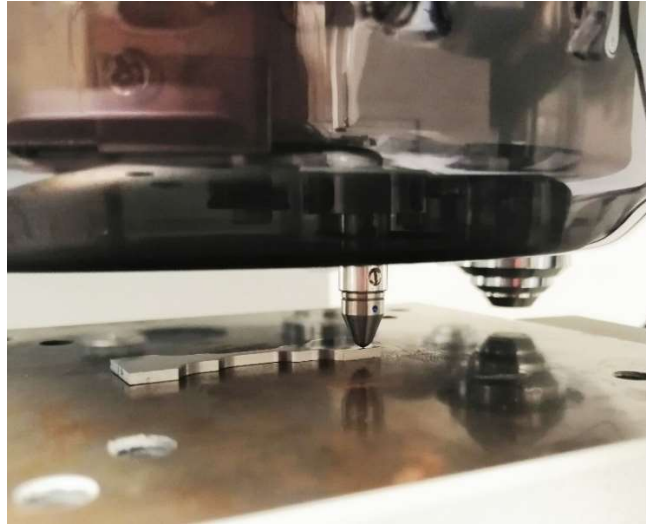


Figure 4.12: Schematic of Vickers indentation [43]

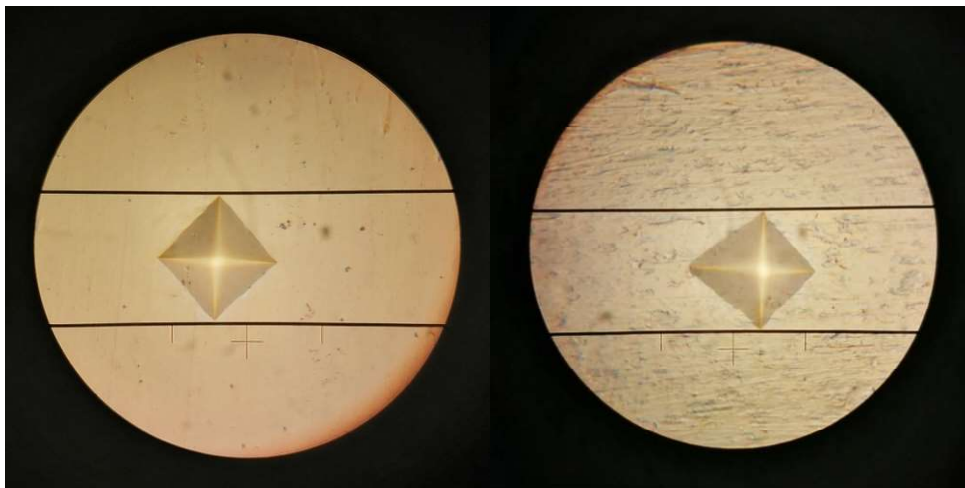


Figure 4.13: Mitutoyo Microwizard Vickers microhardness tester

Mitutoyo Microwizard Vickers microhardness tester reported in Figure 4.13 was adopted. A load of 0.3 gf was applied for 10 seconds. Once set these parameters together with the indenter position, the machine is able to perform the test automatically.



*Figure 4.14: Microhardness indentation*



*(a)*

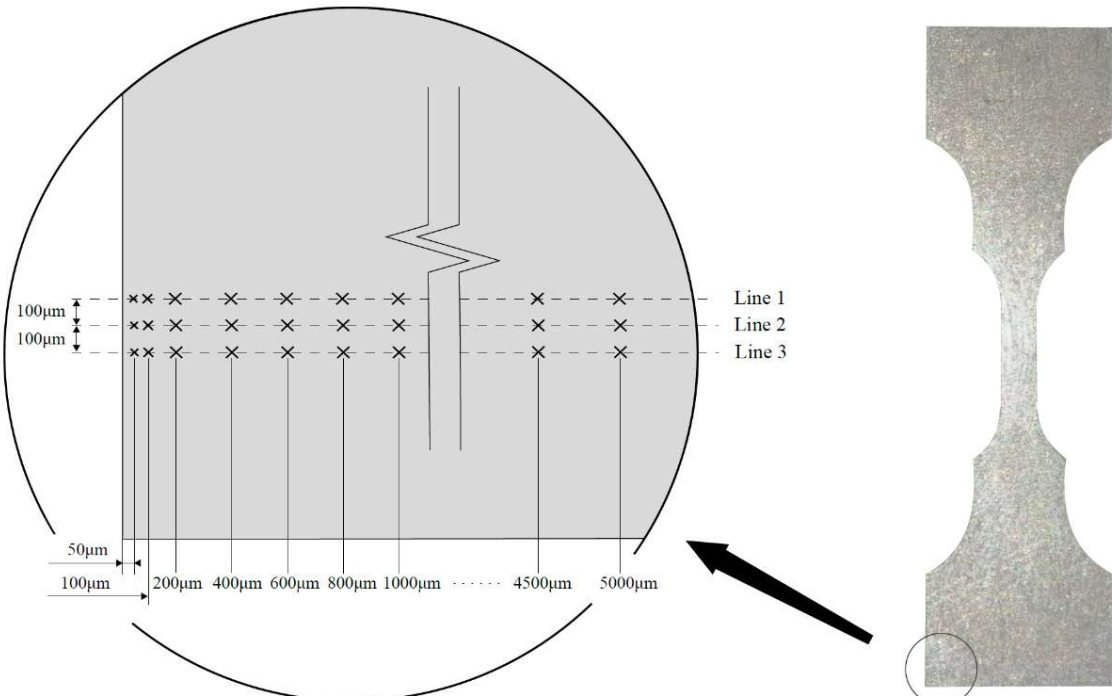
*(b)*

*Figure 4.15: Indentation footprint and diagonal measurement. (a) Regular surface leads to regular footprint. (b) an higher surface roughness may cause footprint distortion*

Then the microscope is turned above the specimen so that measurements can be done. Figure 4.14 shows the indenter while doing the test, fixed on a turntable together with the microscope lens. Indentation dimensions were measured by moving the two parallel lines displayed through the microscope eyepiece on the vertex of the rhombus, as seen in Figure 4.15. Both diagonals were measured and Vickers microhardness value was automatically calculated by using the their mean value. By comparison of pictures in Figure 4.15 it results also that microhardness test is sensitive to surface preparation methods and to microscopic variations from

flatness. Indeed, as shown in Figure 4.15(b), a bit higher surface roughness may cause the formation of an irregular footprint which can affect micro hardness results. So, once again, an optimal surface quality and horizontality is recommended. For matters of preserving structural integrity of the central part, which is the electropolished one, in this study indentation pattern was not performed there but on the specimen side, where however the surface was OP-S polished.

Testing materials with heterogeneity in microstructural phases requires a multiplicity of measurements and averaging of the results [44]. Hence, in the considered case, tests were carried out along 3 lines spaced 100  $\mu\text{m}$  one another, as shown in Figure 4.16: in each line, indentations were performed at increasing distance from the side surface. To quantify the global average value, a mean value was calculated for each series of three measurements equally distant from the surface; Subsequently, among those mean results, a final average value was obtained.



*Figure 4.16: Disposition of microhardness indentations on the specimens: along 3 lines spaced 100  $\mu\text{m}$ , indentations at increasing distance from the side surface. Each series of three measurements equally distant from the surface were averaged and these values, in their turn, gave a global mean value*

### 4.2.3 In situ investigations

#### 4.2.3.1 Introduction and premises

Tensile static tests have always played a priority role on a material mechanical behaviour analysis. Moreover, the possibility to understand how fracture mechanisms occur have been a precious additional information and *in situ* tensile tests represent this opportunity. Indeed, by placing a tensile stage into the chamber of the SEM (Scanning Electron Microscope) equipment it is possible to live monitor and portray specific deformation and failure mechanisms very closely, when instead in traditional testing, possible failure and cracking propagation mechanisms can be obtained only from post-experimental imaging. Observing cracks initiation and propagation at small scale, as well as when they occur, is helpful for the identification of critical locations where deformations events may begin which are then the cause of damage on the macro-level scale [45]. Furthermore, the relationship between microstructure and mechanical properties under tensile loading are investigable by in situ testing and their deep understanding allows also the enhancement of material properties and response by adjusting of process parameters [46].

Although many efforts have being done towards this small-scale approach to reliably characterize mechanical properties, the works that have been published [46]–[54] show several examples of small tensile machines have been recently developed, often adopting specimens that deviate sizes and geometries from the ASTM standards. As stated in [53], this context invites to discern whether and in which way the results measured using such non-standard specimens and devices can be representative of the material behaviour or at least comparable to ASTM standard tests. Actually, a different material behaviour with respect to macro tensile tests can be recognized due to the miniaturisation of the experimental apparatus. This phenomenon is called “scaling effect” and in mechanics involves

principally the dependency of strength on the cross-section area [53]. In a wider perspective, this relation can also concern microstructural features such as grain size through the thickness or microstructural anisotropy. Hence, the need for geometrical or microstructural similarity between the considered specimens to be comparable can be respectively translated in a constant  $L/A$  ratio for flat specimens (where  $L$  is the specimen length and  $A$  the cross-section surface) or  $d/t$  ratio (where  $d$  is the average grain size and  $t$  is the section thickness). Not many studies have been conducted on this scope, to investigate the reliability of micro-scale tests by comparison with the macro ones [52], [53] also because of the micro-structural material properties that limit the miniaturisation of specimens [52]. Thus, the cultural background on this topic is relatively weak, paving the way to the necessity of systematic studies focused on establishing a correlation between scales. Therefore, this premise aims to clarify the meaning of the following analysis which will compare miniature specimens to standard ones reported in literature without pretending to suggest a systematic “scaling effect” correlation due to the absence of similarity criteria. However, in situ investigations described here principally aspire to provide an example of in-depth material characterization in order to support damaging mechanism comprehension with microstructural properties.

#### ***4.2.3.2 In situ tensile tests***

A Kammrath Weiss GmbH DDS-3 in situ testing machine has been adopted to carry out the static tests on the miniature specimens. This machine, shown in Figure 4.17, is a tensile module (with the option of compression) for the Scanning Electron Microscope (SEM) and it can be mounted on the microscope stage just like an oversized specimen. The crosshead is controlled by a linear screw-driven system and its displacement is measured by a linear encoder displacement gauge. The load frame is actuated by using an interface system that connects to the load cell by pass-through connections on the SEM chamber. SEM QUANTA FEG 650



shown in Figure 4.18 was employed to monitor the tests in real-time. Notice that these tests are feasible only on conductive specimens or at least with a conductive coating applied, in order to achieve quality imaging by scanning microscopy.

At first, the machine was placed inside the SEM chamber and secured on the dedicated stage, then the connector was plugged in (Figure 4.19).

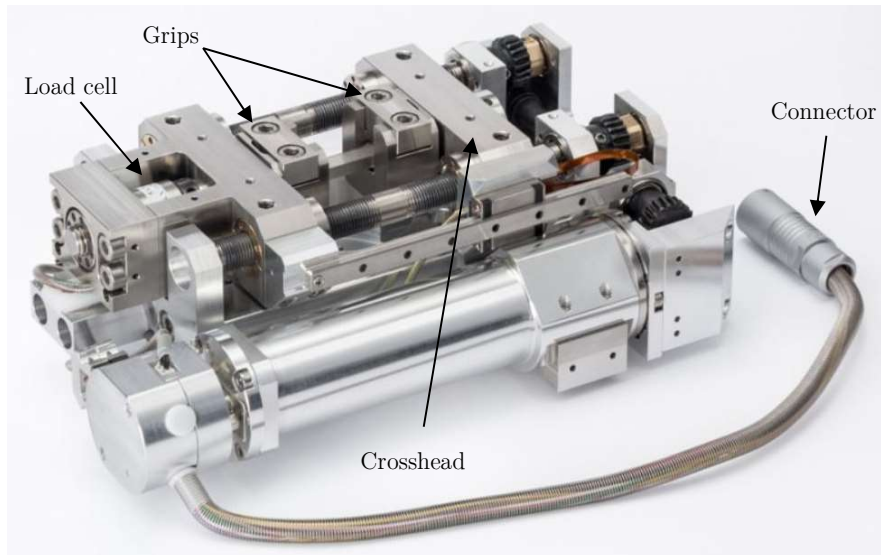


Figure 4.17: Machine used to carry out the tests (Kammrath Weiss GmbH DDS-3)

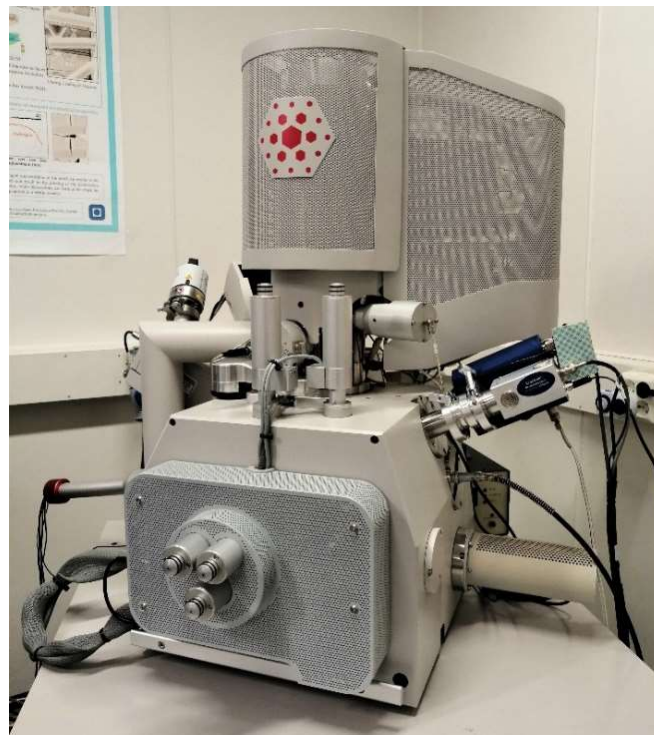
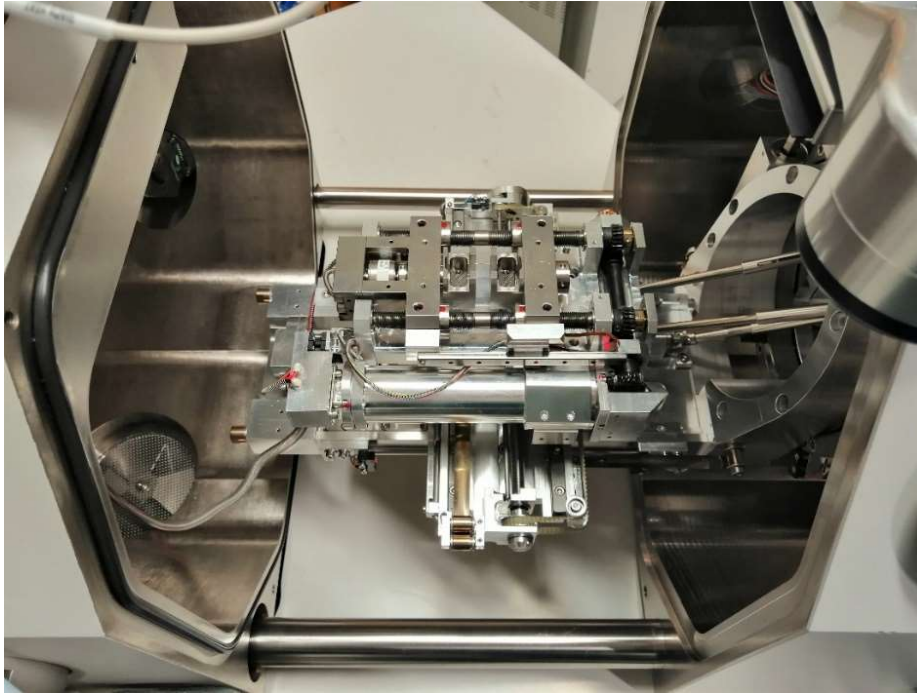


Figure 4.18: SEM QUANTA FEG 650



*Figure 4.19: The tensile module placed within the SEM chamber*

In situ tensile tests are performed by clamping a specimen into the micro-load frame by grips on each side and detailed steps are portraied in Figure 4.20. The specimen was positined on the clamps location with its electropolished surface upwards (Figure 4.20.1). Although the stage can be rotate afterwards with respect to the microscope framing, an accurate alignment in this phase is crucial for the correct orientation of stresses along the specimen while the test is running. Since there are no systematic methods to ensure the right specimen alignment, this phase could take a lot of time, however the tests results strongly depend on this. The securing process is warranted by some metal platelets stacked tightly above the specimens grabbing areas (Figure 4.20.2). These platelets then must be festened to increase grip between the specimen surface and the clamps, avoiding from slipping (Figure 4.20.3). After that the chamber can be closed and made vacuum inside. The specimen was then placed under the electron beam, properly focused and aligned. It has been used a 20 kV voltage with a spotsize of 3. Pictures were taken with a scanning speed of 30  $\mu\text{m/s}$ . The test has been conducted in displacement control, with a crosshead speed of 10  $\mu\text{m/s}$ . Force- displacement curve is displayed while

94

test occurs. Once specimen failure was occurred, several pictures of the broken surface have been taken at different magnifications. Figure 4.20.4 instead shows how the specimen appeared once tested, still grabbed within the clamps. The experimental apparatus requires to be very accurate in handling it both because it is delicate equipment and because even the slightest error, such as a wrong orientation of the specimens or not sufficient clamping force applied, could cause the invalidation of the test. In addition, the possibility to run multiple tests lies on the ability to change the attachment grips quickly, which is the more time consuming operation.

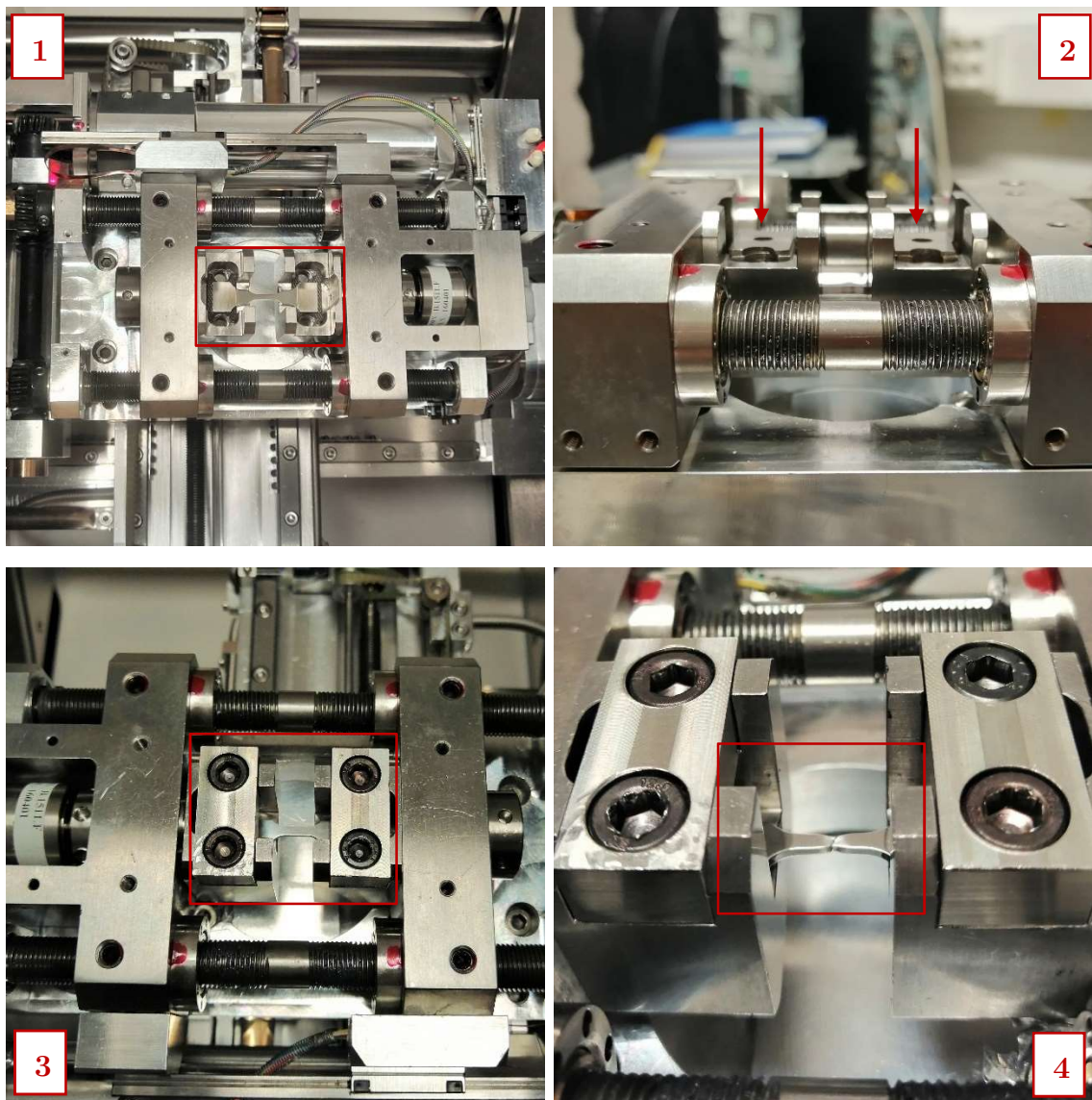
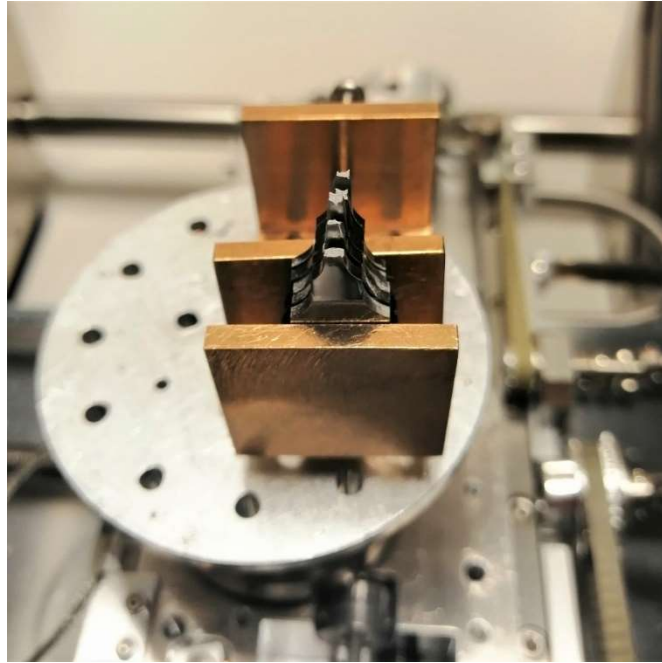


Figure 4.20: (1,2,3) Steps required to anchor the specimen within the machine clamps;  
(4) Fractured specimen after the test

A main problem when performing in situ tensile tests is characterizing the material strain. In absence of adequate extensometer, indeed, the tensile curve in situ tensile tests is often reported as stress-elongation function where elongation is the distance covered by the crosshead. Since the latter may slip, even imperceptibly, and thus move relatively to the specimens or add its own elastic deformation component to the measurement, its travel does not correspond exactly to the displacement of an hypothetical point placed on the specimen surface. Moreover, the crosshead displacement is only a measure of the average strain induced in the specimen and does not consider local strain. Hence, the measured displacement cannot be directly referred to the actual material local deformation if strain was calculated by elongation to initial useful length ratio, it would result higher than reference strain values for the same material. An alternative, can be found by creating a dotted pattern on the specimen surface by etching or spraying and measuring the material strain by dots movements during tests. However, this techniques relies on optical measurements hence requires the video recording to be stationary during testing. Otherwise, as common practice in this type of investigations, as long as test results must not be compared with macro-scale ones, the tensile curve can be plotted as a relation between stress and displacement.

#### ***4.2.3.3 Fractography***

A deep comprehension of fracture mechanism can be supported by the fracture surfaces observation. While in situ tensile tests displayed the upper surface of the specimen showing possible necking events, to better check the fracture surfaces a rotation of the specimens was necessary. Therefore, after completing all the tests, one half specimen each was located together with the others in a dedicated support mounted on the SEM stage, in the way that Figure 4.21 shows. Fracture surface was hence oriented upwards, perpendicularly to the detector. These investigations can reveal how the crack nucleated and subsequently propagated.



*Figure 4.21: Failed specimens placed together on a support on the SEM stage*



# Chapter 5

## Results and Discussion

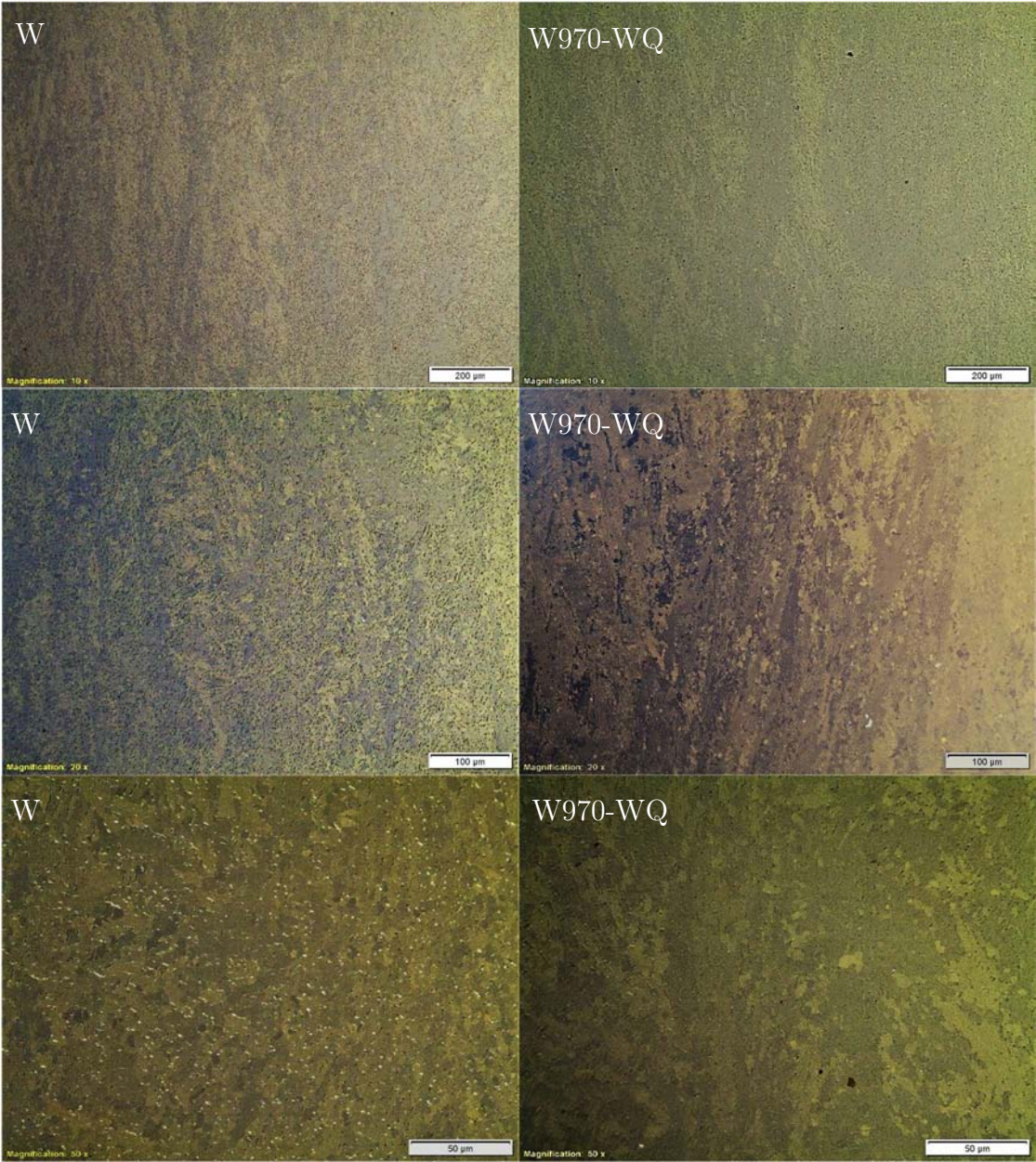
### 5.1 Microstructural properties

Micrography of the received wrought specimen (W) showed long columnar  $\alpha$  grains along the transversal axis distributed into the  $\beta$  matrix. After rolling and annealing treatment above the  $\beta$  transus, the microstructure has recrystallized and lost the typical anisotropy commonly given by a forming process. The W970-WQ, although the rapid cooling from the upper limit of the  $\alpha+\beta$  field, presented a very similar microstructure to the non-treated one. Indeed long columnar  $\alpha$  grains are recognizable also in the W970-WQ case. This condition shows that the applied treatment has not produced the desired grain refinement and, thus, the maintaining at 970°C should have been longer. Indeed, due to the aforementioned uncertainties related to the assessment of the actual temperature of the specimens, it is probable that the latter have not completely reached the set temperature and as a consequence have not allowed  $\alpha$  phase to properly dissolve into  $\beta$  phase and subsequently transform by displacive mechanism, during quenching. The treatment only contributed to homogenize the orientation of  $\alpha$  grains, in wider columnar grains. Pictures in Figure 5.1 show at different magnifications the two microstructure compared: on the left is reported the as received W, on the right W970-WQ. This similarity in microstructure configuration is supported also by comparable microhardness results, as it will be discussed later in this section.

The annealed specimen, named W1015-FC, showed a slight increase of average grain size and nearly equiaxed  $\alpha$  grains. By exceeding  $\beta$  transus temperature during the treatment for just sufficient time, grain swelling process has been activated and stabilized by the slow cooling. Figure 5.2 shows W1015-FC specimen with coarser and equiaxed  $\alpha$  grains. By comparison with the reported scale on each picture, the

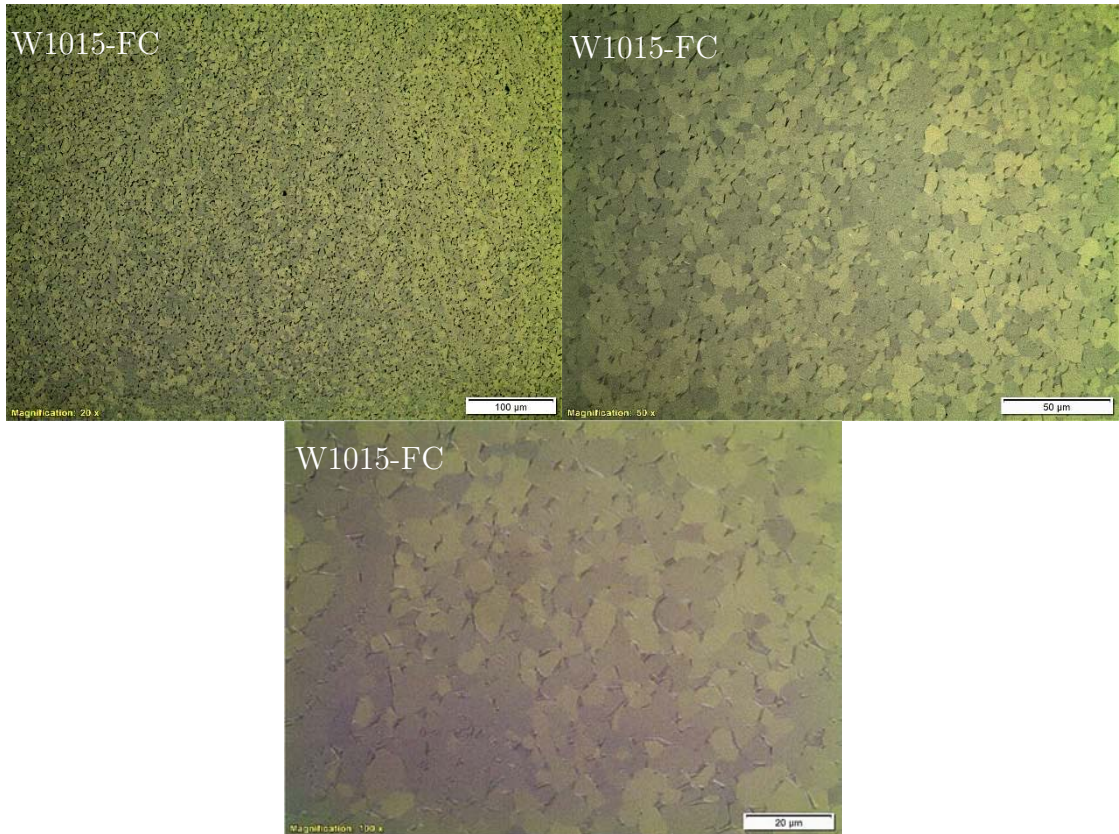
average grain size of W1015-FC has been estimated of approximately  $8 \mu\text{m}$ . In this case, the longer maintenance time has probably helped the specimen to reach the furnace temperature.

The AM specimens are very different in microstructure compared to the wrought ones. In accordance with the typical microstructure of additive manufactured titanium that have been found out in others works, such as [31], [32], [55], both the considered AM specimens showed columnar prior  $\beta$  grains that grow across layers.



*Figure 5.1: Microstructure of wrought specimens without etching; On the left column is reported the microstructure of the as received specimen (W), on the right column is shown the W970-WQ specimen at increasing magnification*

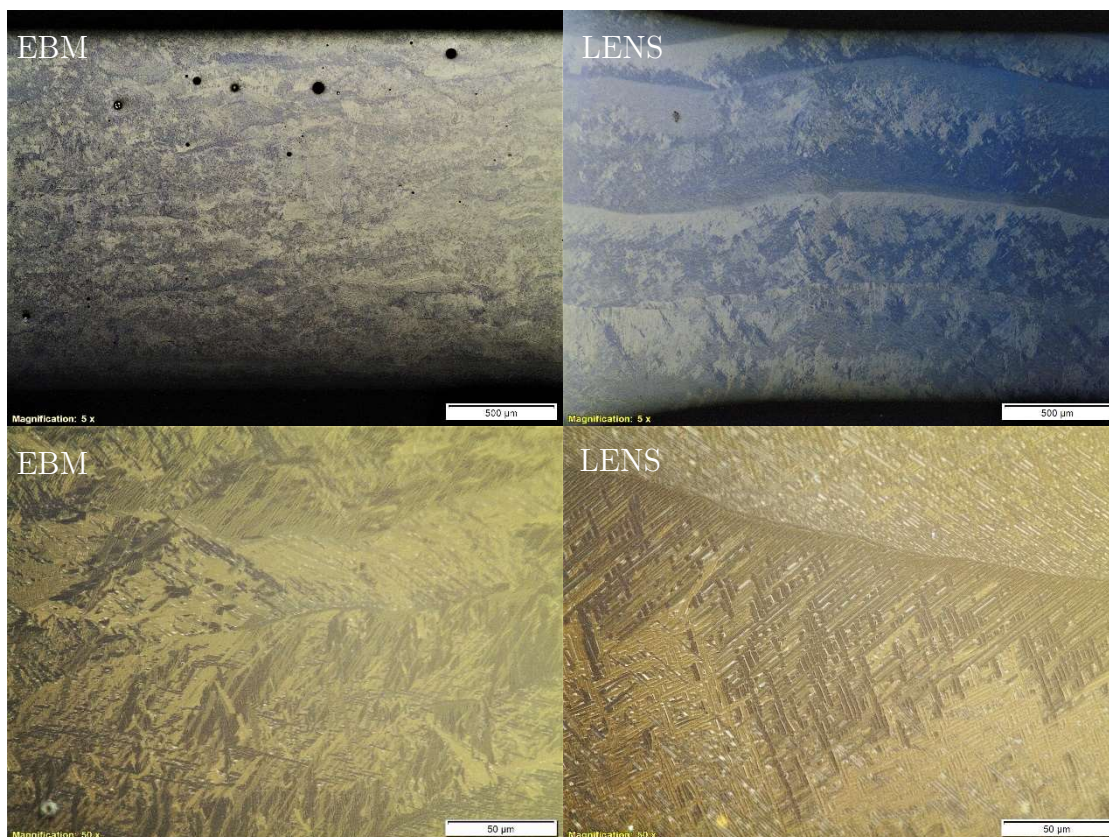




*Figure 5.2: Annealed specimen W1015-FC microstructure: coarse equiaxed  $\alpha$  grains distributed into the  $\beta$  matrix at increasing magnifications*

As explained in [30] these prior grains are firstly formed when the melt approaches the solidus temperature during its solidification and it is able to grow across layers following heat dissipation direction. In Appendix A, at the lowest magnifications, prior grains extending along the longitudinal axis are visible on both AM samples. Perpendicularly to those, an alternance of heat-affected zones appears on the pictures, which corresponds to the thickness of deposited material layers during the manufacturing process. The AM workpieces are cooled as well as they are built, so while the local temperature on the material falls below the  $\beta$  transus temperature,  $\alpha$  phase start to form, depending on the speed of cooling process: generally the  $\alpha$  phase begin with growing on the  $\beta$  grain boundaries and then it can grow along them or within the  $\beta$  grains in lamellae form. In case of rapid cooling, a lower amount of alpha phase is found at the boundaries and the thickness of the  $\alpha$  laths decreases with increasing cooling rate [32]. By comparison of the considered

specimens, EBM result in prior grains averagely  $15\ \mu\text{m}$  wide and a combination of weaved  $\alpha$  platelets and similarly oriented  $\alpha$  colonies of variable thickness; LENS instead appeared having wider prior  $\beta$  grains, estimated  $500\ \mu\text{m}$  thick, that often resulted in crossing the specimen throughout all its length, and very fine basket-weaved  $\alpha$  and acicular  $\alpha'$  within the prior grains (Figure 5.3). It has been pointed out [32] that an increased size of prior  $\beta$  grains must be mainly related to longer time and higher temperature at which the material is exposed above  $\beta$  transus. As occurred in [32], it is evident that, due to different process setups, the Powder Bed Fusion (PBF) endures shorter time above the  $\beta$  transus compared to Direct Energy Deposition (DED) method, leading to smaller prior grain size. As stated before, faster cooling rates result in thinner  $\alpha$  platelets growing towards the center of the prior grain. This situation is clearly recognizable in LENS specimen where the temperature gradient is higher than in EBM.



*Figure 5.3: Microstructure of AM specimens is commonly characterized by prior  $\beta$  grains and lamellar or acicular  $\alpha$  grown within as a basket-weaved pattern; Appendix A completes the description with more micrographies*

Despite laser source is not as powerful and narrow as the electron beam, laser beam in LENS technology results much more focused in all its affected surface generating a sharper gradient of temperature around the beam, which automatically leads to higher cooling rates. An example of phase transformation model for SLM technology is proposed in [56]. Since both SLM and LENS are laser-based processes, the prediction of finding a fully martensitic microstructure in that work is very close to the LENS case. Indeed, looking also at the pictures in Appendix A, LENS microstructure contains also acicular  $\alpha'$  martensite, formed by displacive transformation upon rapid cooling. The existence of martensite in LENS specimen is supported by its microhardness value. The latter not only it is the highest among the considered cases as shown in Figure 5.4, but above all is consistent with results of martensite microhardness for cast and additively manufactured Ti6Al-4V alloy published in [57] and [58], where the presence of martensitic phase was proved by EBSD analysis.

Microhardness test confirmed what has been previously stated about the effect of the undergone thermal history on samples microstructures. Figure 5.4 shows the mean global value calculated as described in section 4.2.2, while in Appendix B is

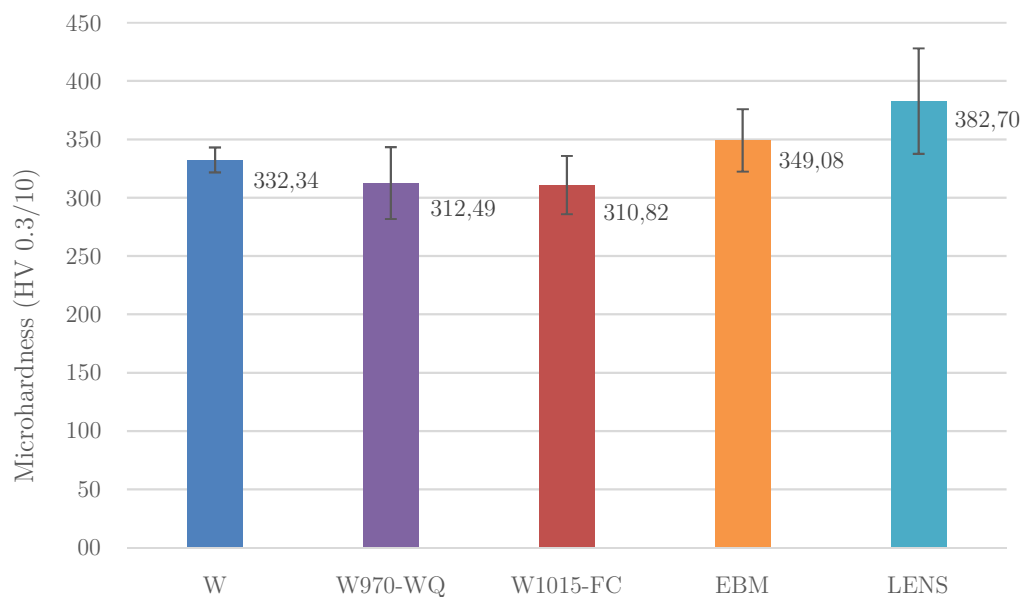


Figure 5.4: Results of microhardness test

reported the mean microhardness of three lines as a function of the distance from the side surface. At first glance, additive manufactured specimens resulted harder than the all the wrought ones due to their averagely finer microstructure compared to the more equiaxed and, in some cases, coarser  $\alpha$  phase and this is in accordance with other works [55]. The as-received wrought specimen showed the higher hardness value if compared to the treated ones. This confirms the softening role of both the thermal cycle conducted on W970-WQ and W1015-FC specimens, which have very similar hardness as better shown in the diagram in Appendix B. On average, the annealed specimen showed a slightly lower microhardness due to the grains coarsening treatment subjected. The AM specimens are well differentiated due to the occurrence of  $\alpha'$  martensite in LENS specimen. Notice that, as mentioned in Chapter 3, titanium martensitic phase has not the same embrittlement and hardening effect than that of steel martensite, thus, even if LENS is harder than EBM only slightly, this increase can be anyway lead to the presence of martensitic phase. In conclusion, since hardness is normally related to strength by a coefficient depending on the strain hardening coefficient and being strength, in turn, promoted by smaller grain size by the Hall-Patch law, it has been observed that it is possible to link also a finer microstructure with a higher hardness.

## 5.2 Fracture mechanism

Performing in situ tensile tests allowed to monitor real-time the failure mechanism of the different specimens. By the qualitative analysis based on pictures taken during tests and on the fractured surfaces, it is possible to understand fracture mechanisms. In Appendix C are reported the test sequence of pictures that precede failure. Figure 5.5 shows the last frame for each case, when fracture has occurred. At very first sight, it is possible to note that EBM specimen behaviour is strongly

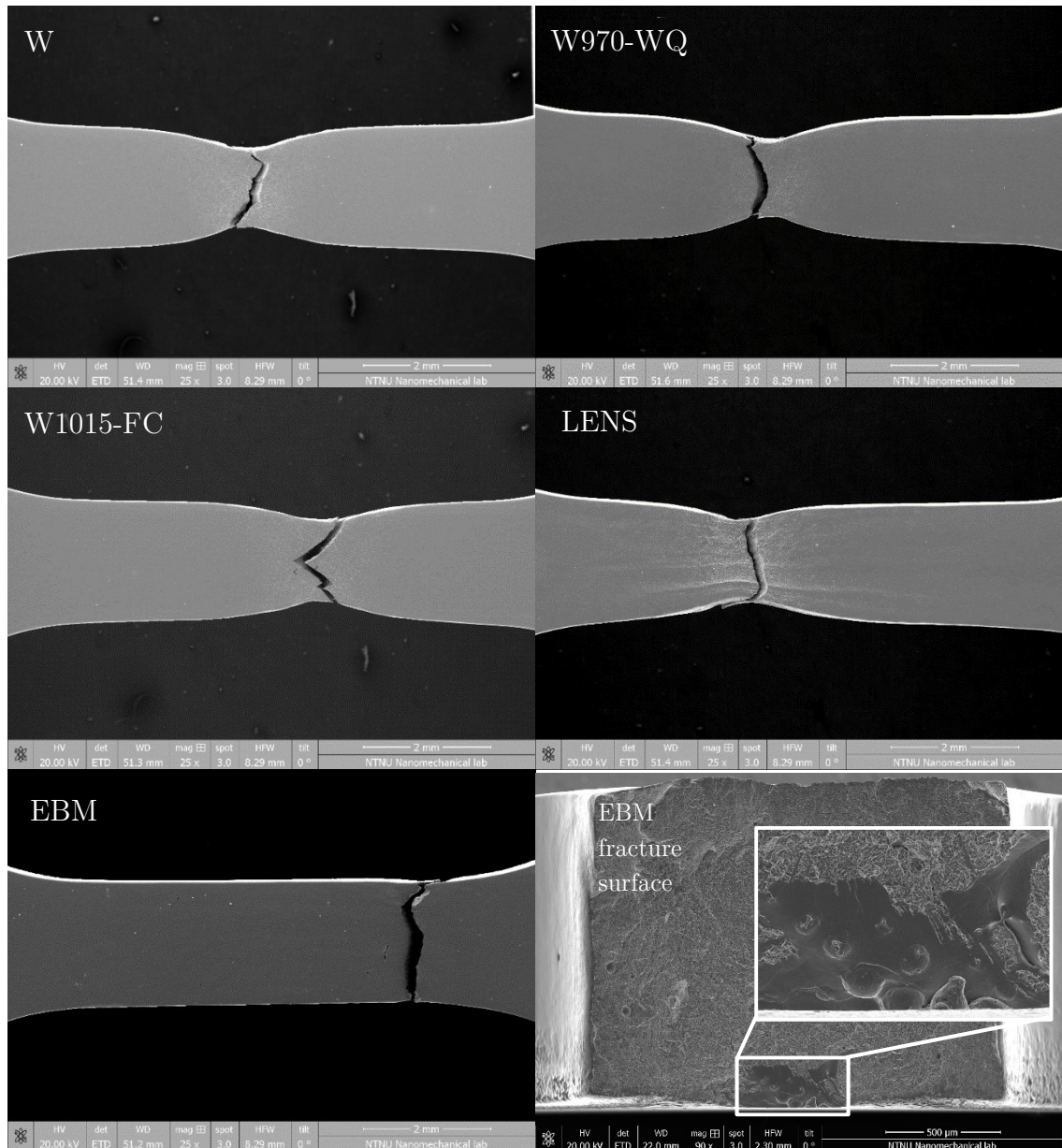


Figure 5.5: SEM pictures of specimens at the end of the *in situ* test;  
EBM one has prematurely failed due to a lack-of-fusion pore

defect-dependent since, even testing other samples, its failure occurs without even necking and never in the central part of the gage length. Indeed, as shown in Figure 5.5, in its fracture surface a lack-of-fusion pore has been found and, as written in [30], [42], this kind of defects for additive manufactured workpieces are the most fatal because of their sharpness, which acts as stress concentrator. These pores are actually cracks that occur in boundary zone of two adjacent layers where, due to the occurrence of some unfavourable conditions for effective powder melting, the

layers result weakly bonded. Since the loading direction is parallel to that of the specimen building, it tend to open the defect and make fracture happen. For this reason, specimens produced by EBM process result in a brittle behaviour. These defects are widely common in EBM products and they are usually solved with a Hot Isostatic Pressing treatment after their fabrication.

Except for premature break of EBM, which has not given cross section a chance to shrink, all the other specimens showed necking phenomenon that is the first indicator of a ductile fracture. Figure 5.6 aims to represent necking behaviour by displaying W1015-FC specimen, that in this case must be considered as representative of all the others (Appendix C shows every case). Necking mechanism is the evidence of plastic deformation resulting by exceeding yield strength and it is accompanied by shear deformation. Indeed, the plane stress condition make shear stress the main responsible of ductile fracture. For these reason, the maximum slip plane is inclined of  $45^\circ$  with respect to the tensile direction and not always this inclination is recognizable on the fracture surface, as instead occurred for the lucky case of W1015-FC shown in Figure 5.6a. Visually, shear deformation is translated in an opacification of the surface (notable in all stages before fracture in test sequence pictures in Appendix C), which at higher magnifications corresponds to the appearance of microcracks along the  $\alpha$  plates (Figure 5.6b) due to stress concentration and grains gliding along the shear direction. The plastic deformation zone appears in tortuous grain boundaries configuration induced by plastic flow and shear motion (Figure 5.6c) and at the lower level, within the grain, slip bands are visible along their slip directions which exhibit stepped staircase-like features (Figure 5.6d). Opacification is particularly evident in the LENS specimen exemplified in Figure 5.7a, where  $\alpha$  phase on the prior boundaries serves as preferential path where dislocations can freely move and damage can accumulate [46], thus delaying failure to higher elongation, and lower stress. This phenomenon

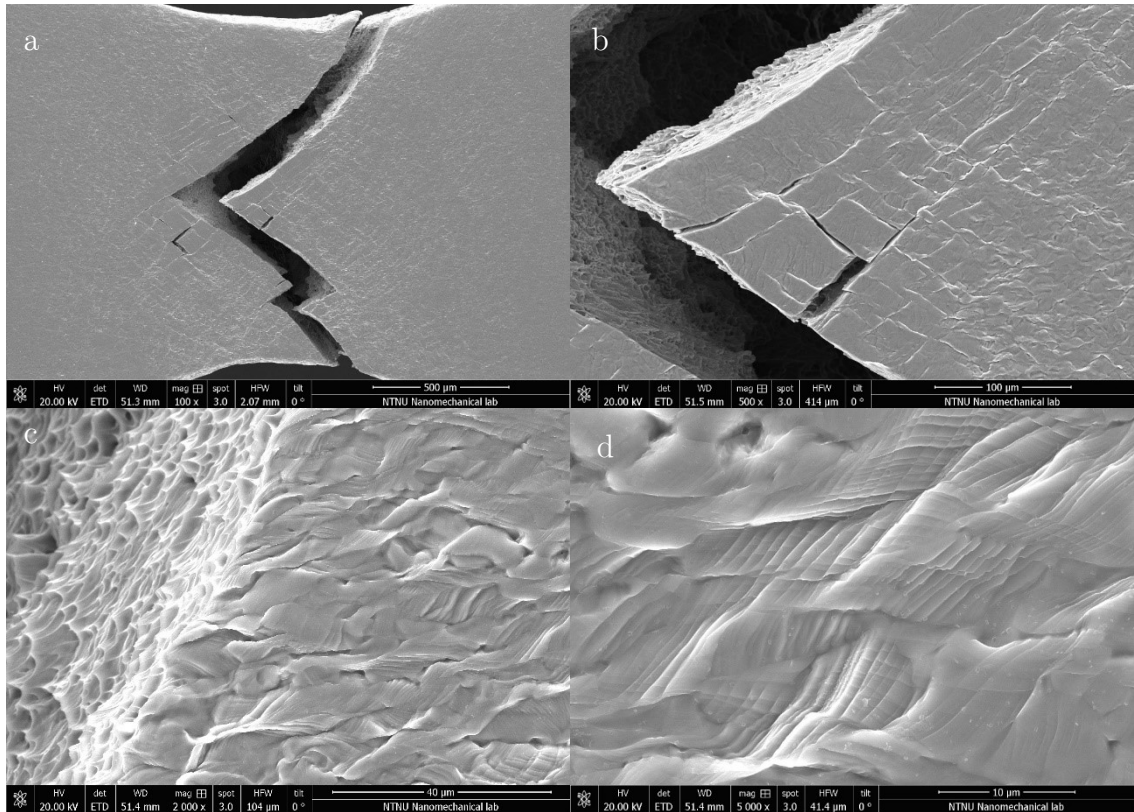


Figure 5.6: W1015-FC as representative of ductile fracture mechanism; (a) Opacification is created by (b) 45° shear bands (c) which induce chaotic grain boundary tortuosity; (d) Slip bands are visible within the grains.

is verified by tensile stress-elongation curves that will be presented later. Ductile behaviour is typical for longitudinally built AM specimens, in which tensile direction is along the growth direction of the large prior  $\beta$  grains. The opacification in LENS is highlighted by the contrast of boundary  $\alpha$  preferentially accumulating damages, versus the interior part of prior grains where basket-weaved and  $\alpha$  colonies represent barriers that inhibit damage from passing through. Hence, the sliding phenomenon is more pronounced on the prior boundaries. Furthermore, in case of both AM specimens, more tangled stretched grains due to plastic flow have been observed on the surface compared to wrought specimens (Figure 5.7b). This can be linked to the elongated and woven  $\alpha$  microstructure already present in AM specimens.

The comparison between fractographies in Figure 5.8 showed similarities on the fracture mechanisms. In all fracture surfaces two different zones have been

identified: a central one, rougher, in which micro-voids nucleated from microstructural defects or dimples and subsequently coalesced perpendicularly to the loading direction; the outer zone in the fracture surfaces represent the change in direction of the propagating crack front, tilted of approximately 45°, resulting in the so-called *cup-cone* fracture (visible also in pictures of Figure 5.5).

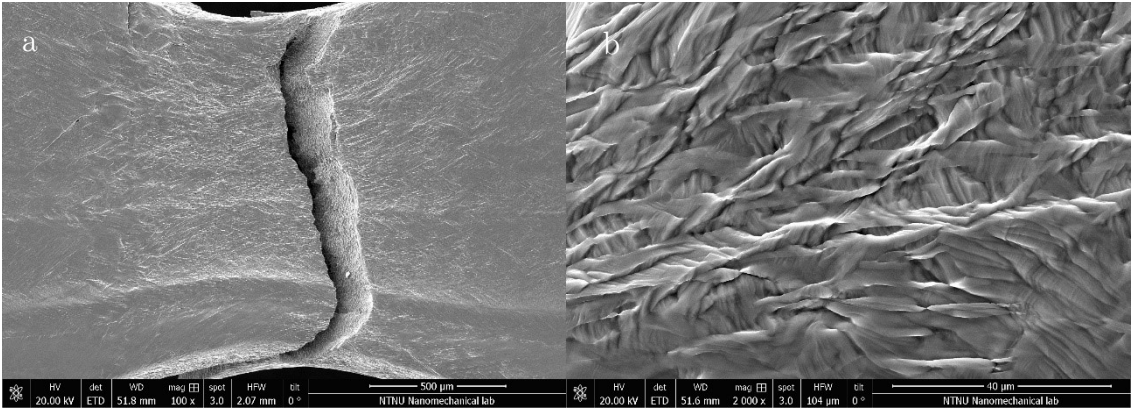


Figure 5.7: LENS specimen as representative of AM behaviour; (a)  $\alpha$  boundary on the prior grains are a privileged for damage accumulation; (b) grains are way more stretched and tortuous in AM specimens (see also Appendix C)

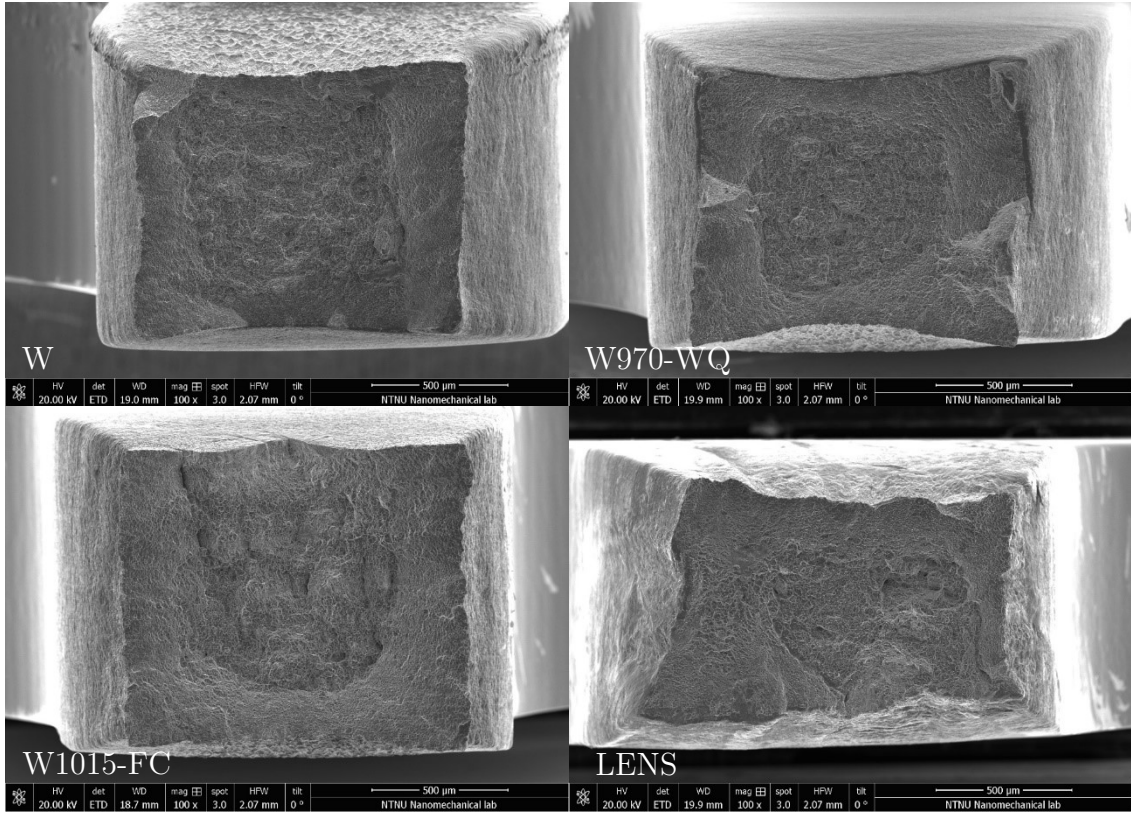


Figure 5.8: Fracture surfaces in comparison (except for EBM, shown in Figure 5.5)



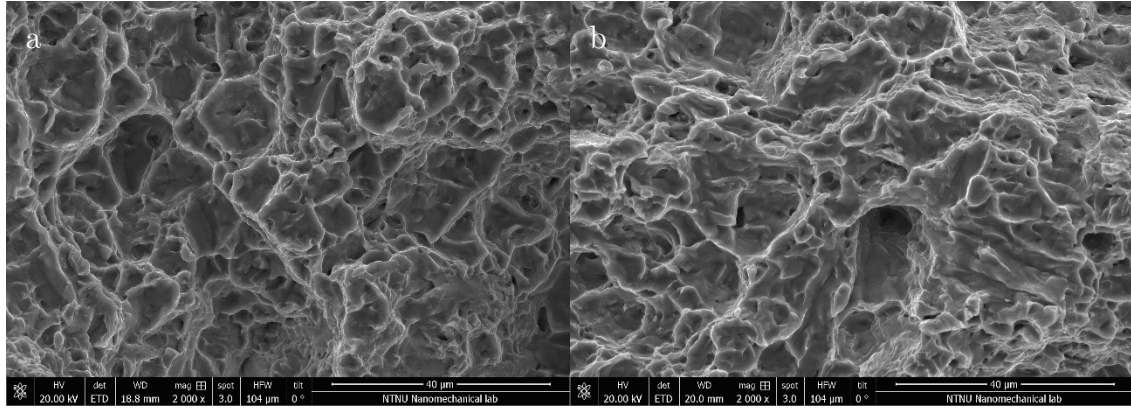


Figure 5.9: (a) W1015-FC and (b) LENS detail of the center of fracture surface

The fracture features in Figure 5.9 are representative for all wrought and AM cases (that are reported in Appendix C) and illustrate the presence of dimples in the center of fracture surface, typical causes of ductile fracture initiation. Compared to AM specimens, wrought ones showed equiaxed and slightly wider dimples, accordingly to their round-like grains, which leads to an increase of tensile ductility [59] and this comparison is consistent with previous works [55]. AM specimens showed, instead, deeper dimples which are a sign of higher elongation, due to the aforementioned preferential path for damage given by prior grains boundaries aligned with the loading direction. Despite its finer microstructure, LENS is still characterized by a ductile fracture due to its  $\beta$  matrix.

In conclusion, fractographies have shown that plastic deformation preceding failure results in maximum sliding planes  $45^\circ$  tilted due to the predominance of shear stresses, equally tilted, and it is governed by microstructure and, in AM specimens, the occurrence of bonding defects between layers. However, the fracture mechanisms observed in all the defect-free specimens consist in the nucleation of dimples in the center of the section and subsequently coalesced, which bring specimen to typical ductile failure. The common fracture process must be explained, despite different microstructural configurations, as a consequence of the coexistence of both  $\alpha$  and  $\beta$  phases in all Ti-6Al-4V specimens.

### 5.3 Mechanical properties and size effect

Small-scale tensile tests have resulted in the stress-elongation curves reported in Figure 5.10. As anticipated in the premises of in situ tests in section 4.2.3.1, the main problem in testing miniature specimen is the characterization of strain. In this case no extensometer was available, hence stress is here expressed as a function of the crosshead displacement (elongation) which has been measured by a linear encoder. Notice that this measurement contains not only the actual material elongation, but considers also elastic components of the clamps and possible slippage. Therefore, by dividing elongation by the initial gauge length of the specimen, here equal to 5000  $\mu\text{m}$ , the strain obtained results higher than it should actually be because of the just mentioned additional components included in elongation measure. The stress value is the engineering stress  $S$ , calculated as:

$$S = \frac{F}{A_0} \quad (5.1)$$

where  $F$  is the measured load and  $A_0$  the initial cross sectional area of the specimen, calculated by measuring the medium thickness of each specimen, which having been deeply polished could deviate from the nominal value. Values of cross sectional area are reported in Appendix E. Among in situ tensile tests premises, it has been stated that these analysis are a preliminary work to establish limits and opportunities of this experimental approach. With this in mind, no reliable correlations can be drawn by comparison of the different specimens due to low statistical sample available. However, it can be observed that elastic behavior is approximately coincident between specimen, thus Young's modulus appears not to be significantly affected by microstructure. Moreover, it is confirmed the higher ductility in LENS specimen that was expected after the fractographies analysis: despite martensitic phase within it, the  $\alpha$  phase boundaries contributed to accumulate damage and delayed failure, resulting in higher elongation. Instead, EBM resulted in the lower elongation value due to its premature fracture caused by a lack of fusion defect.

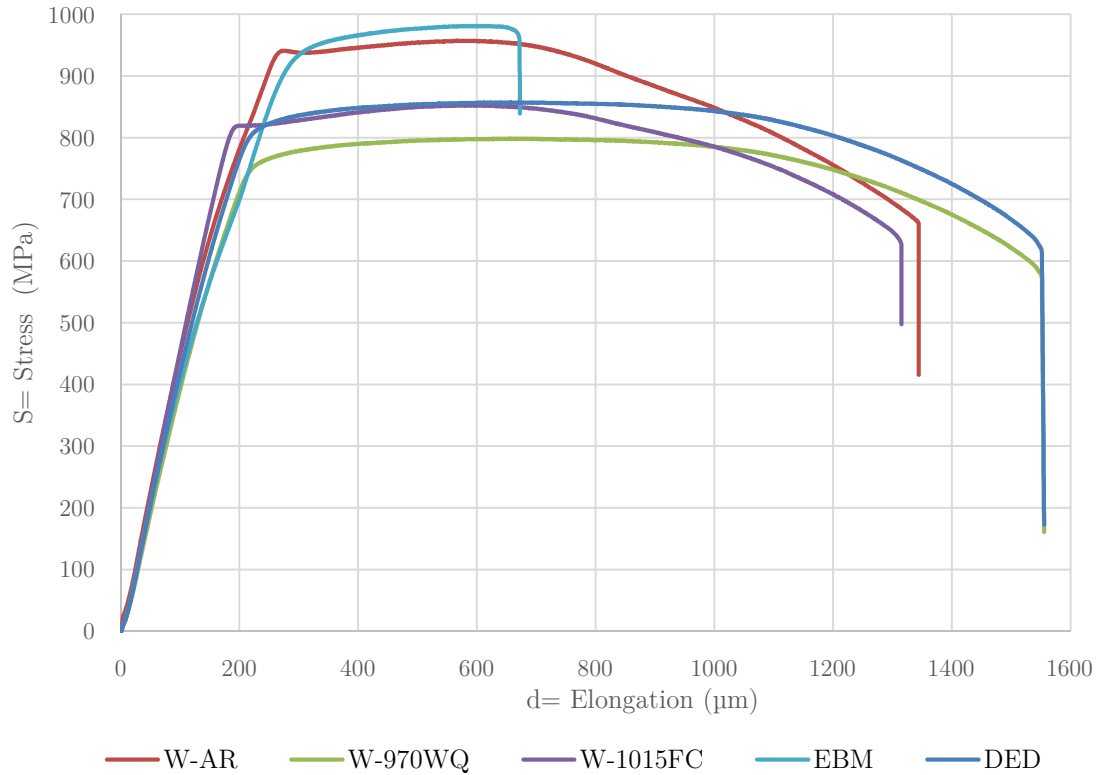


Figure 5.10: Stress- Elongation curves measured by in situ tensile tests

Reliability of small-scale investigations has been widely investigated, not only due to the characterization of strain, but also because of the awareness of possible “size effects”. The term “size effect” refers to a variation in mechanical response with decreasing component or specimen sizes. Models and experimental procedures have been developed in order to take it into account and, possibly, predict the material behaviour in case of decreasing in scale. It has been pointed out that “size effect” in metallic materials may appear as the component scale approaches the order of magnitude of its material grains. Often this “size effect” can also occur when the specimen sizes become sufficiently small relatively to the spatial distribution of critical defects [5]. In other words, a smaller section has a lower probability of being affected by the defects, the size of which often depends on manufacturing or material constraints and thus they can be equally found in both micro and macro workpieces. Sometimes “size effect” is translated into a “grain-size effect” considering the contribute given by the ratio  $N$  between a characteristic dimension

of the specimen and the average grain size. It has been observed in various tensile conditions and for different alloys, that the grain size effect ruled by Hall-Patch law is significant at all scales until the  $N$  ratio value is around 10-15. At that point it has been noted that this “grain-size effect” starts to affect the material behaviour by a decrease in the flow stress, reaching a minimum value for  $N$  in the range of about 2-4, and then increasing again for decreasing  $N$  [6].

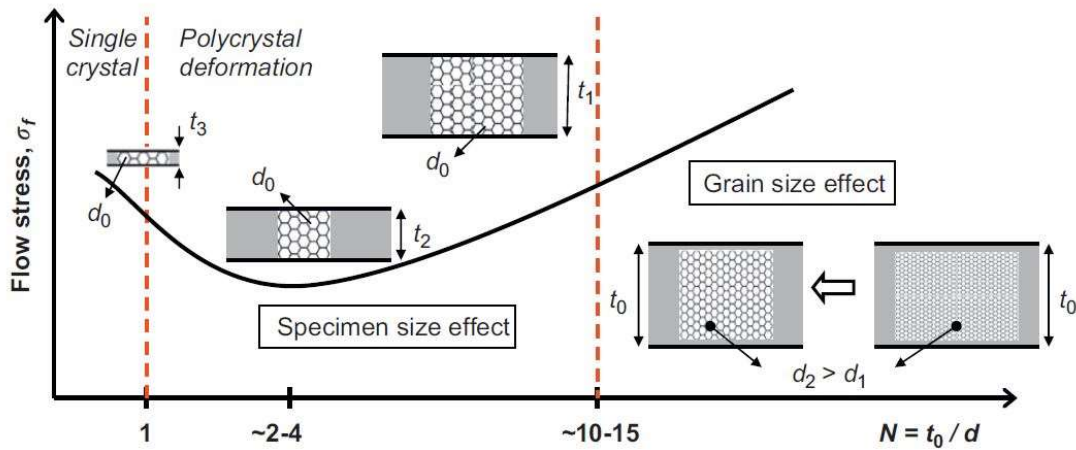


Figure 5.11: Grain vs. specimen size effect on the flow stress as a function of  $N$  [6]

Figure 5.11 illustrates this prediction model on flow stress, which is the instantaneous value of stress required to sustain plastic deformation at a particular strain. Practically, since flow stress expresses a middle value between yield strength and ultimate strength, it can be considered the dominant stress in the strain hardening zone of the tensile curve and it is modeled as the Hollomons equation:

$$Y_f = K \varepsilon^n$$

where  $Y_f$  is the flow stress,  $K$  is the strength coefficient,  $\varepsilon$  is the instantaneous strain and  $n$  is the strain hardening exponent.

Therefore, in this work strain hardening effect has been evaluated in order to investigate if a similar influence can be verified by the considered Ti-6Al-4V miniature specimens. An experimental procedure to determine strain hardening exponent has been found in the Ramberg-Osgood relationship [60]. R-O formulation

provides the same exponential relationship between stress and strain given by Hollomons with some precautions. At first, R-O equation is often formulated by using true strain  $\varepsilon$  and true stress  $\sigma$ , which are defined as:

$$\varepsilon = \ln \frac{L}{L_0} \quad , \quad \sigma = \frac{FL}{A_0 L_0} \quad (5.3)$$

where  $L$  is the current length,  $L_0$  is the initial gauge length,  $F$  and  $A_0$  as above. Hence, these values have been obtained following ASTM standards [61]:

$$\varepsilon = \ln(1 + e) \quad , \quad \sigma = S(1 + e) \quad (5.4)$$

where  $e$  is engineering strain here approximated as:

$$e = \frac{d}{L_0} \quad (5.5)$$

where  $d$  is the elongation measured during the test and  $L_0$  is equal to 5000  $\mu\text{m}$ .

Ramberg-Osgood exponential relationship is given as follows:

$$\sigma = H\varepsilon_p^n \quad (5.6)$$

where  $H$  is a strength coefficient,  $n$  is the strain hardening exponent and  $\varepsilon_p$  is the plastic true stress. Indeed, the formulation proposed by Ramberg and Osgood considers strain as a sum of the elastic and plastic strain contributes:

$$\varepsilon = \varepsilon_e + \varepsilon_p \quad (5.7)$$

as illustrated also in Figure 5.12a.

Since elastic strain is proportional to stress according to:

$$\varepsilon_e = \frac{\sigma}{E} \quad (5.8)$$

where  $E$  is the elastic modulus, the plastic component in R-O relationship can be calculated as:

$$\varepsilon_p = \varepsilon - \frac{\sigma}{E} \quad (5.9)$$

Thus, Young's modulus  $E$  has been extracted as slope of the elastic part of the  $\sigma - \varepsilon$  curve (true stress-true strain calculated curve) and reported in Appendix E. Then, the plastic strain has been calculated following the (5.9) for a range of equivalent elongation values included between 300 and 600  $\mu\text{m}$ , which corresponds to the strain hardening behavior zone on the tensile curve. By plotting  $\sigma - \varepsilon_p$

relationship expressed in (5.6) in a log-log plot,  $H$  results to be the value of  $\sigma$  at  $\varepsilon_p=1$ , and  $n$  is the slope of the log-log plot reported in red in Figure 5.12b, where total strain  $\varepsilon$  is plotted and at large strains, it approaches the plastic strain line of slope  $n$ . Values of  $n$  close to 0 lead to perfectly plastic materials, while values near 1 indicate perfectly elastic behaviors. Values of  $n$  and  $H$  coefficients are reported in Table 5.1 with the reference ones obtained at the same strain rates ( $10^{-3} \text{ s}^{-1}$ ). Figure 5.13 also reports a comparison diagram for strain hardening exponents of Table 5.1. Firstly, the calculated values of strain hardening exponents resulted in being similar for all the specimens, meaning that there is no evidence for a microstructure influence on strain hardening behavior at this scale. Furthermore, by comparison with reference values measured on standard-size specimens, both strain hardening exponent and strength coefficient result of the same order of magnitude, which leads to conclude that strain hardening behavior does not appear to be affected by size effect neither. Anyway, it is worth reminding that accuracy of the calculation just described is based on the assumption that engineering strain  $e$  has been estimated using the measure of the crosshead displacement during the static test, which does not correspond to local material strain.

Anyway, another investigation on possible size effect has been carried out, for which it has been possible to develop a more realistic approach to evaluate strain. This method is based on the estimation of material elongation by measuring on the test

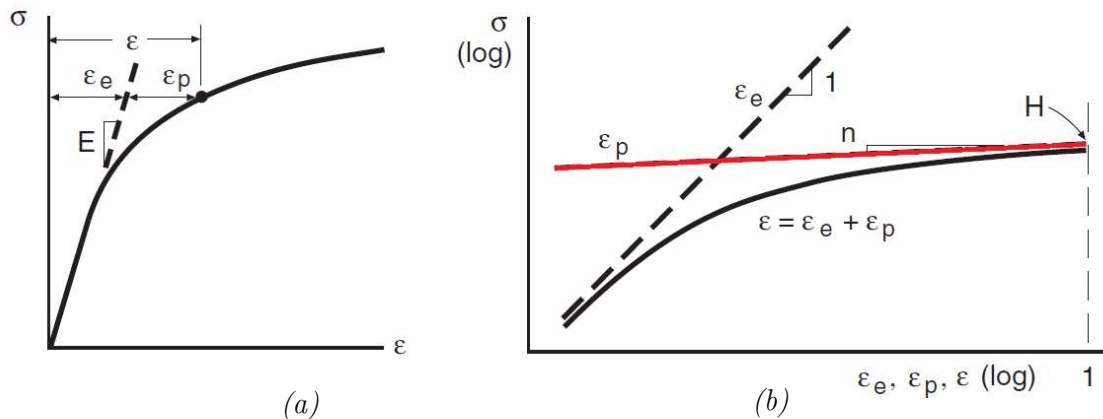


Figure 5.12: Stress–strain curves on linear and logarithmic coordinates for the Ramberg-Osgood relationship [60]

	<b>n</b>	<b>H (MPa)</b>
W	0.0554	1240.085
W970-WQ	0.0594	1042.972
W1015-FC	0.0718	1149.403
EBM	0.0603	1297.432
LENS	0.0594	1119.912
Ref1 [62]	0.040	1050
Ref2 [63]	0.085	895

Table 5.1: Strain hardening coefficient values: calculated with experimental data and reference values for the same strain rate

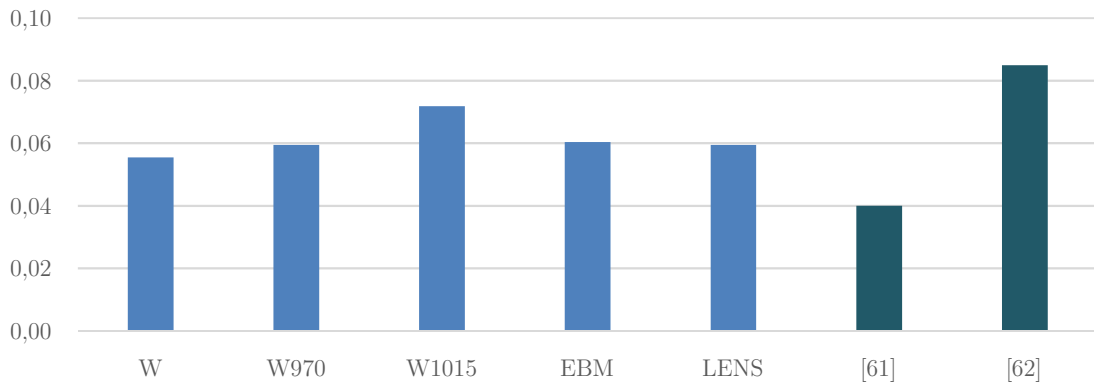


Figure 5.13: Strain hardening exponents compared to reference values reported in Table 5.1

sequence photograms the displacement of two known points on its surface, through a proportion with the reported scale. By calculating the difference between the distance of the know points in two subsequent photograms, the material elongation is given by dividing it for the initial distance as:

$$e = \frac{L_f - L_0}{L_0} \quad (5.10)$$

where  $L_0$  is the initial length measured in the first photogram and  $L_f$  is length obtained in the following picture. Since photograms are not directly correlated to a specific point on the tensile curve, the only moment of the test in which strain was evaluable with a restrained error was the failure. Hence, the first photogram of the test sequence has been compared with the one just before the crack occurrence, and elongation has been estimated as illustrated in Figure 5.14 and described by (5.10).

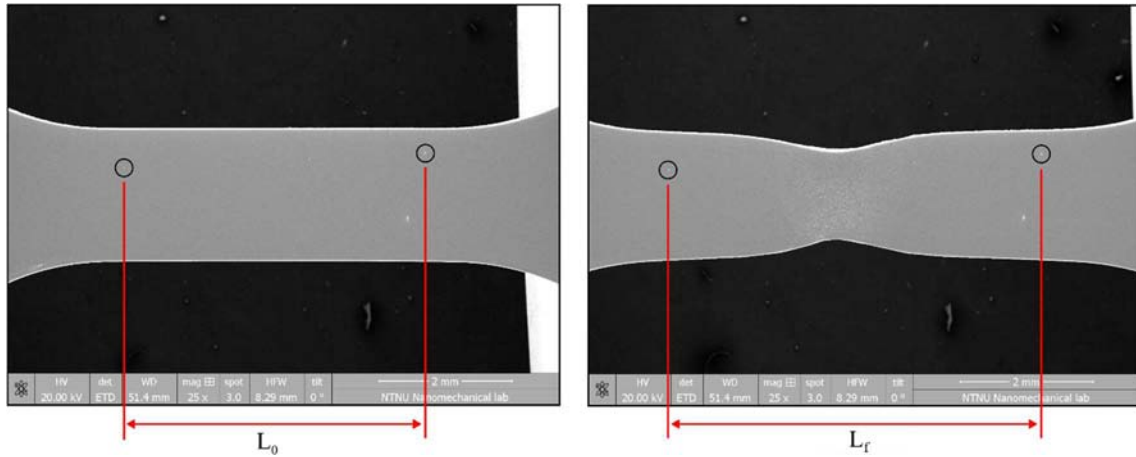


Figure 5.14: Graphical method to measure fracture strain

The accuracy of this method relies on the stability of camera (in this case of the detector of SEM), on the resolution of pictures and on the uncertainty of the length measure. However, compared to strain estimation by means of the crosshead displacement, this measurement is free from grips compliance and slippage components.

The graphical method has been adopted in this study to evaluate strain to failure for each specimens, in order to make a comparison with standard-size specimens. The Table 5.2 summarises the values estimated for the miniature specimens tested and some references from literature referred to standard ones.

Considering all the different specimens as a unique sample representative for the generic miniature specimen tested in this work, a significant increase of elongation to failure is observed in small-scale tested specimens. This finding is also consistent with what it has been proved in the comparative study reported in [52], where the

Specimen	e %	Reference	e %
W	24.18	[52] W	1.2 - 15.1
W970-WQ	21.9	[9] W solution treated	16
W1015-FC	29.4	[30] EBM	1.7 - 14.9
EBM	7	[30] DED	10.8 - 11.9
LENS	33.6		

Table 5.2: Strain to failure calculated and reported in other works



displacement was more accurately measured by means of a laser extensometer. This means that for small specimens, failure occurs later than for standard ones. Since, in the common practice, elongation to failure value is mostly controlled by the amount of internal defects, this “super-ductile” behaviour can be interpreted as a lower incidence of defects in a specimens with sizes comparable to theirs. Therefore, one of the consequences of size effect has been detected and it leads to a delayed failure of miniature specimens under tensile loading, likely due to a decreasing dependence on defects by decreasing of specimens sizes.



# Conclusions

The results obtained by in situ testing on wrought and additively manufactured Ti-6Al-4V miniature specimens have underlined some findings on experimental techniques.

Firstly, the effectiveness of heat treating Ti-6Al-4V miniature specimen cannot rely on the small sizes of the specimen in order to contain solution treatment time, but rather on a practical solution to ensure the actual temperature reached by the specimen in the vacuum atmosphere, where the workpiece must be put not to oxidize. The temperature gradient while processing and the cooling rate significantly affects microstructure: a sufficiently long permanence of the workpiece above the  $\beta$  transus temperature combined with a subsequent slow cooling allows most of  $\alpha$  to dissolve into  $\beta$  phase and solidify as coarse equiaxed grains, while the fast cooling rate to which an AM component is subjected while processing activates displacive mechanisms that result in lamellar basket-weaved or acicular martensitic microstructure. The latter has been recognized in the Laser Engineering Net Shape specimen, and confirmed by its high microhardness value, generated by a highly focused beam which creates a high temperature gradient, leading to fast cooling and inhibiting diffusive processes. The weaved pattern within relatively thin prior  $\beta$  grains have been noticed in specimens manufactured by means of Electron Beam Melting technology, where, since the beam is less focused and the powder bed is pre-heated, the temperature gradient is lower.

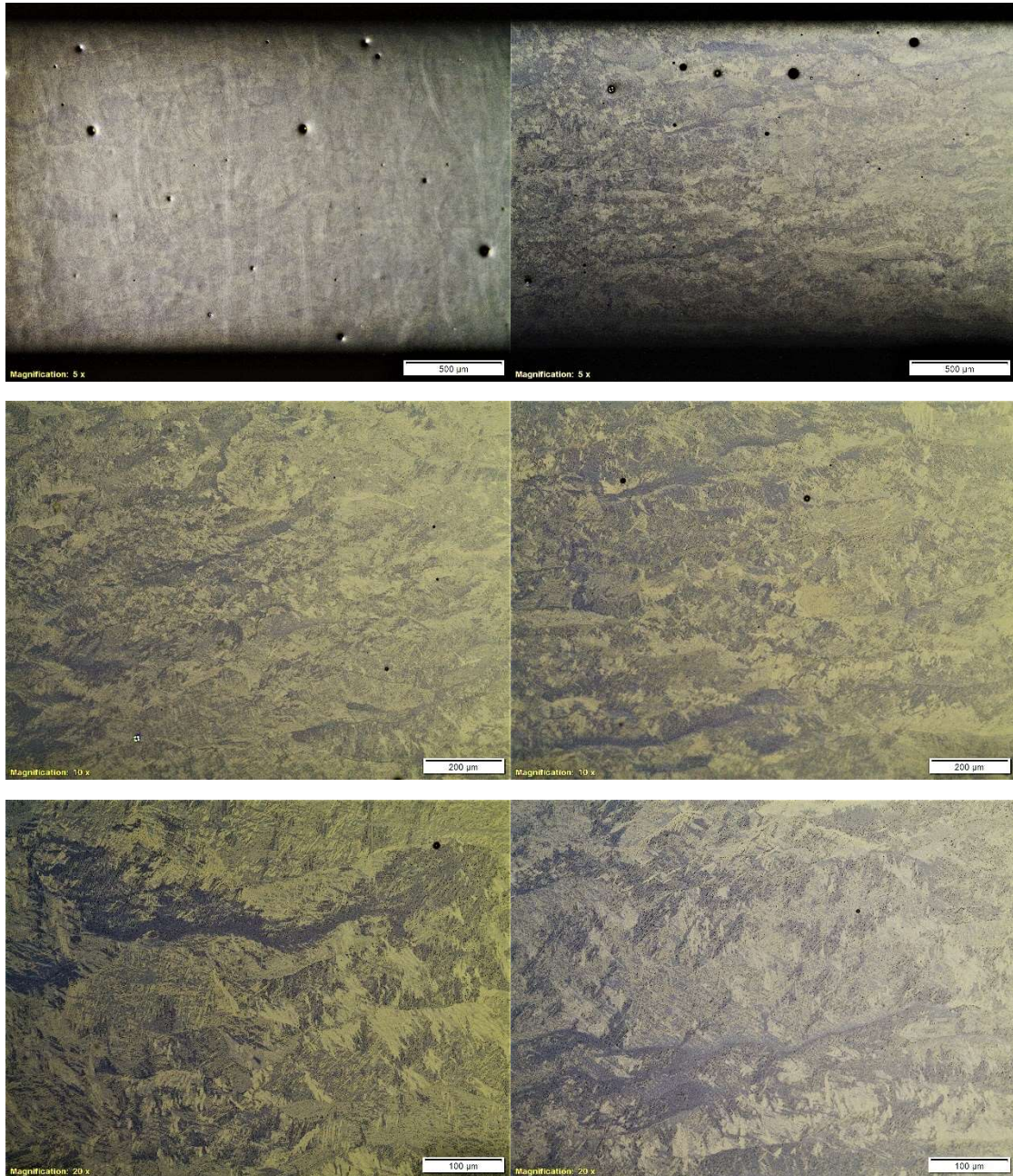
By performing in situ tensile tests, ductile fracture mechanisms have been observed among all the tested specimens because of the coexistence of  $\alpha$  grains and  $\beta$  matrix, despite different microstructure configurations. However, the behavior of specimens fabricated by Electron Beam Melting technique is consistently defects-dependent due to the frequent presence of lack-of-fusion pores which can cause premature failure.

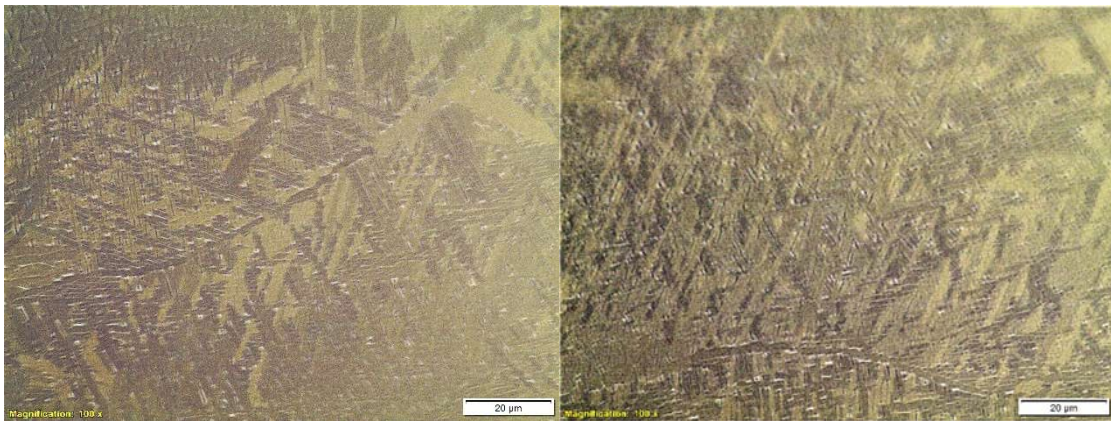
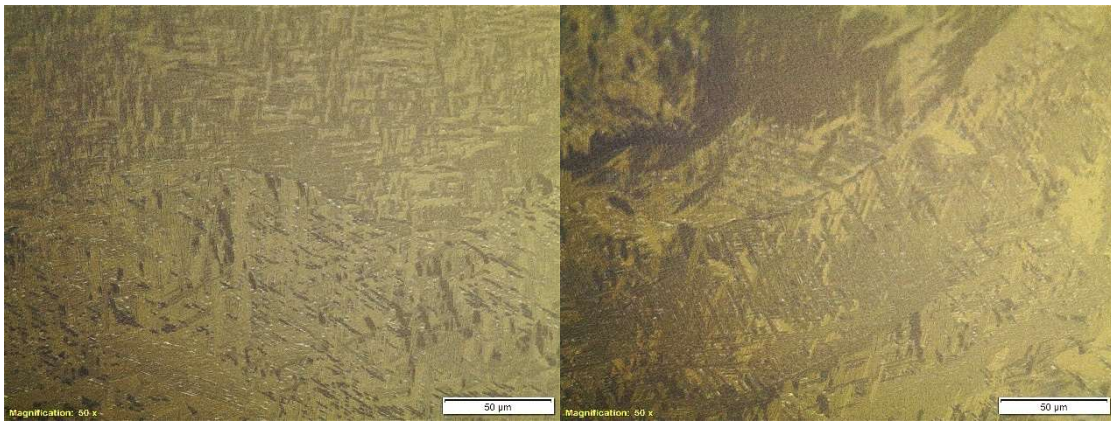
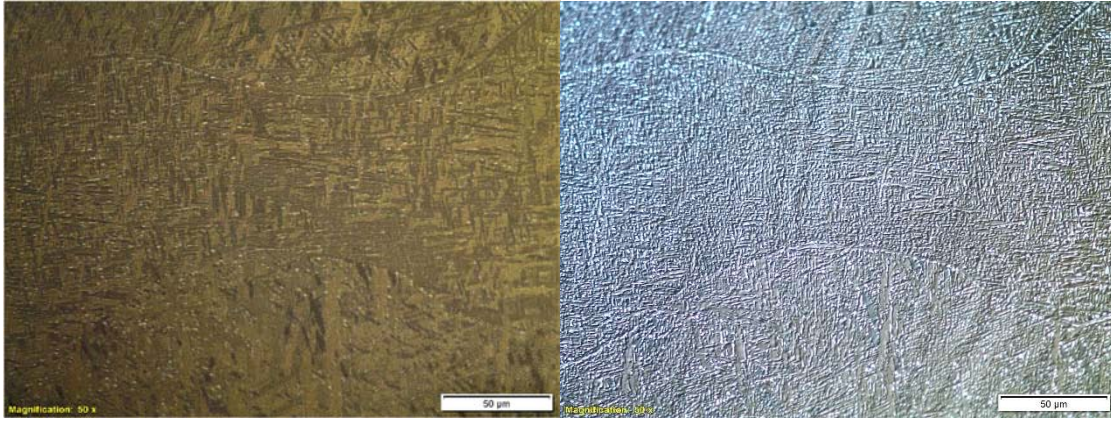
Static stress-elongation curves have been derived, highlighting uncertainties on data interpretation linked both to the scarce sample of processable tests due to the accurate preparation required for the experimental apparatus, and both to the possibility of a “size effect” that would make tensile curves less predictable because of the variation of mechanical properties with decreasing specimen sizes. Therefore, strain hardening behaviour has been investigated by means of the Ramberg-Osgood formulation and no evidence for the “size effect” has been found related to that. Strain hardening does not appear to be affected from the microstructure either. However, since no extensometer was available, the calculation of engineering strain does not correspond to the actual material one because also compliance grip and slippage components are contained in the crosshead displacement measure. A graphical method has been proposed in this regard, based on the measurement of the distance between two known points in two subsequent test sequence photograms. Despite its dependence on the quality of the imaging process, this procedure is more realistically applicable to calculate the elongation to failure of the specimens. This calculation highlighted that failure seems delayed in miniature specimens, likely due to a lower incidence of defects related to “size effect”.

In conclusion, since in situ tests are generally conducted on equipments and specimens tailored for specific purposes, the need for common experimental criteria is strongly felt in order to unify results and pave the way to the developing of more systematic models for prediction of “size effects”. Many improvements on the experimental method can be easily brought through experience, in order to fully exploit the numerous and interesting potentialities that this method can offer for in-depth material characterization.

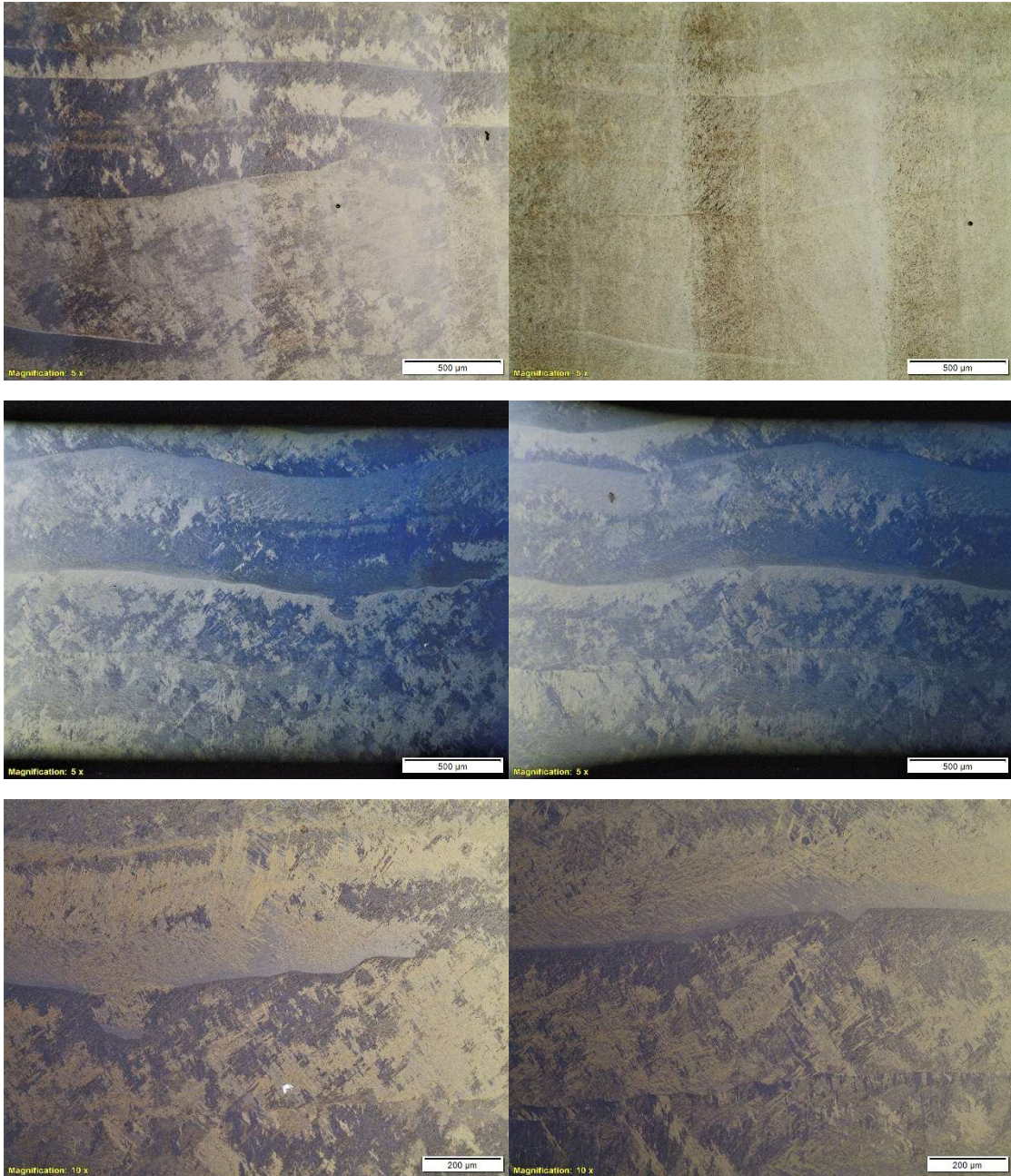
# Appendix A: AM Micrographies

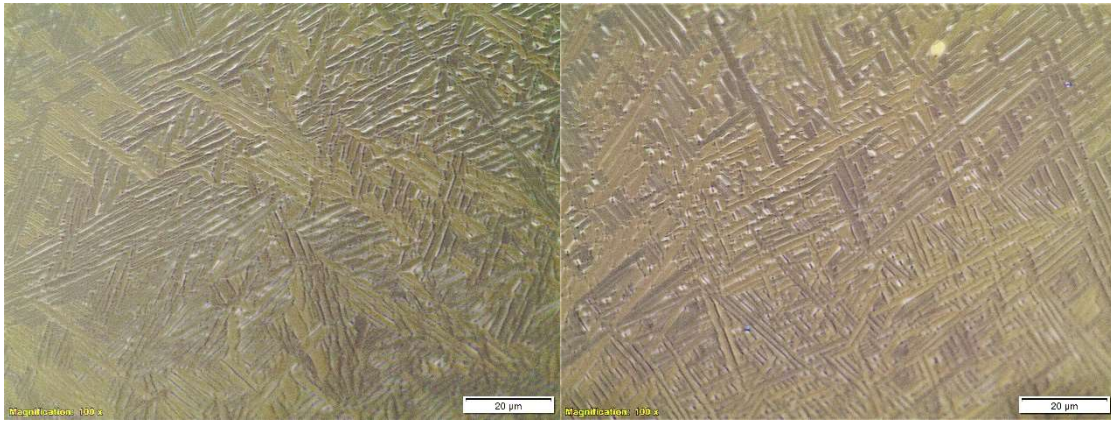
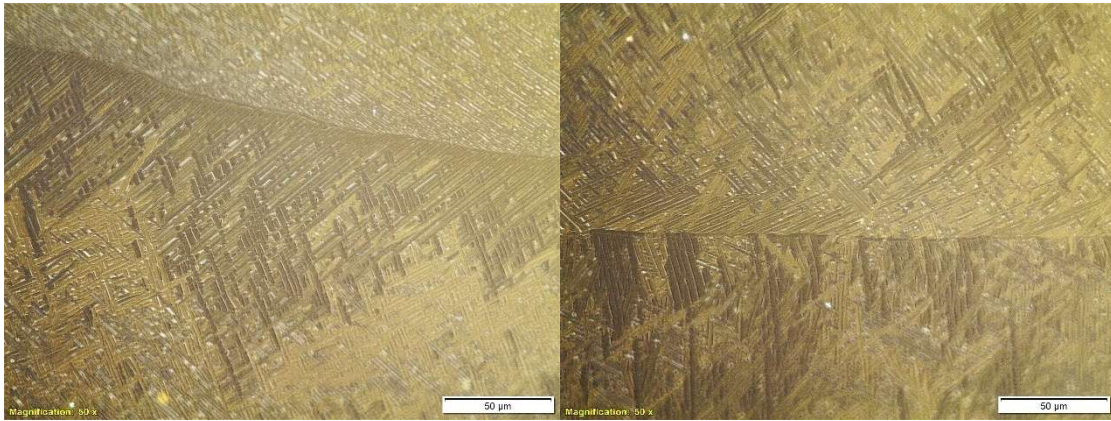
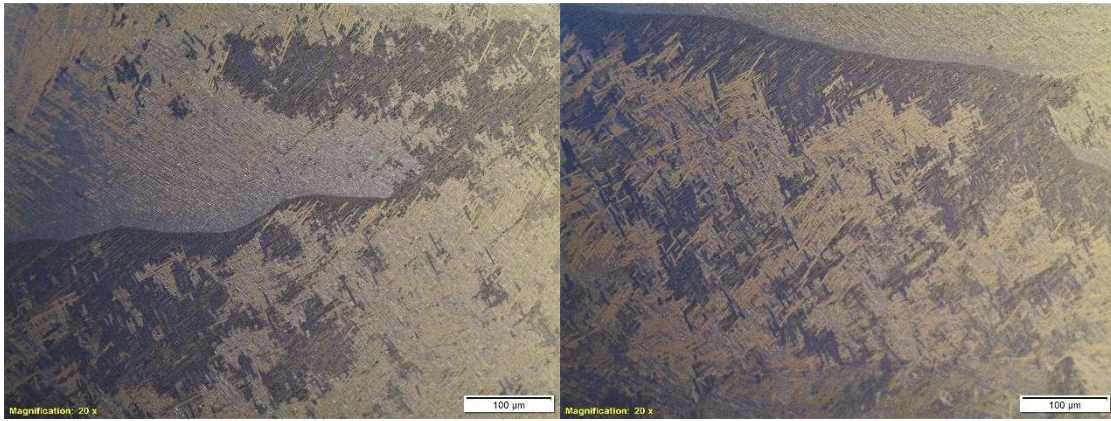
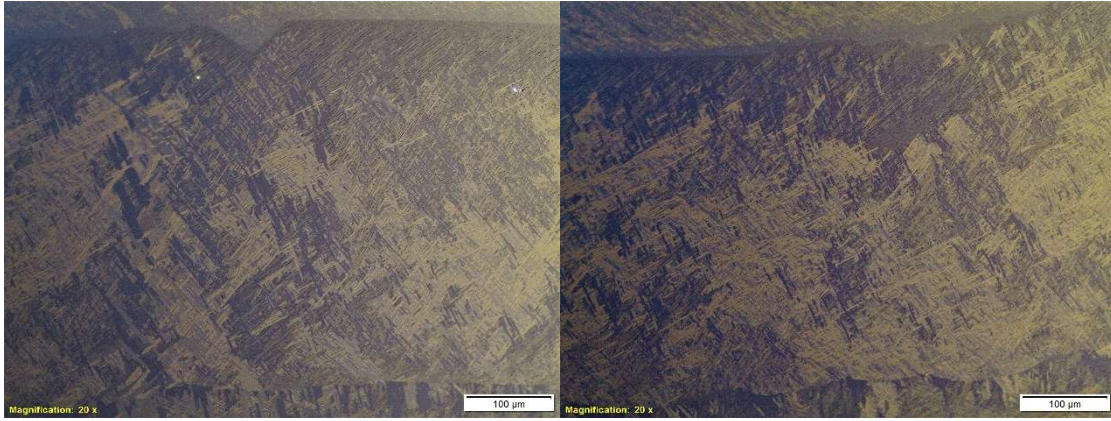
*EBM micrography.* Prior  $\beta$  grains 10-20  $\mu\text{m}$  wide,  $\alpha$  basket-weaved platelets.





*LENS micrography*: layer thickness of 508  $\mu\text{m}$  visible in the first two pictures taken with polarized lens; Prior  $\beta$  grains 500  $\mu\text{m}$  wide, acicular  $\alpha'$  and basket-weaved  $\alpha$

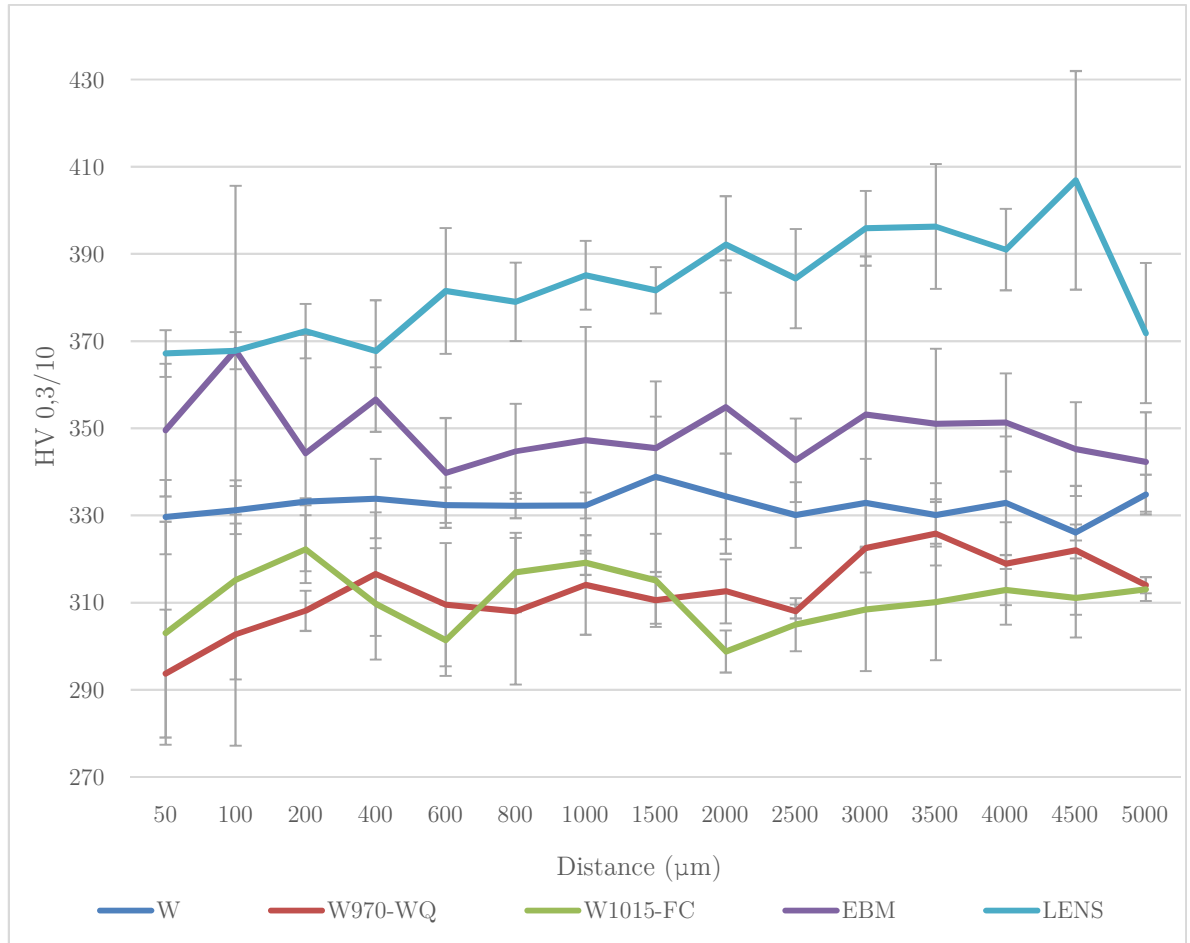






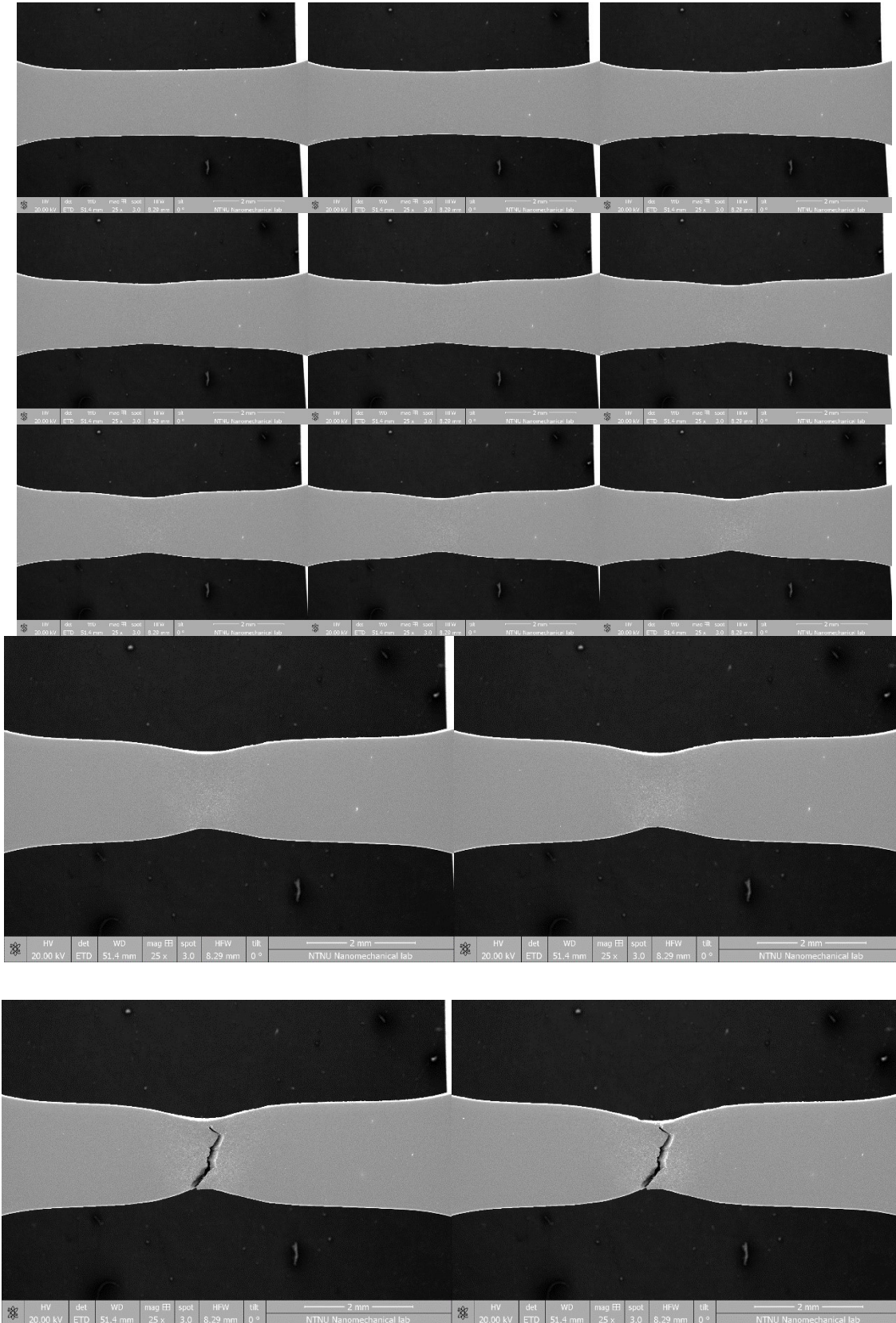
# Appendix B: Microhardness

Microhardness profiles as a function of the distance from the surface; The plotted values are equal to the mean between three lines measurements (see Figure 4.16).

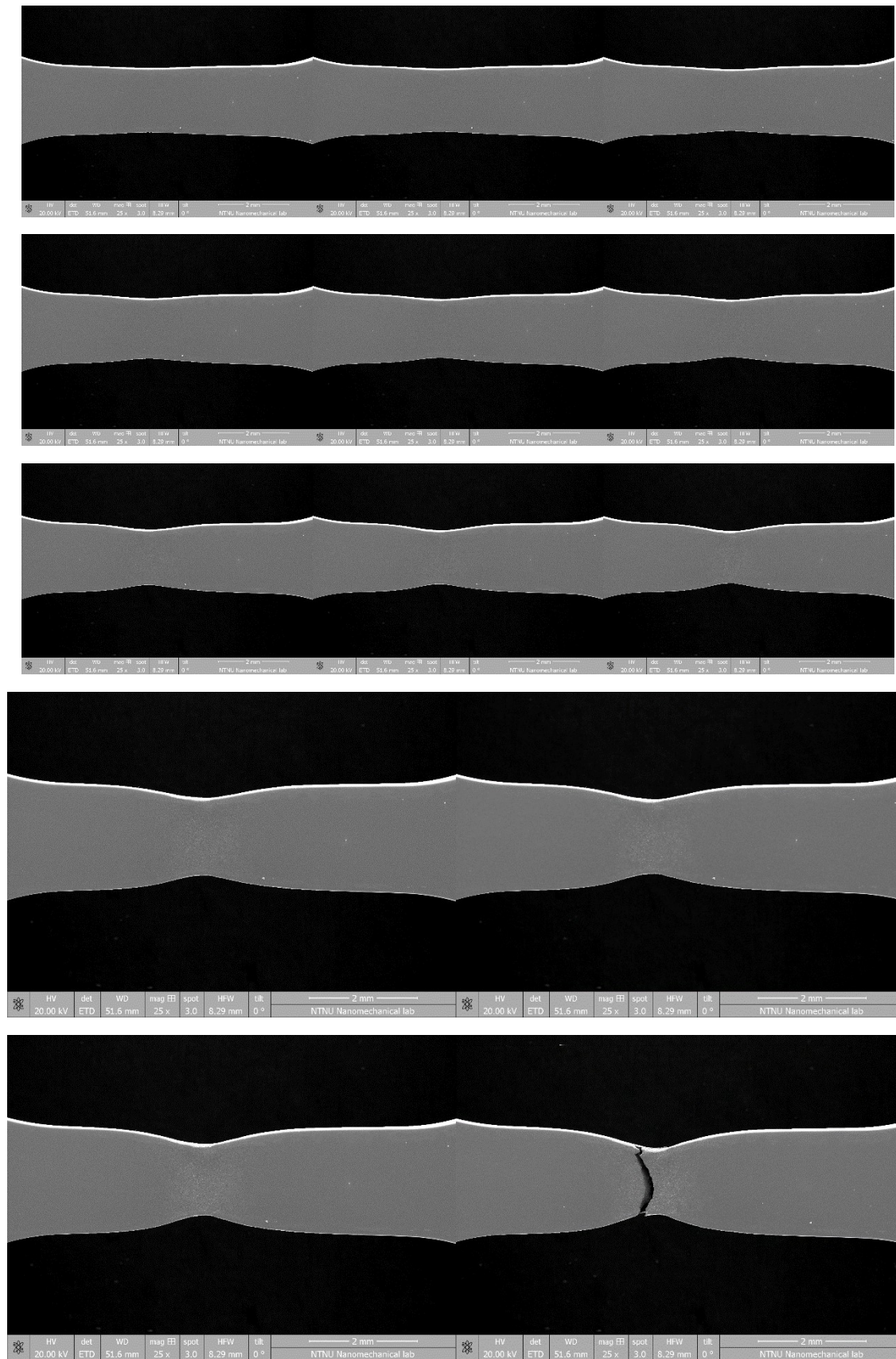


# Appendix C: Test sequences

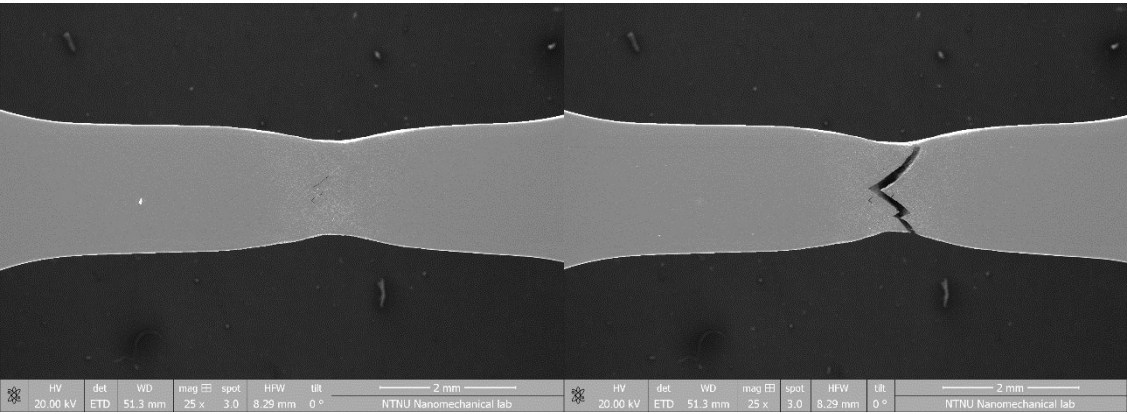
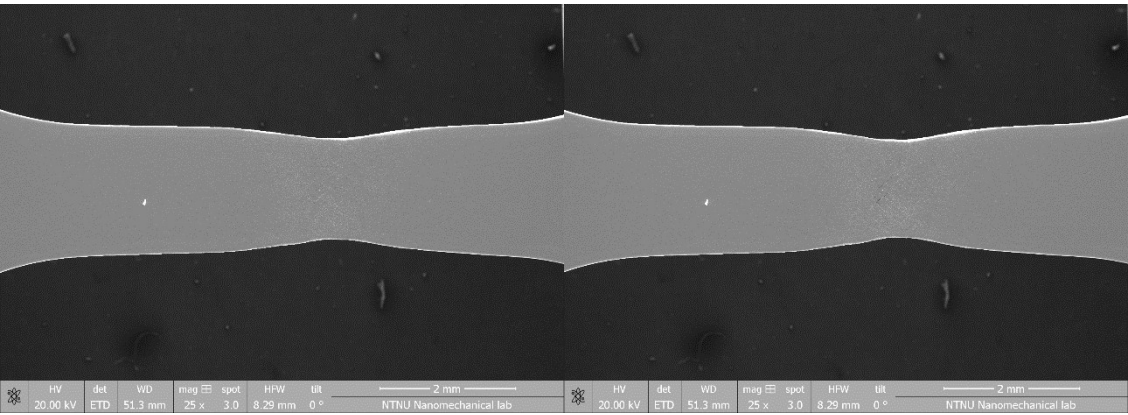
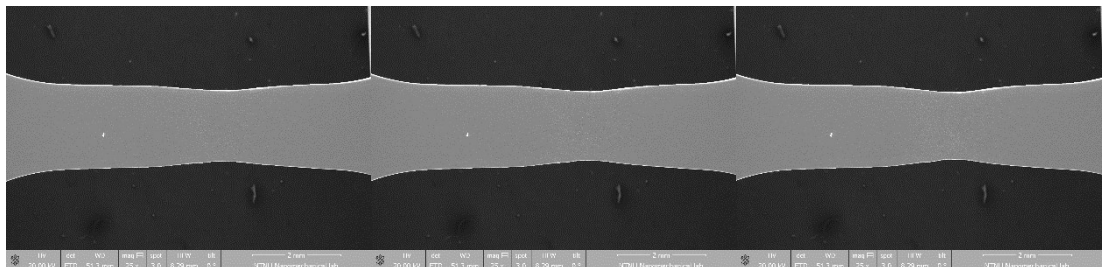
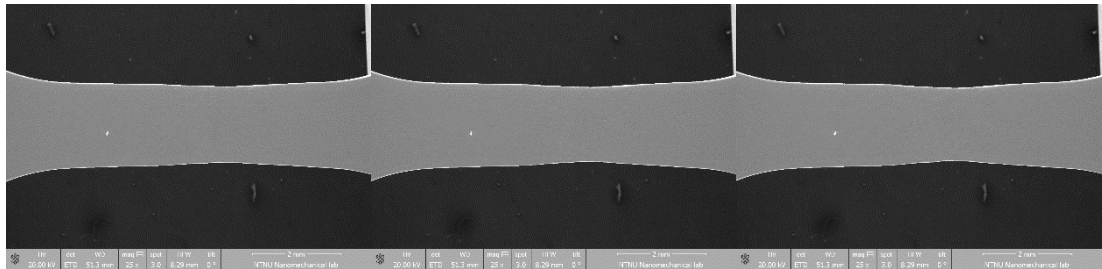
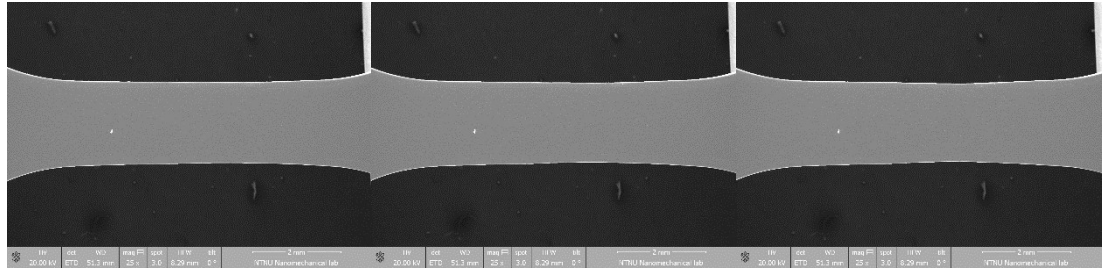
*Last steps of in situ test sequence for W*



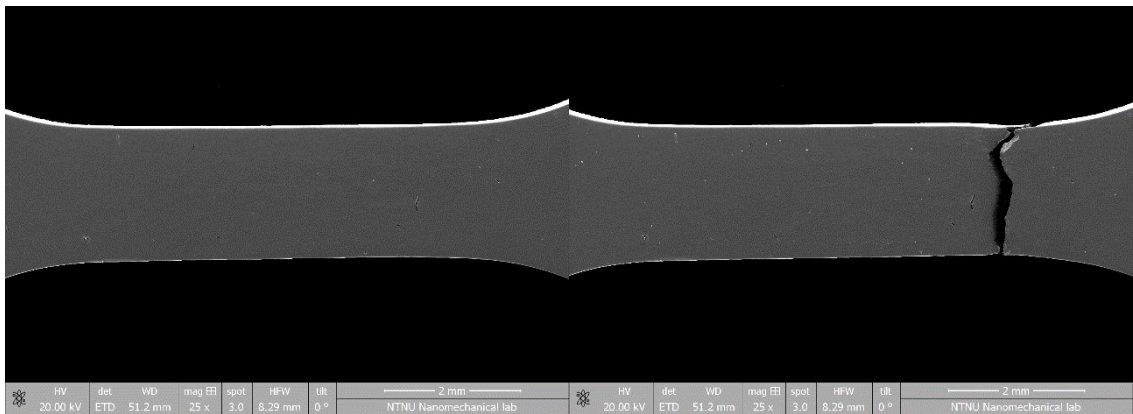
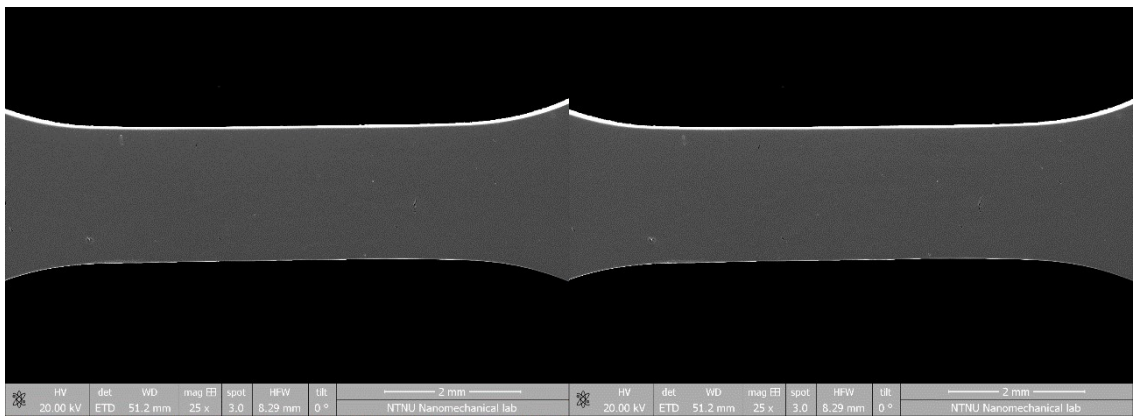
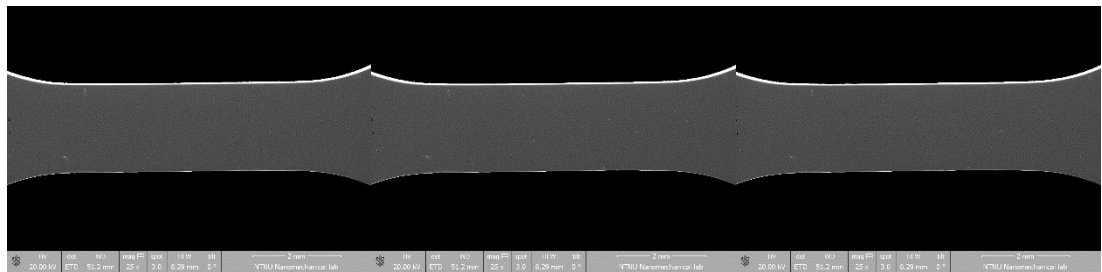
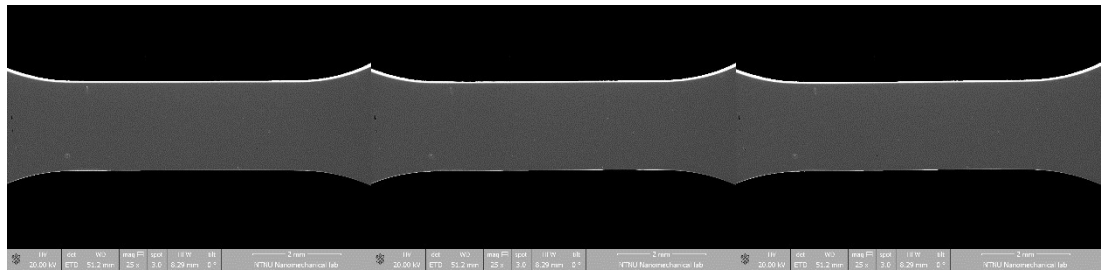
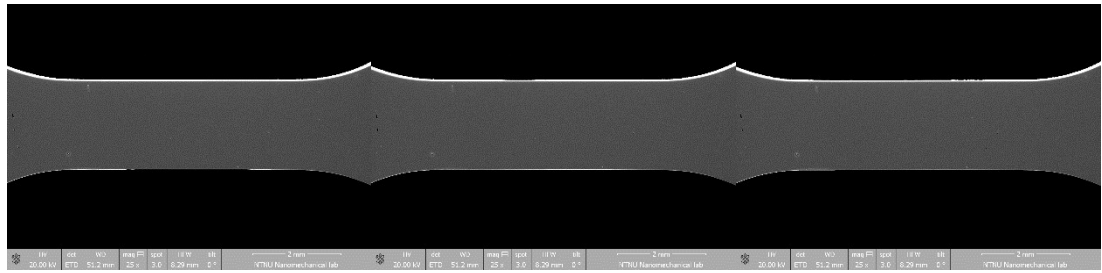
*Last steps of in situ test sequence for W970-WQ*



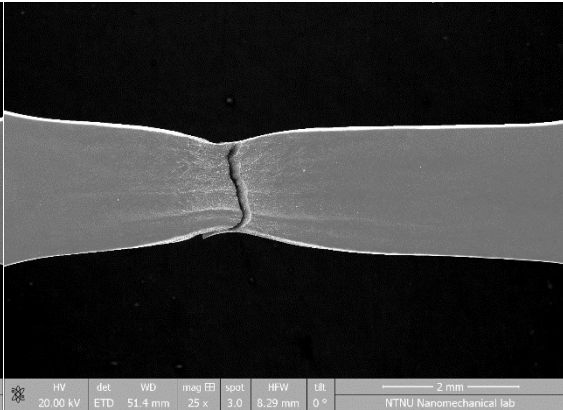
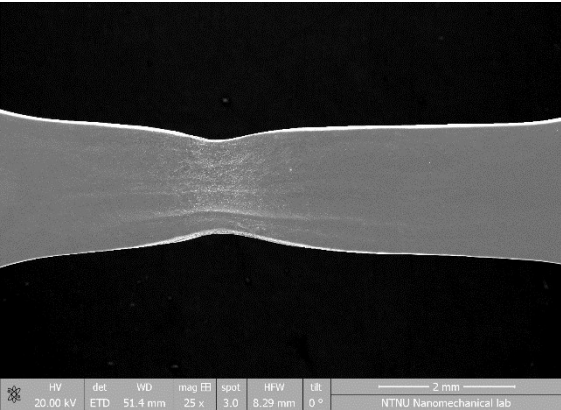
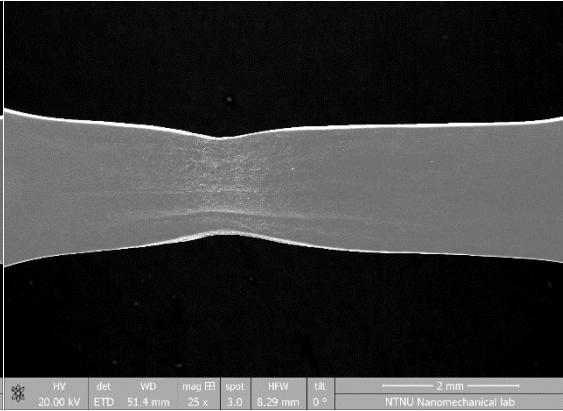
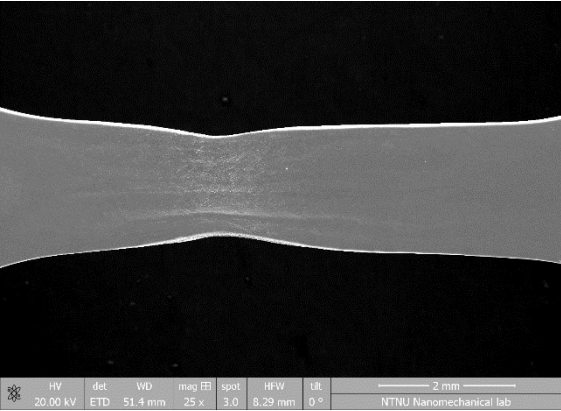
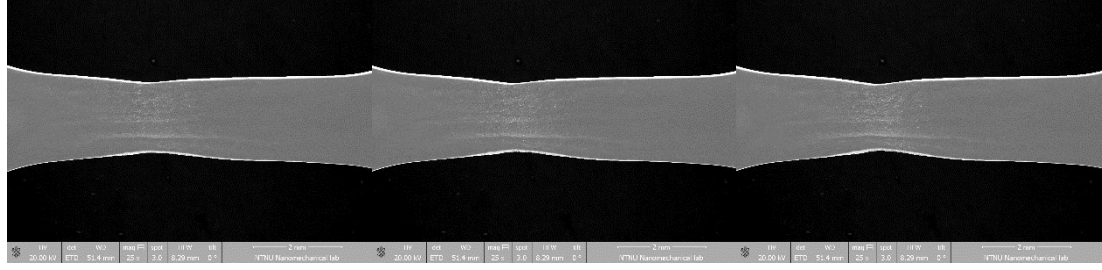
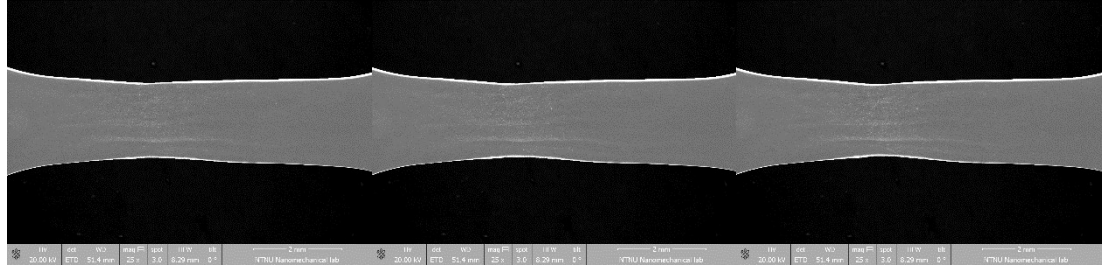
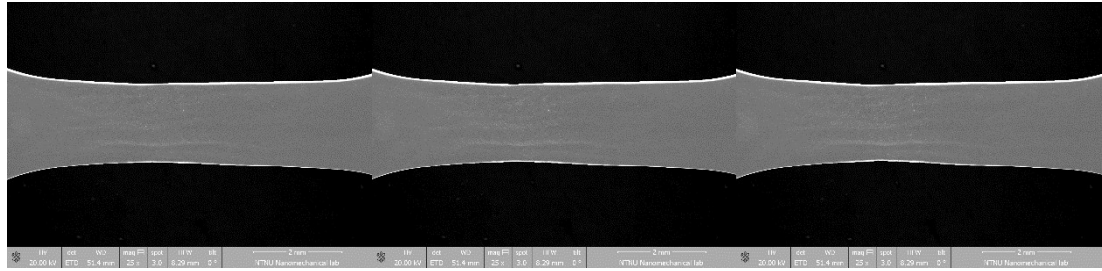
*Last steps of situ test sequence for W1015-FC*



*Last steps of situ test sequence for EBM*

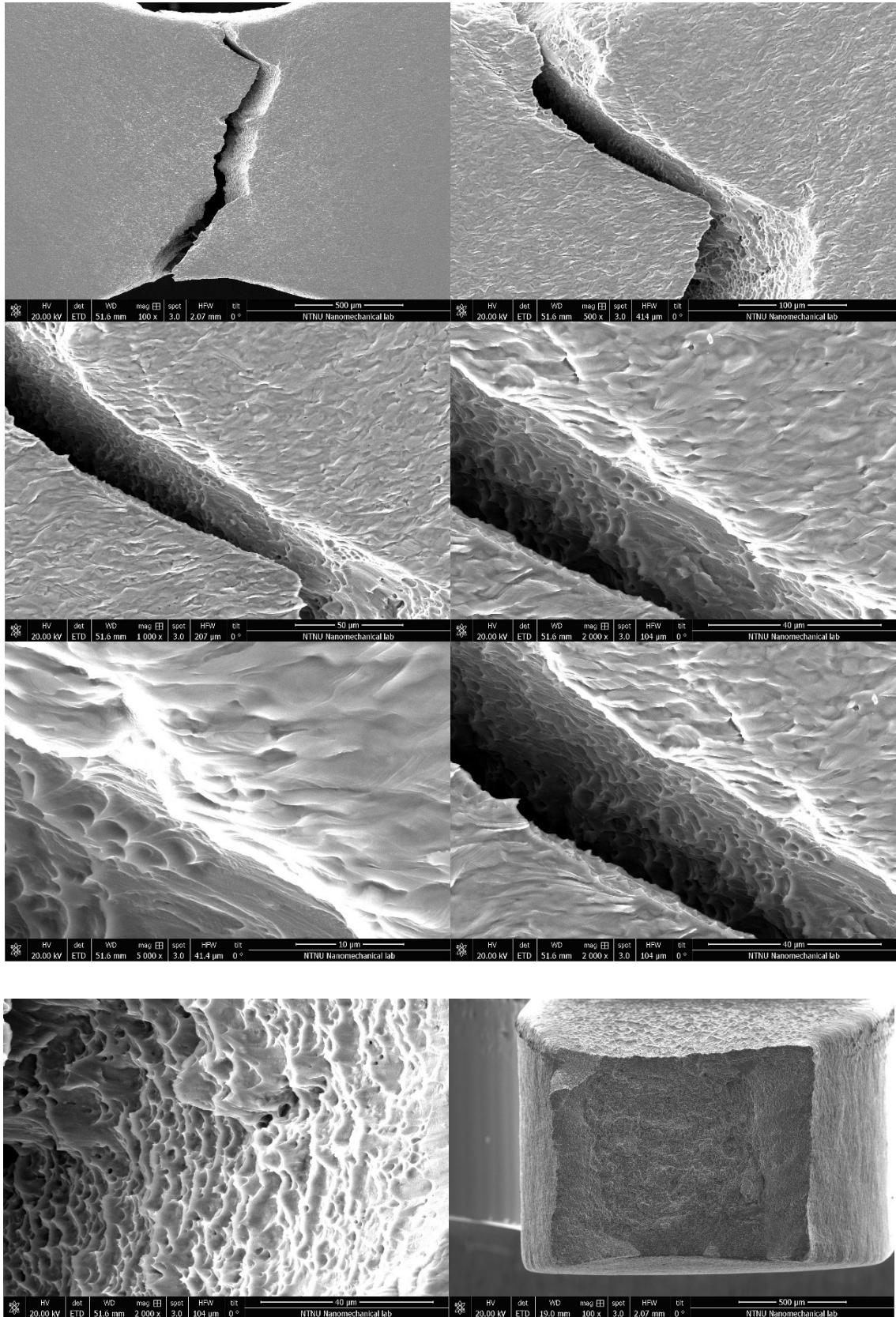


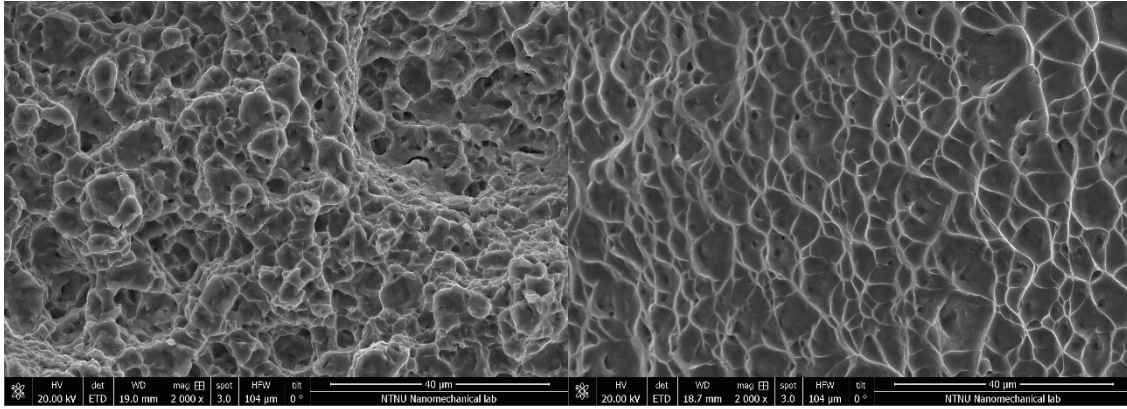
*Last steps of situ test sequence for LENS*



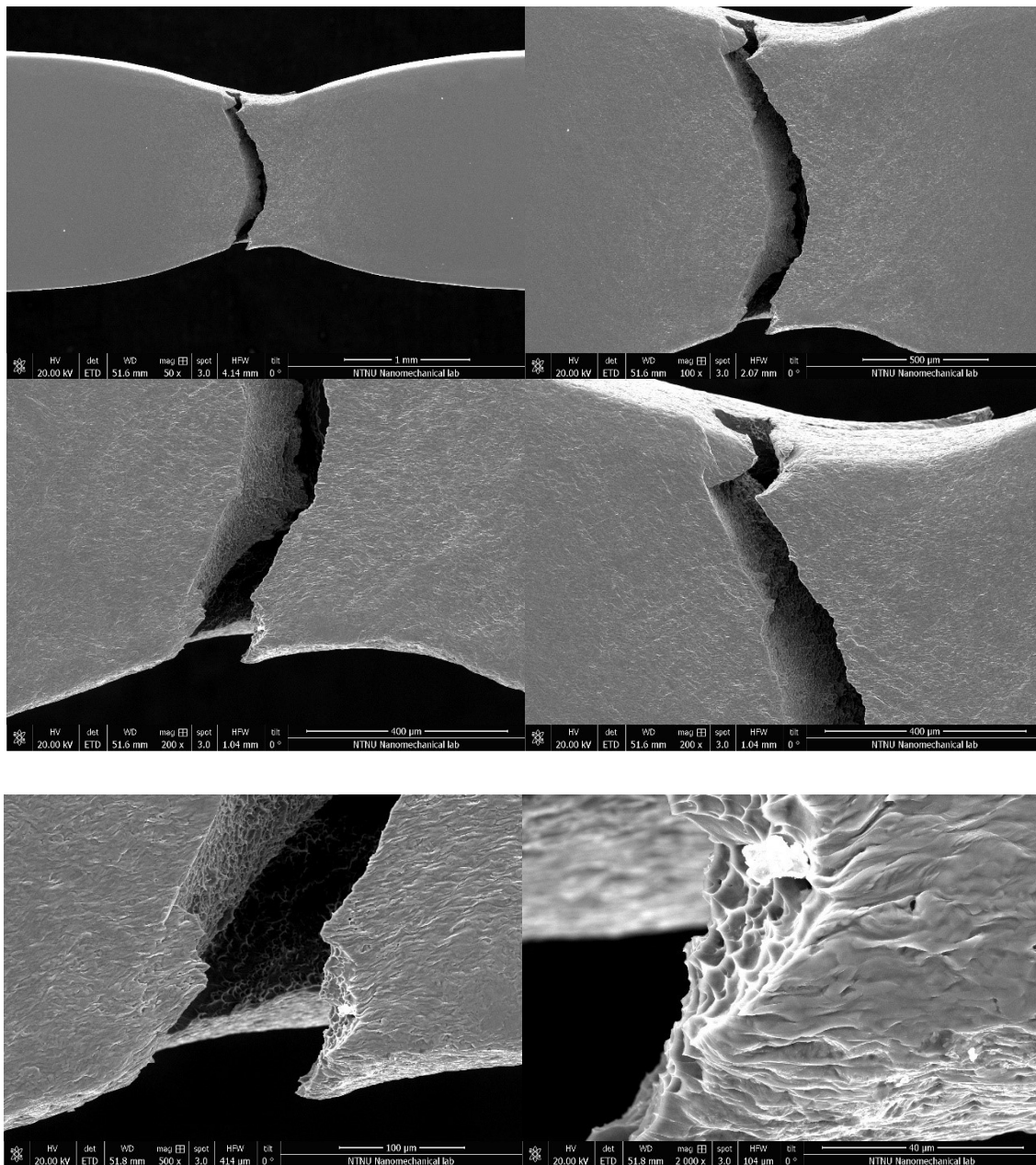
# Appendix D: Fractographies

## *Fractography W*

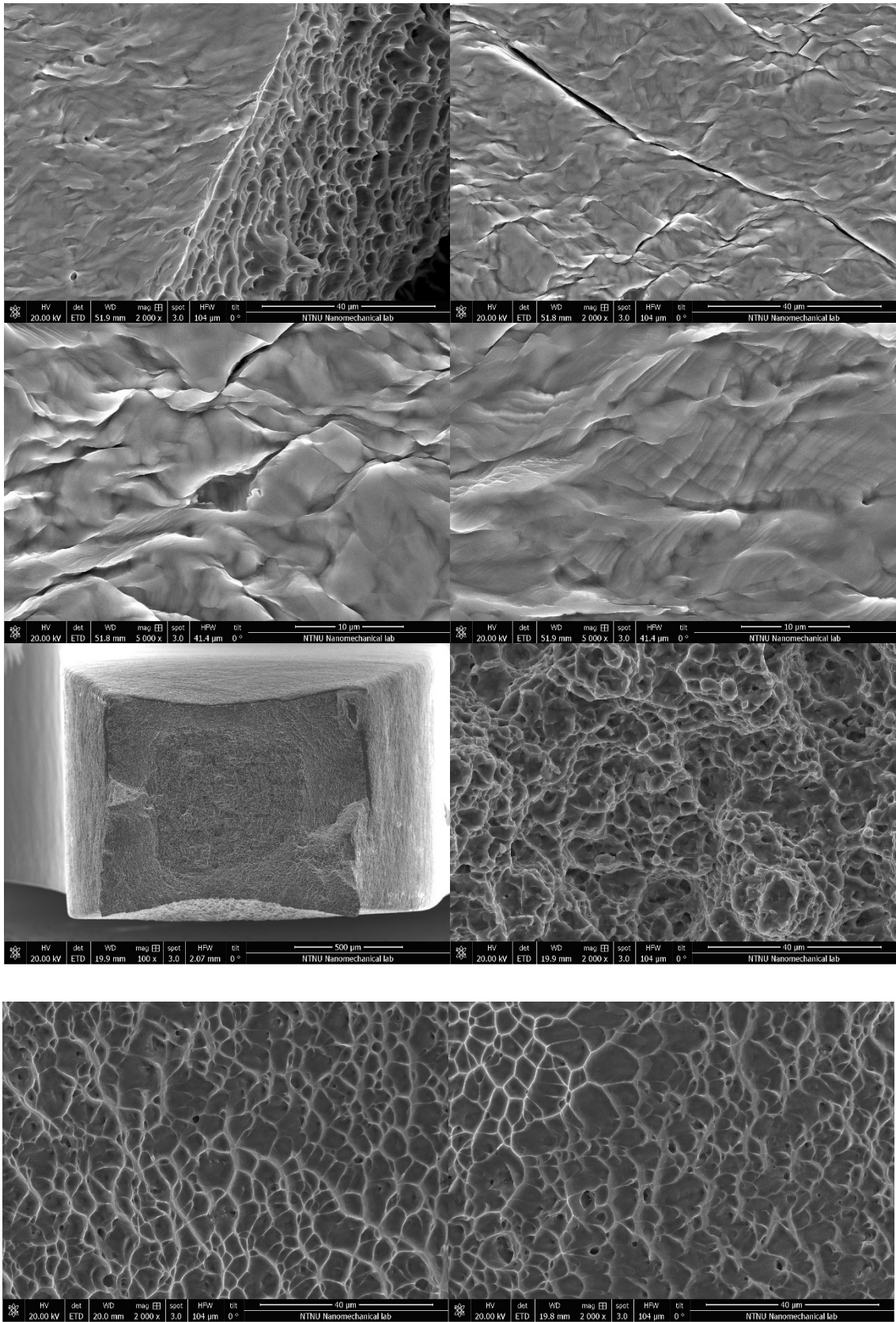




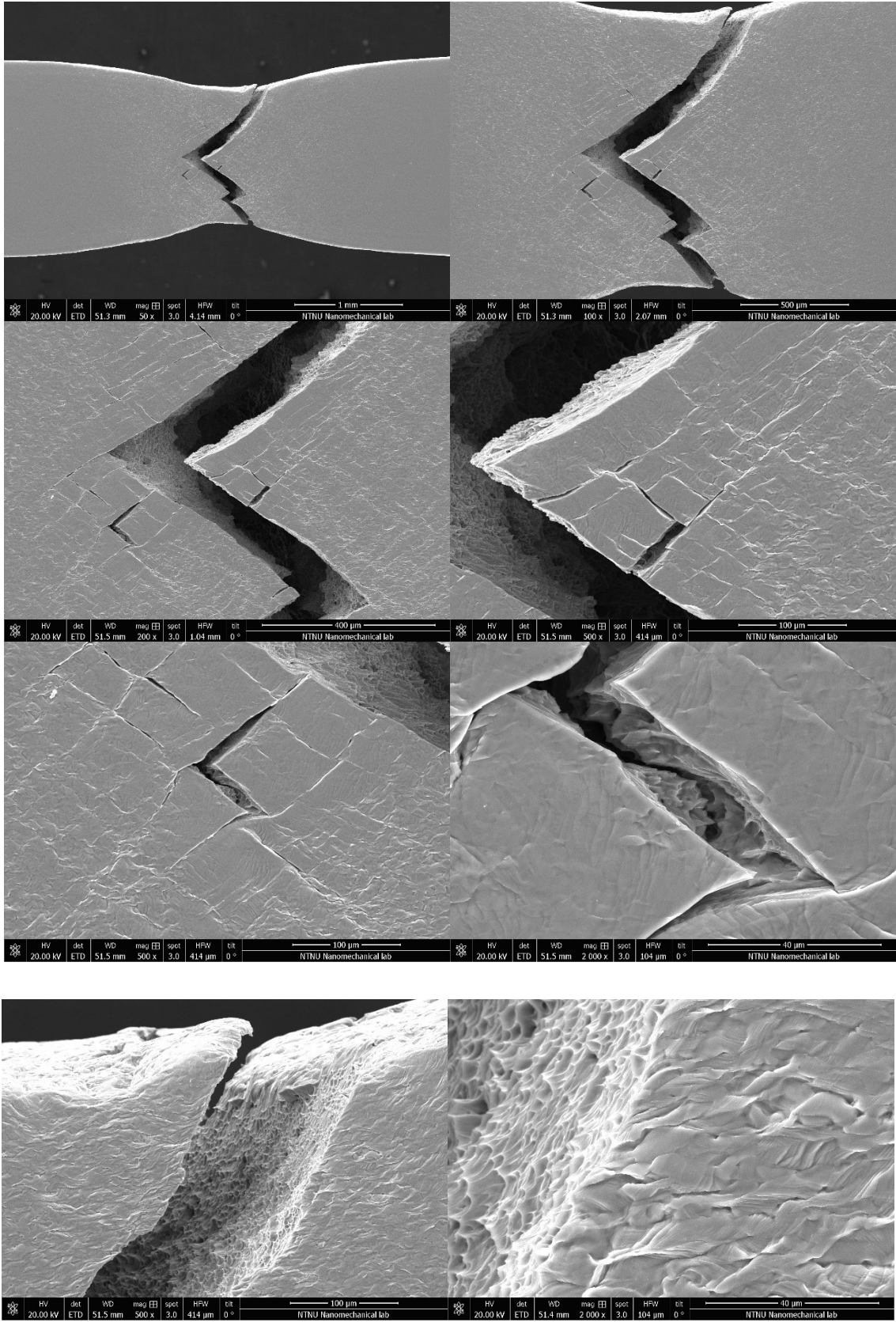
*Fractography W970-WQ*

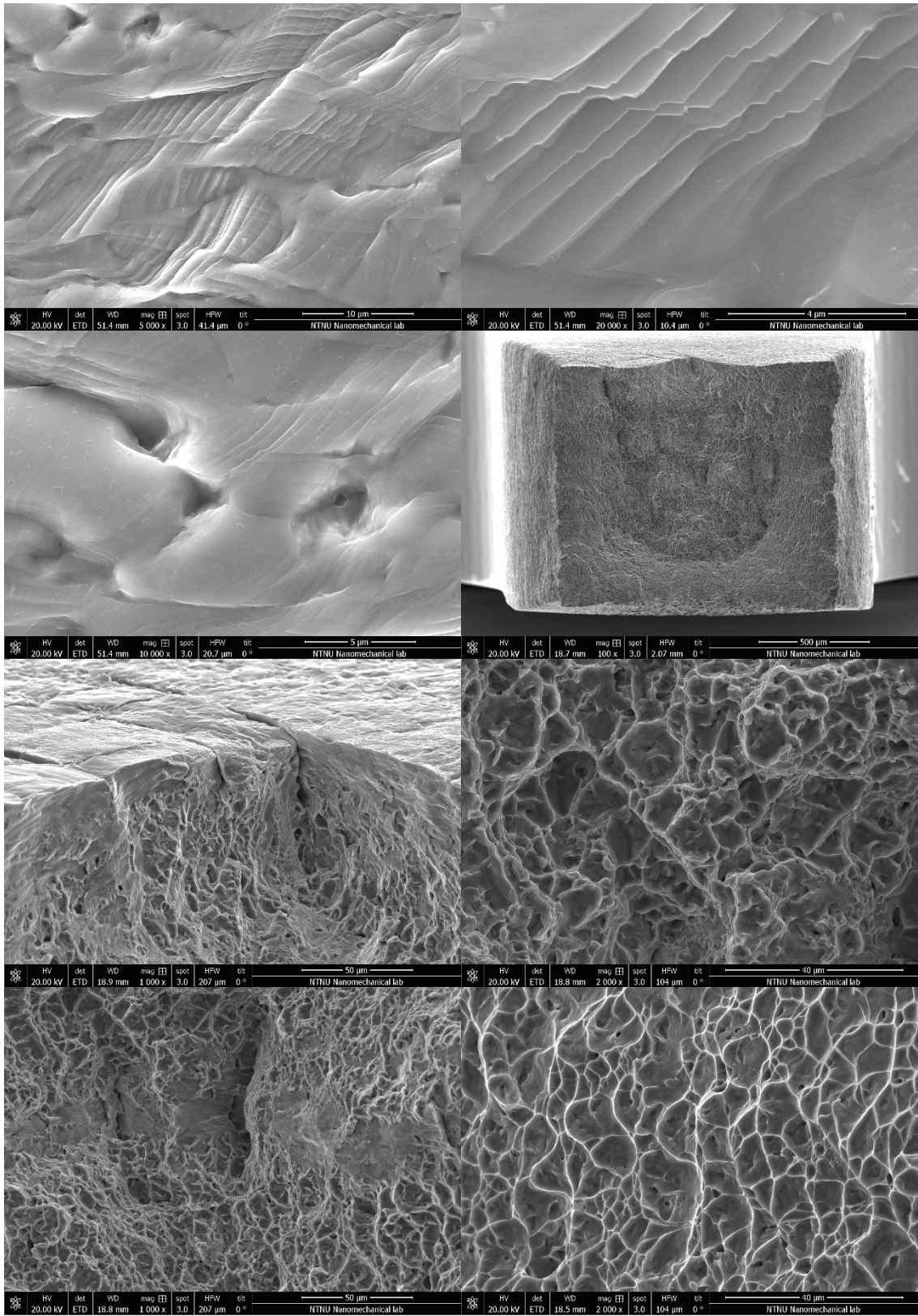




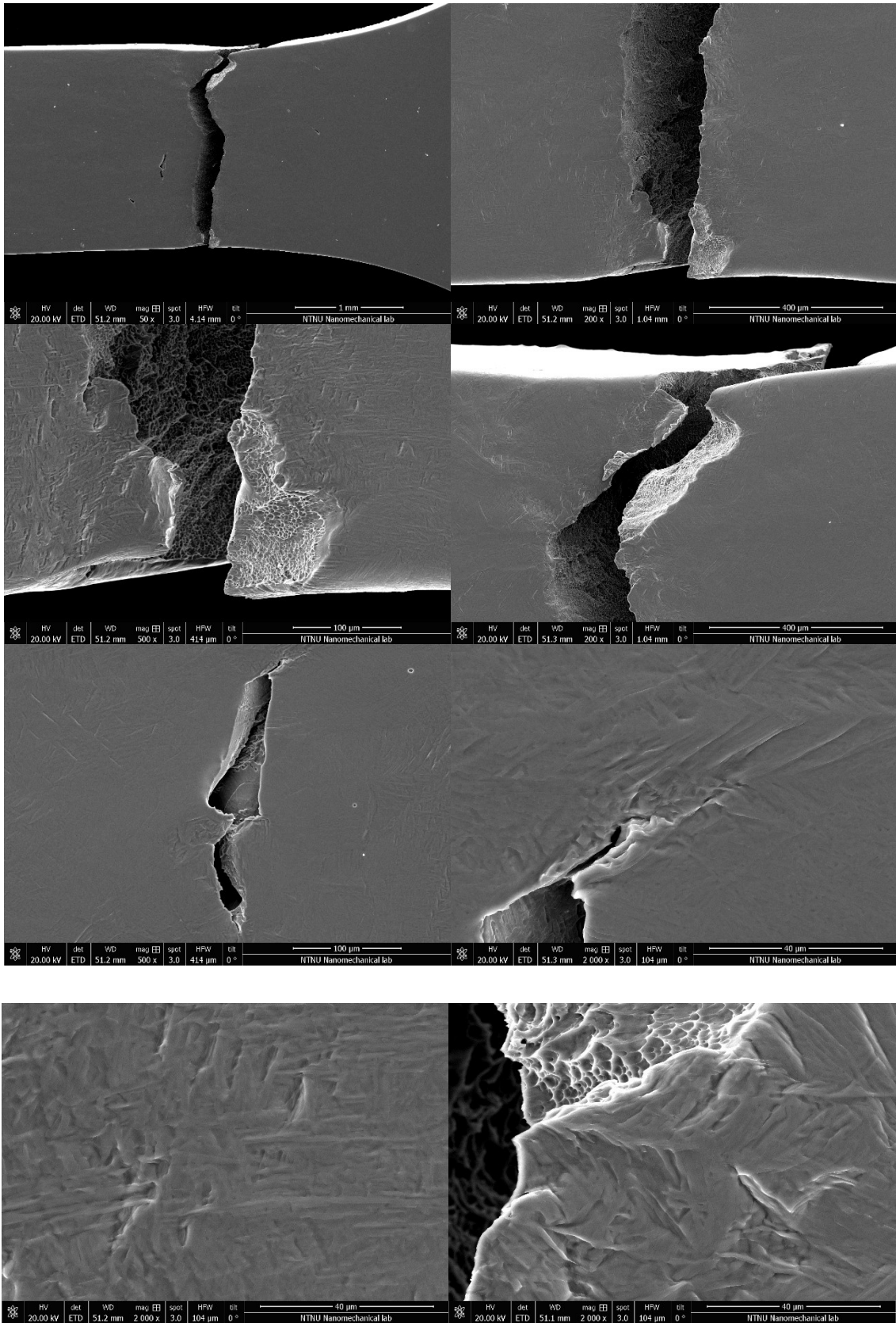


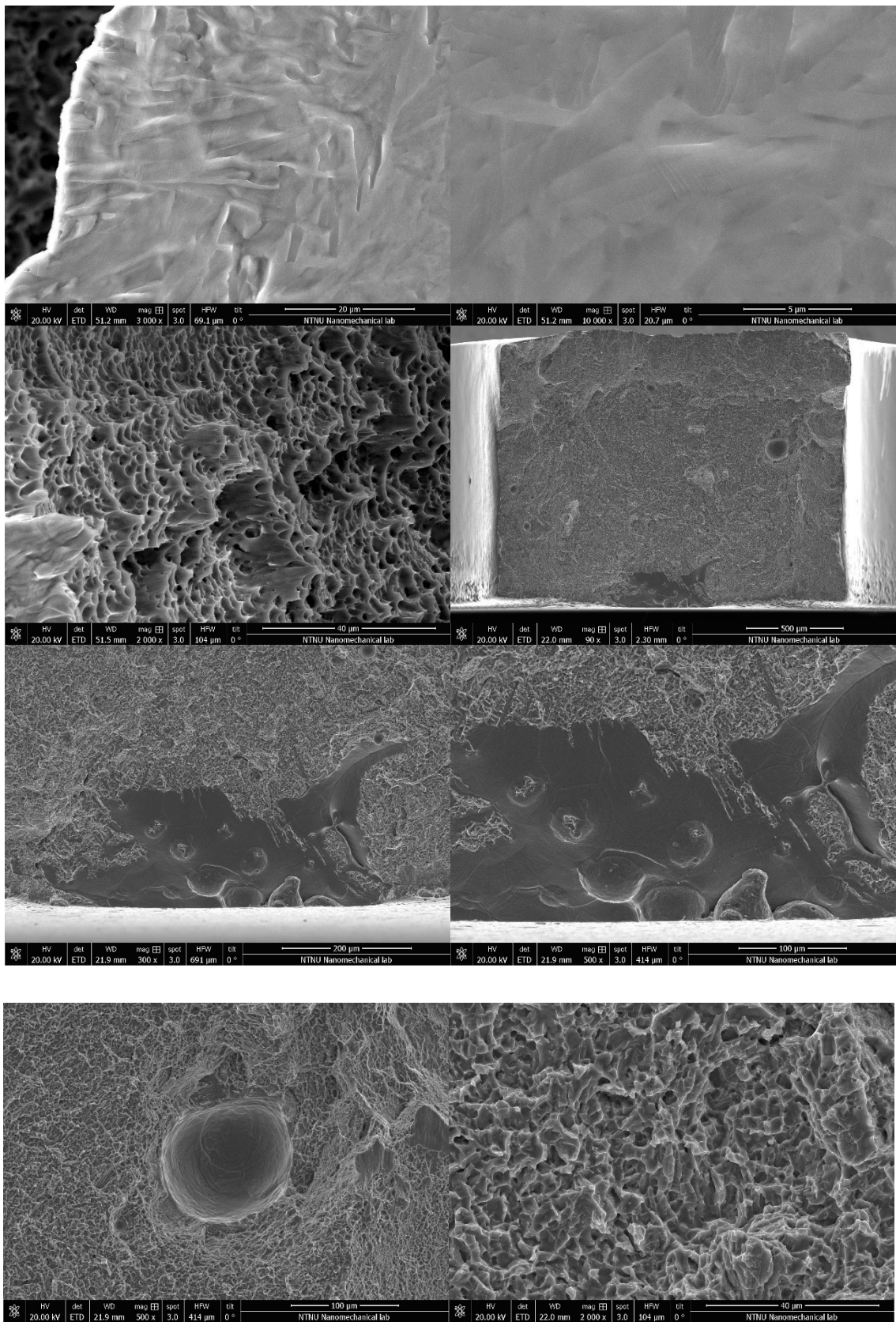
*Fractography W1015-FC*

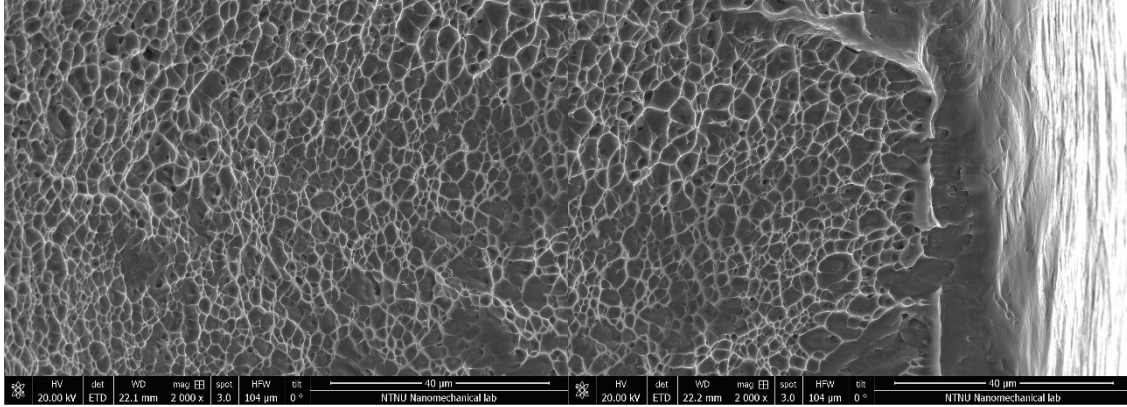




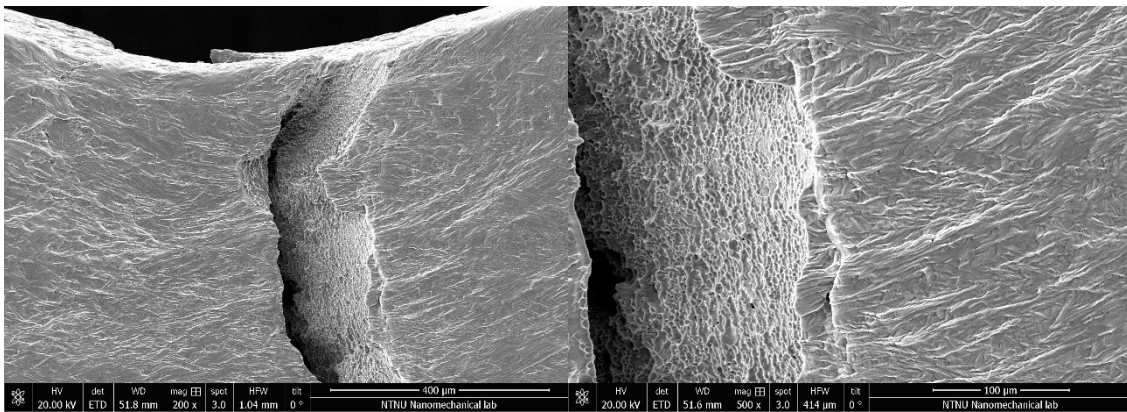
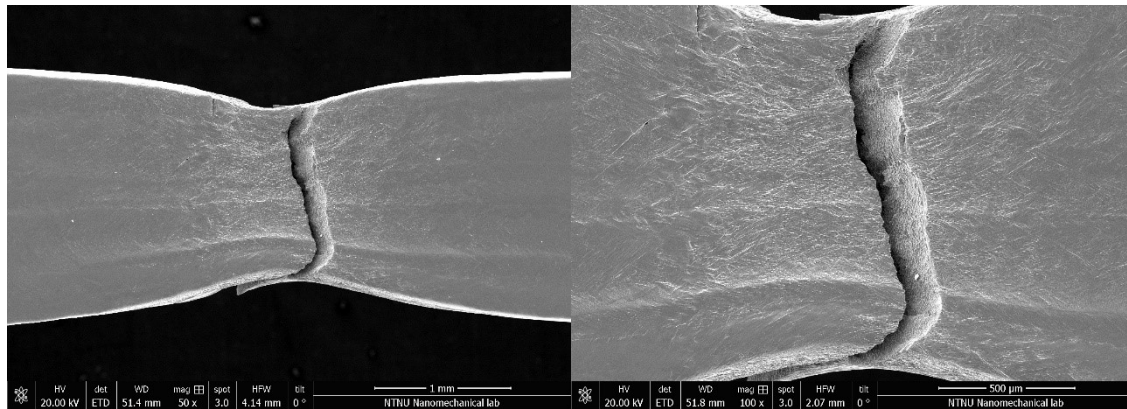
# Fractography EBM

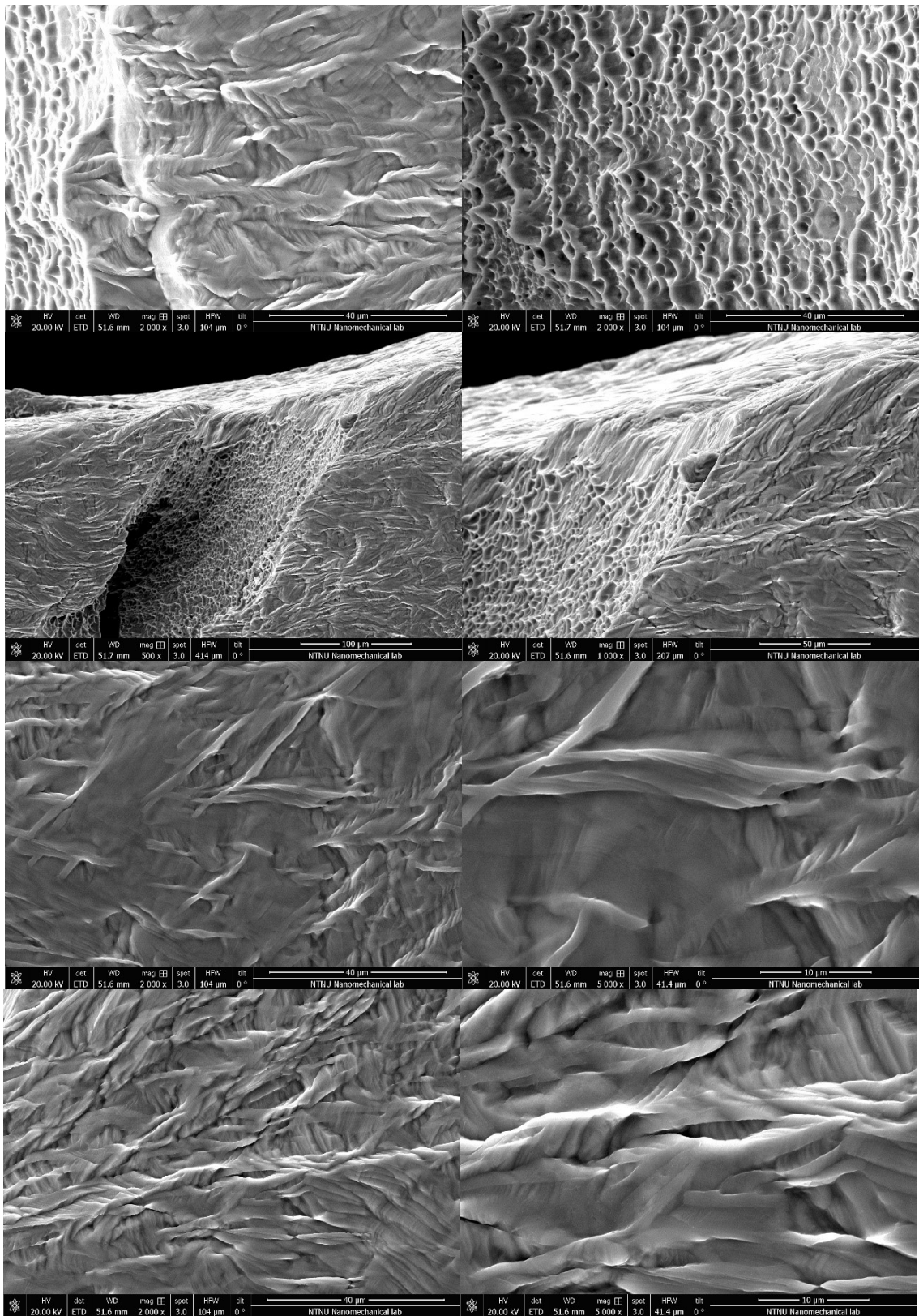


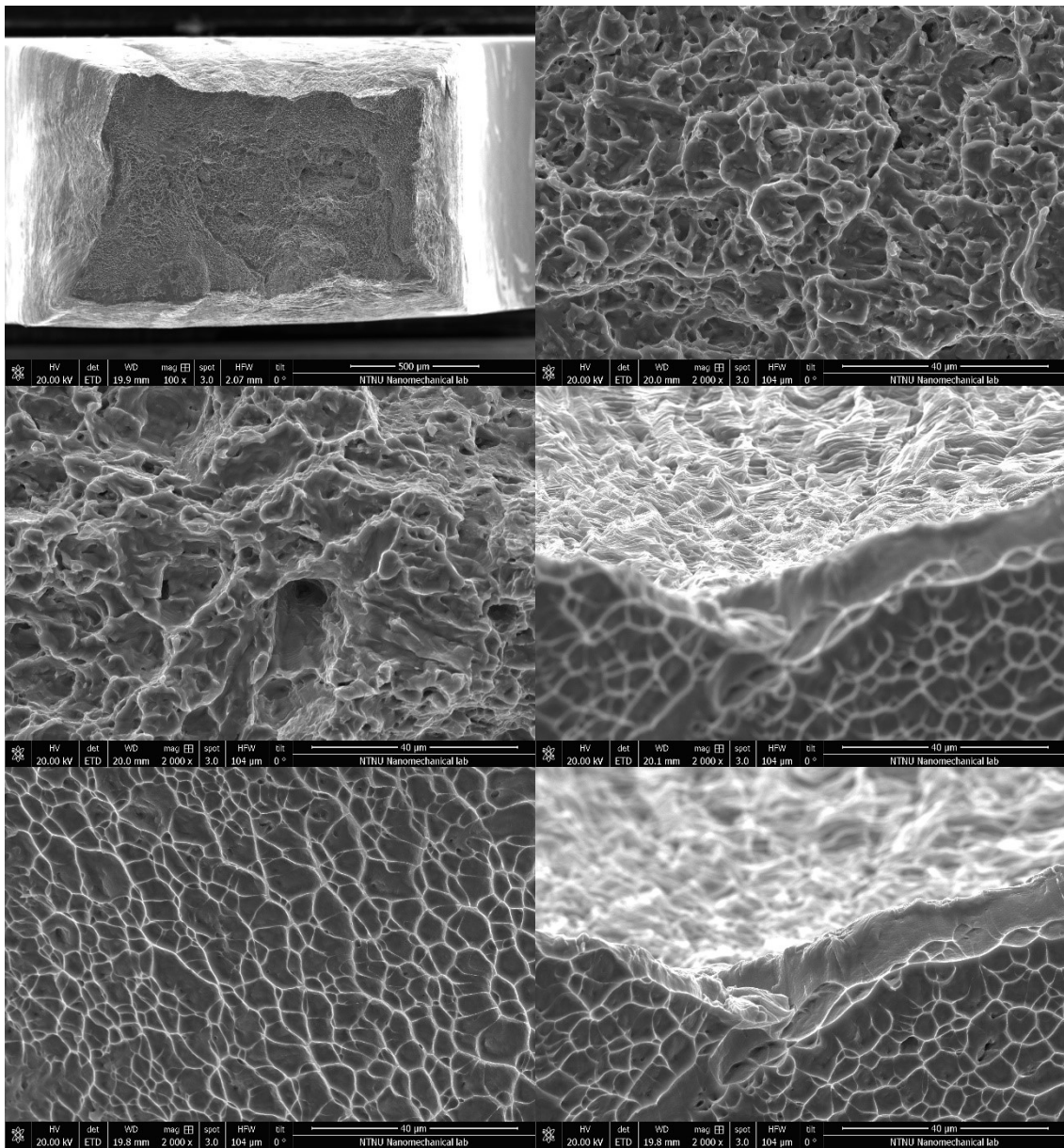




*Fractography LENS*









## Appendix E: Tensile test values

*Medium thickness values and cross sectional areas, calculated for width= 2 mm*

	Thickness (mm)	Area (mm <sup>2</sup> )
W	1.33	2.66
W1015-FC	1.395	2.79
W970-WQ	1.31	2.62
EBM	1.43	2.860
LENS	1.22	2.44

*Young's Modulus values calculated as slope of elastic part of  $\sigma - \epsilon$  (true stress-true strain) curve with  $L_0$  =initial gauge length=5000 $\mu$ m*

	Young's Modulus (MPa)
W	22970
W970	20466
W1015	23900
EBM	21197
LENS	21976

# References

- [1] A. Safdar, *A Study on Electron Beam Melted Ti-6Al-4V* Adnan Safdar Division of Solid Mechanics Department of Construction Sciences. 2012.
- [2] Bhaskar Dutta, *Additive Manufacturing of Titanium Alloys Additive Manufacturing of Titanium Alloys State of the Art , Challenges , and Opportunities*. 2014.
- [3] J. E. Barnes, A. B. Kingsbury, E. Bono, "Does " Low Cost " Titanium Powder Yield Low Cost Titanium Parts?," *PowderMet 2016 International Conference on Powder Metallurgy*, n. January, 2016.
- [4] J. Dzuga *et al.*, "Effects of thickness and orientation on the small scale fracture behaviour of additively manufactured Ti-6Al-4V," *Materials Characterization*, Vol. 143, n. October 2017, 2018, pp. 94–109.
- [5] T. Connolly, P. E. Mchugh, M. Bruzzi, "A review of deformation and fatigue of metals at small size scales," *Fatigue and Fracture of Engineering Materials and Structures*, Vol. 28, n. 12, 2005, pp. 1119–1152.
- [6] S. Mahabunphachai, M. Koç, "Investigation of size effects on material behavior of thin sheet metals using hydraulic bulge testing at micro/meso-scales," *International Journal of Machine Tools and Manufacture*, Vol. 48, n. 9, 2008, pp. 1014–1029.
- [7] R. Boyer, G. Welsch, E. W. Collings, *Materials properties handbook : titanium alloys*. 1994.
- [8] H. Warlimont, *Titanium and titanium alloys*. 2018.
- [9] M. J. Donachie, *Titanium: a technical guide*. 2000.
- [10] P. C. Turner, J. S. Hansen, S. J. Gerdemann, "Doe/arc-2001-086," n. Figure 1, 2001.
- [11] "Titanium Alloys - Ti6Al4V Grade 5." [Online]. Available: <https://www.azom.com/article.aspx?ArticleID=1547>. [Accessed: 30-Mar-2020].
- [12] M. Peters, J. Kumpfert, C. H. Ward, C. Leyens, "Titanium alloys for aerospace applications," *Advanced Engineering Materials*, Vol. 5, n. 6, 2003, pp. 419–427.
- [13] "Titanium: applications and uses-Metalpedia." [Online]. Available: <http://metalpedia.asianmetal.com/metal/titanium/application.shtml>. [Accessed: 30-Mar-2020].
- [14] "Boeing: The Boeing Company." [Online]. Available: <https://www.boeing.com/>. [Accessed: 02-Apr-2020].
- [15] E. Uhlmann, R. Kersting, T. B. Klein, M. F. Cruz, A. V. Borille, "Additive Manufacturing of Titanium Alloy for Aircraft Components," *Procedia CIRP*, Vol. 35, 2015, pp. 55–60.

- [16] and B. S. Gibson, Ian, David W. Rosen, *Additive Manufacturing Technologies*, Vol. 17. 2015.
- [17] D. T. Pham, R. S. Gault, “A comparison of rapid prototyping technologies,” *International Journal of Machine Tools and Manufacture*, Vol. 38, n. 10–11, 1998, pp. 1257–1287.
- [18] ASTM International, “F2792-12a - Standard Terminology for Additive Manufacturing Technologies,” *Rapid Manufacturing Association*, 2013, pp. 10–12.
- [19] T. D. Ngo, A. Kashani, G. Imbalzano, K. T. Q. Nguyen, D. Hui, “Additive manufacturing (3D printing): A review of materials, methods, applications and challenges,” *Composites Part B: Engineering*, Vol. 143, n. December 2017, 2018, pp. 172–196.
- [20] HP, “HP Metal Jet technology,” 2018, pp. 1–8.
- [21] N. B. Crane, “Impact of part thickness and drying conditions on saturation limits in binder jet additive manufacturing,” *Additive Manufacturing*, Vol. 33, n. February, 2020, p. 101127.
- [22] L. Thijs, F. Verhaeghe, T. Craeghs, J. Van Humbeeck, J. P. Kruth, “A study of the microstructural evolution during selective laser melting of Ti-6Al-4V,” *Acta Materialia*, Vol. 58, n. 9, 2010, pp. 3303–3312.
- [23] D. D. Gu, W. Meiners, K. Wissenbach, R. Poprawe, “Laser additive manufacturing of metallic components: Materials, processes and mechanisms,” *International Materials Reviews*, Vol. 57, n. 3, 2012, pp. 133–164.
- [24] R. Yan *et al.*, “Electron beam melting in the fabrication of three-dimensional mesh titanium mandibular prosthesis scaffold,” *Scientific Reports*, Vol. 8, n. 1, 2018, pp. 1–10.
- [25] K. Osakada, M. Shiomi, “Flexible manufacturing of metallic products by selective laser melting of powder,” *International Journal of Machine Tools and Manufacture*, Vol. 46, n. 11 SPEC. ISS., 2006, pp. 1188–1193.
- [26] N. Taniguchi *et al.*, “Effect of pore size on bone ingrowth into porous titanium implants fabricated by additive manufacturing: An in vivo experiment,” *Materials Science and Engineering C*, Vol. 59, 2016, pp. 690–701.
- [27] P. Heintz, L. Müller, C. Körner, R. F. Singer, F. A. Müller, “Cellular Ti-6Al-4V structures with interconnected macro porosity for bone implants fabricated by selective electron beam melting,” *Acta Biomaterialia*, Vol. 4, n. 5, 2008, pp. 1536–1544.
- [28] B. Vandenbroucke, J. P. Kruth, “Selective laser melting of biocompatible metals for rapid manufacturing of medical parts,” *Rapid Prototyping Journal*, Vol. 13, n. 4, 2007, pp. 196–203.
- [29] S. M. J. Razavi, F. Berto, “Directed Energy Deposition versus Wrought Ti-6Al-4V: A Comparison of Microstructure, Fatigue Behavior, and Notch

- Sensitivity,” *Advanced Engineering Materials*, Vol. 1900220, 2019, pp. 1–15.
- [30] S. Liu, Y. C. Shin, “Additive manufacturing of Ti6Al4V alloy : A review,” *Materials & Design*, Vol. 164, 2019, p. 107552.
- [31] T. Vilaro, C. Colin, J. D. Bartout, “As-fabricated and heat-treated microstructures of the Ti-6Al-4V alloy processed by selective laser melting,” *Metallurgical and Materials Transactions A: Physical Metallurgy and Materials Science*, Vol. 42, n. 10, October 2011, pp. 3190–3199.
- [32] M. Neikter, P. Åkerfeldt, R. Pederson, M. L. Antti, “Microstructure characterisation of Ti-6Al-4V from different additive manufacturing processes,” *IOP Conference Series: Materials Science and Engineering*, Vol. 258, n. 1, 2017.
- [33] “Heat Treating of Titanium and Titanium Alloys.” [Online]. Available: <http://www.totalmateria.com/Article97.htm>. [Accessed: 30-Mar-2020].
- [34] A. Morri, “Trattamenti termici delle leghe di titanio  $\alpha+\beta$ , correlazioni fra microstruttura e comportamento meccanico,” *Metallurgia Italiana*, Vol. 100, n. 10, 2008, pp. 1–10.
- [35] S. El-Hadad, M. Nady, W. Khalifa, A. Shash, “Influence of heat treatment conditions on the mechanical properties of Ti-6Al-4V alloy,” *Canadian Metallurgical Quarterly*, Vol. 57, n. 2, 2018, pp. 186–193.
- [36] X. Yao, “Quenching of Titanium and Control of Residual Stresses,” *Heat Treating of Nonferrous Alloys*, Vol. 4, 2018, pp. 546–554.
- [37] T. Depover, T. Hajilou, D. Wan, D. Wang, A. Barnoush, K. Verbeken, “Assessment of the potential of hydrogen plasma charging as compared to conventional electrochemical hydrogen charging on dual phase steel,” *Materials Science and Engineering A*, Vol. 754, n. October 2018, 2019, pp. 613–621.
- [38] C. Implications, “Surface roughness and fatigue performance of commercially pure titanium and Ti-6Al-4V alloy after different polishing protocols,” Vol. 93, n. 4.
- [39] B. Chou, R. Jain, D. Mcgervey, U. Landau, G. Welsch, “Electropolishing of Titanium,” p. 300.
- [40] A. Guesnier, “Preparation of ferrous metals for Electron Backscatter Diffraction Application Notes,” *Oxford Instruments NanoAnalysis*, 2010, p. 12.
- [41] S. Zhang, X. Lin, J. Chen, W. Huang, “Heat-treated microstructure and mechanical properties of laser solid forming Ti-6Al-4V alloy,” *Rare Metals*, Vol. 28, n. 6, 2009, pp. 537–544.
- [42] T. Vilaro, C. Colin, J. D. Bartout, “As-fabricated and heat-treated microstructures of the Ti-6Al-4V alloy processed by selective laser melting,” *Metallurgical and Materials Transactions A: Physical Metallurgy and Materials Science*, Vol. 42, n. 10, 2011, pp. 3190–3199.

- [43] R. E. Smallman, A. H. W. Ngan, “Characterization and Analysis,” *Modern Physical Metallurgy*, 2014, pp. 159–250.
- [44] T. Vickers, “Small-specimen Mechanical Testing,” Vol. 1, n. 1, pp. 1–5.
- [45] C. Z. X. Microscopy, “In Situ Observation of Mechanical Testing at the Nanoscale In Situ Observation of Mechanical Testing at the Nanoscale.”
- [46] J. Lu, L. Chang, J. Wang, L. Sang, S. Wu, Y. Zhang, “In-situ investigation of the anisotropic mechanical properties of laser direct metal deposition Ti6Al4V alloy,” *Materials Science and Engineering A*, Vol. 712, n. December 2017, 2018, pp. 199–205.
- [47] P. Hosemann, C. Shin, “Small scale mechanical testing of irradiated materials Small scale mechanical testing of irradiated materials,” n. May, 2015.
- [48] K. Kumar *et al.*, “Use of miniature tensile specimen for measurement of mechanical properties,” *Procedia Engineering*, Vol. 86, 2014, pp. 899–909.
- [49] W. V. Vaidya *et al.*, “Structure-property investigations on a laser beam welded dissimilar joint of aluminium AA6056 and titanium Ti6Al4V for aeronautical applications Part I: Local gradients in microstructure, hardness and strength,” *Materialwissenschaft und Werkstofftechnik*, Vol. 40, n. 8, August 2009, pp. 623–633.
- [50] P. H. Hou, T. Y. Chen, “An automatic tensile test measurement system for miniature specimens,” *Experimental Techniques*, Vol. 29, n. 4, July 2005, pp. 32–36.
- [51] K. J. Hemker, W. N. Sharpe, “Microscale Characterization of Mechanical Properties,” *Annual Review of Materials Research*, Vol. 37, n. 1, August 2007, pp. 93–126.
- [52] N. Kashaev, M. Horstmann, V. Ventzke, S. Riekehr, N. Huber, “Comparative study of mechanical properties using standard and micro-specimens of base materials Inconel 625, Inconel 718 and Ti-6Al-4 v,” *Journal of Materials Research and Technology*, Vol. 2, n. 1, 2013, pp. 43–47.
- [53] A. V. Sergueeva, J. Zhou, B. E. Meacham, D. J. Branagan, “Gage length and sample size effect on measured properties during tensile testing,” *Materials Science and Engineering A*, Vol. 526, n. 1–2, 2009, pp. 79–83.
- [54] C. Rudolf, B. Boesl, A. Agarwal, “In Situ Mechanical Testing Techniques for Real-Time Materials Deformation Characterization,” *Jom*, Vol. 68, n. 1, 2016, pp. 136–142.
- [55] K. Beyl, K. Mutombo, C. P. Kloppers, “Tensile properties and microstructural characterization of additive manufactured, investment cast and wrought Ti6Al4V alloy,” *IOP Conference Series: Materials Science and Engineering*, Vol. 655, n. 1, 2019.
- [56] P. Tan, F. Shen, B. Li, K. Zhou, “A thermo-metallurgical-mechanical model for selective laser melting of Ti6Al4V,” *Materials and Design*, Vol. 168, 2019, p. 107642.

- [57] X. Yan *et al.*, “Effect of heat treatment on the phase transformation and mechanical properties of Ti6Al4V fabricated by selective laser melting,” *Journal of Alloys and Compounds*, Vol. 764. pp. 1056–1071, 2018.
- [58] T. Trnava, S. Republic, B. Polytechnic, “The influence of heat treatment on the microstructure of the casted ti6al4v titanium alloy,” *Materials World*, Vol. 2, 2007, pp. 1–6.
- [59] L. E. Murr *et al.*, “Microstructures and mechanical properties of electron beam-rapid manufactured Ti – 6Al – 4V biomedical prototypes compared to wrought Ti – 6Al – 4V,” *Materials Characterization*, Vol. 60, n. 2, 2008, pp. 96–105.
- [60] Norman E. Dowling, *Mechanical Behavior of Materials - Engineering Methods for Deformation, Fracture and Fatigue*, 4th ed. 2013.
- [61] ASTM Internationnal, “Standard Test Method for Tensile Strain-Hardening Exponents ( n -Values ) of Metallic,” *ASTM International*, 2016, pp. 1–9.
- [62] R. K. Gupta, V. A. Kumar, C. Mathew, G. S. Rao, “A Strain hardening of Titanium alloy Ti6Al4V sheets with prior heat treatment and cold working,” *Materials Science & Engineering A*, Vol. 662, 2016, pp. 537–550.
- [63] U. Bathini, T. S. Srivatsan, A. Patnaik, T. Quick, “A study of the tensile deformation and fracture behavior of commercially pure titanium and titanium alloy: Influence of orientation and microstructure,” *Journal of Materials Engineering and Performance*, Vol. 19, n. 8, 2010, pp. 1172–1182.